NASA TECHNICAL MEMORANDUM

NASA TM X-72671

COPY NO.

NASA TM X-72671

LOW-SPEED WIND-TUNNEL TESTS OF A 1/10-SCALE MODEL OF A BLENDED-ARROW ADVANCED SUPERSONIC TRANSPORT

By

H. Clyde McLemore and Lysle P. Parett

March 1975

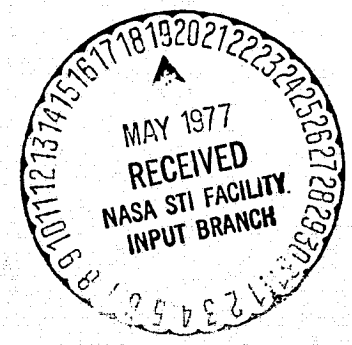

RELEASED FOR PUBLIC AVAILABILITY
MARCH 1977

NATIONAL AERONAUTICS AND SPACE ADMINISTRATION
LANGLEY RESEARCH CENTER, HAMPTON, VIRGINIA 23665

1. Report No.	2. Government Accession No.	3. Recipient's Catalog No.
TM X-72671		

4. Title and Subtitle	5. Report Date
LOW-SPEED WIND-TUNNEL TESTS OF A 1/10-SCALE MODEL OF A BLENDED-ARROW ADVANCED SUPERSONIC TRANSPORT	March 1975
	6. Performing Organization Code

7. Author(s)	8. Performing Organization Report No.
H. Clyde McLemore and Lysle P. Parlett	

9. Performing Organization Name and Address	10. Work Unit No.
NASA Langley Research Center Hampton, VA 23665	743-04-12-02
	11. Contract or Grant No.
	13. Type of Report and Period Covered
12. Sponsoring Agency Name and Address	Technical Memorandum
National Aeronautics and Space Administration Washington, DC 20546	14. Sponsoring Agency Code

15. Supplementary Notes

16. Abstract

Tests have been conducted in the Langley full-scale tunnel to determine the low-speed aerodynamic characteristics of a 1/10-scale model of a blended-arrow advanced supersonic transport. Tests were made for the clean configuration and a high-lift configuration with several combinations of leading- and trailing-edge flaps deflected for providing improved lift and longitudinal stability in the landing and takeoff modes. The tests were conducted for a range of angles of attack from about -6^{o} to 30^{o}, sideslip angles from -5^{o} to 10^{o}, and for Reynolds numbers from 6.78×10^{6} to 13.85×10^{6} corresponding to test velocities of 41 knots to 85 knots, respectively.

17. Key Words (Suggested by Author(s)) (STAR category underlined)	18. Distribution Statement
Aerodynamics, Low-Speed Stability and Control, Advanced Supersonic Transport	

19. Security Classif. (of this report)	20. Security Classif. (of this page)	21. No. of Pages	22. Price*
Unclassified	Unclassified	69	$4.25

*Available from { The National Technical Information Service, Springfield, Virginia 22151
STIF/NASA Scientific and Technical Information Facility, P.O. Box 33, College Park, MD 20740

LOW-SPEED WIND-TUNNEL TESTS OF A 1/10-SCALE MODEL OF A BLENDED-ARROW ADVANCED SUPERSONIC TRANSPORT

By H. Clyde McLemore and Lysle P. Parlett

Langley Research Center

SUMMARY

Tests have been conducted in the Langley full-scale tunnel to determine the low-speed aerodynamic characteristics of a 1/10-scale model of a blended-arrow advanced supersonic transport. Tests were made for the clean configuration and a high-lift configuration with several combinations of leading- and trailing-edge flaps for providing improved lift and longitudinal stability in the landing and takeoff modes. The tests were conducted for a range of angles of attack from about -6° to 30°, sideslip angles from -5° to 10°, and for Reynolds numbers from 6.78×10^{6} to 13.85×10^{6} corresponding to test velocities of 41 knots and 85 knots, respectively.

The clean configuration exhibited static longitudinal instability (pitchup) at an angle of attack of about 3°; however, deflecting inboard wing leading-edge flaps delayed the pitchup to an angle of attack of about 18°. Deflecting full-span trailing-edge flaps and leading-edge flaps increased the lift coefficient from a value of about 0.35 for the clean configuration to a value of about 0.50 (untrimmed) at an angle of attack of 9.5° (estimated tail scrape angle). The model exhibited satisfactory lateral-directional characteristics to angles of attack of about 16°. Above this angle of attack the directional stability increased markedly; however, the effective dihedral decreased to nearly zero at an angle of attack of about 24°.

INTRODUCTION

The present study is part of the overall effort of the NASA to provide the technology base for the formulation and development of advanced supersonic-cruise vehicles. This paper will report the results of initial low-speed tests of a supersonic transport concept designed to utilize very low wing weight (blended wing-fuselage contours), variable-cycle engines or quiet, duct-burning fan engines, and thrust vectoring.

The distinguishing features of the present concept are the platypus-nosed, all-wing planform, and the centerline-mounted four-engine propulsion package. The planform with its long root chord was selected for sonic-boom reasons as discussed in reference 1. The location of the propulsion system was dictated in part by the desire to avoid aeroelastic problems associated with the placing of mass outboard and rearward of the torsional axis of the flexible, lightweight structure. The propulsion system is designed to incorporate a thrust vectoring capability intended to provide increased circulation for improvement in both lift and lift-drag ratio (see refs. 2 and 3), and additional longitudinal control. To effectively use vectored thrust in improving airframe flight efficiency in the critical low-speed mode where thrust reduction is important to noise alleviation, active controls are also a necessary feature of the present design. Beyond the features cited, the aerodynamic design philosophy is largely that reported in references 4 and 5.

The objectives of these preliminary tests are to determine some of the low-speed static aerodynamic characteristics of the basic configuration concept and to provide the data base from which configuration modifications might be made to alleviate any low-speed aerodynamic problems.

The tests were conducted in the Langley full-scale tunnel on a 1/10-scale model of an advanced blended-arrow supersonic transport configuration. The tests were conducted for a range of Reynolds numbers from 6.78×10^6 to 13.85×10^6 based on the mean aerodynamic chord. The tests were

conducted for a range of angle of attack of about -6^{o} to 30^{o} and for sideslip angles from -5^{o} to 10^{o}. The configuration variables included combinations of leading- and trailing-edge flap deflections; and thrust and engine nozzle deflection angle were varied to provide for additional lift. A few tests were conducted with the vertical tails removed to determine the contribution of the tails to lateral-directional stability and in addition tests were conducted to determine rudder effectiveness.

SYMBOLS

The data are referred to the stability of axes illustrated in figure 1. The origin of the axes was located to correspond with the 35-percent location of the mean aerodynamic chord.

The dimensional quantities are given in the International System of Units (SI) and in U.S. Customary Units. Conversion factors for the two systems are given in reference 6.

b	wing span, 4.570 m (15.00 ft)
B.S.	body station (longitudinal distance from model nose), m (ft)
$\bar{c}$	mean aerodynamic chord, 4.600 m (15.10 ft)
C_D	drag coefficient, Drag/qS
C_L	lift coefficient, Lift/qS
C_ℓ	rolling moment coefficient, Rolling moment/qSb
C_m	pitching moment coefficient, Pitching moment/q$S\bar{c}$
C_n	yawing moment coefficient, Yawing moment/qSb
C_Y	side force coefficient, Side force/qS
i_c	canard deflection angle, positive leading-edge up, deg
L.E.	leading edge
q	free stream dynamic pressure, N/m^2 (lb/ft^2)

S	wing area, 15.15 m^2 (163.00 ft^2)
T	engine thrust (thrust above the value for $T_c' = 0$), N (lb)
T_c'	thrust coefficient, T/qS
($T_c' = 0$)	thrust coefficient where engine exhaust total pressure is equal to free stream total pressure
T.E.	trailing edge
V	free stream velocity, m/sec (ft/sec)
X	longitudinal stability axis
α	angle of attack referred to wing reference line (fig. 1), deg
β	angle of sideslip, deg
δ_f	trailing-edge flap deflection, deg
δ_n	leading-edge flap deflection referenced to undeflected leading-edge position, deg
δ_N	engine exhaust deflection angle, positive downward, deg
δ_r	rudder deflection, positive for trailing-edge left, deg

Subscripts:

1,2,3,4,5,6,7 (with δ_n symbol) wing leading-edge flap segments (1, nearest wingtip, and 7, nearest nose of model (see fig. 2))

1,2,3 (with δ_f symbol) wing trailing-edge flap segments (1, inboard, and 3, outboard (see fig. 2))

MODEL

The dimensional characteristics of the 1/10-scale model are shown in figures 2 through 4. Photographs of the model mounted for tests in the Langley full-scale tunnel are presented in figures 5 through 7. The

model construction was an aluminum framework filled with a strux filler with the surface covered with several layers of fiberglass. The model was essentially rigid for these low-speed tests.

The model was equipped with wing leading- and trailing-edge flaps, twin vertical tails, and for a few tests, a 2-percent (aspect-ratio-6) canard. The leading-edge flap segments could be deflected from 0^{o} to 60^{o} downward (referenced normal to the wing leading-edge hingeline and to the mean line of the leading-edge section). The location, length, and chord of the leading-edge flap segments are shown in figures 2 and 3.

As shown in figure 3, the trailing-edge flaps were divided into three segments and each side could be deflected downward 30^{o} perpendicular to the hingeline - the maximum allowable angle to prevent scraping the runway on landing or takeoff.

The canard was equipped with a double-slotted full-span flap and a full-span slat. Since the incremental trimming effect was the only point of interest for the current investigation, the canard was installed at a fixed angle of incidence on the lower surface of the nose of the model. The physical characteristics of the canard and its location on the fuselage are noted in figure 4.

The model was equipped with fixed twin tails with full-span rudders with the size and positioning of fins and rudders as shown in figure 2.

The model was also equipped with four 0.14 m (5.50 in.) diameter fans (engines) mounted in an underslung nacelle. (See figure 3.) These fans were free to windmill with tunnel speed, or to be powered by externally supplied compressed air. The fans were tip driven (air ejected from blade tips to cause fan rotation), and for the current installation the fans could be driven to about 18,000 rpm (total combined static thrust $\approx$290 N (65 lb)) with the available compressed air supply.

TESTS AND CORRECTIONS

Tests

Force tests were conducted on the 1/10-scale model in the Langley full-scale tunnel for several values of Reynolds numbers, based on the mean aerodynamic chord from 6.78×10^6 to 13.85×10^6 (corresponding to test velocities of about 41 knots and 85 knots, respectively). Most of the tests were conducted at about 54 knots (Reynolds number = 8.92×10^6). For the powered tests, the test speed was restricted to about 23 knots to 34 knots (T_C' range of 0.1 to 0.2) because of a limited air supply system for the fans. (Maximum engine revolution speed was about 18,000 rev/min.)

Tests were conducted for angles of attack from about -6^o to 30^o and for sideslip angles from -5^o to 10^o. Tests were conducted for several combinations of wing leading-edge flap segments and deflections, and for combinations of trailing-edge flap segments and deflection angles - the latter for longitudinal and lateral control as well as for improved lift.

A few tests were conducted (at zero sideslip) to determine the effectiveness of the twin rudders, and a few tests were conducted with an aspect-ratio-6, double-slotted-flap canard installed on the nose.

Most of the tests were conducted with the model drive fans (engines) windmilling with a drag correction applied to the force data to account for the excess drag of the windmilling fans and the internal drag of the fan duct ($T_C' = 0$). The drag correction was determined by comparing the windmilling drag to the drag measured with the fans operating at sufficient speed to generate free stream total pressure at the fan nozzle (zero flow-through loss). Tests were conducted for thrust coefficients (T_C') to about 0.20 to determine the effects of thrust on the aerodynamic forces and moments.

Wool tufts were attached to the wing upper surface to aid in the interpretation of the force test results.

Corrections

The test data have been corrected for tunnel airflow angularity, buoyancy, and for strut tares. The sidewash angle has not been accounted for in the data presentation, and this, in general, resulted in an initial offset, from zero, of the lateral and directional data. The sidewash angle was approximately 0.5° ($\beta \approx -0.5^{\circ}$).

Tunnel wall corrections were found to be negligible by both theory (ref. 7) and by experiment wherein a 1/150-scale model of the test model was tested in a 1/15-scale model of the full-scale tunnel.

PRESENTATION OF DATA

Type of data:	Figure Number
Longitudinal:	
Tuft studies	8-14
Effect of Reynolds number	15
Effect of vertical tails	16
Effect of L.E. and T.E. flaps	17
Effect of full-span T.E. flaps	18
Effect of inboard L.E. flaps	19
Effect of outboard L.E. flaps	20
Effect of canard	21
Effect of increasing canard area and incidence	22
Effect of engine thrust	23
Effect of thrust vectoring	24
Control effectiveness of T.E. flaps	25, 26
Effect of sideslip for several Reynolds numbers	27
Effect of vertical tails with sideslip	28
Effect of sideslip for high-lift configuration	29
Effect of sideslip for canard configuration	30

RESULTS AND DISCUSSION

In order to expedite the publication and dissemination of the data of this paper, the data will be presented with only a cursory analysis. The data are briefly analyzed with regard to the achievement of high lift and adequate stability and control for the low to moderate angles of attack that would be encountered during landing and takeoff maneuvers.

Tuft studies.- As an aid in interpreting the force and moment characteristics, flow studies were made of a few select configurations by observing the action of wool tufts attached to the upper surface of the wing. Photographs of the tuft studies are presented in figures 8 through 14. The missing photographs for a few angles of attack was caused by camera malfunction.

Flow over the clean wing ($\delta_f = \delta_n = 0$) at zero sideslip and with tails removed (fig. 8) is seen to develop into a large chordwise vortex on each wing panel that sweeps the flow outboard for angles of attack above $\alpha = 10^\circ$. Installing the vertical tails (fig. 9) constrains the large vortices and causes rough flow outboard of the fins at $\alpha = 14^\circ$. Some stall exists outboard of the tails at $\alpha = 18^\circ$ and the tips are stalled by $\alpha = 28^\circ$. Sideslipping the clean configuration ($\beta = 10^\circ$) (fig. 10), caused the advancing wingtip to stall earlier than the unyawed wing, and the retreating wing did not stall through the full angle-of-

attack range investigated. This characteristic will be related to the dihedral effect exhibited by the configuration in a later section. Deflecting inboard leading- and full-span trailing-edge flaps (high lift configuration) resulted in spanwise flow at the wingtips by $\alpha = 2^{o}$. (See figure 11.) Both wingtips and the mid-trailing-edge flaps were stalled by $\alpha = 22^{o}$. The effect of deflecting the outboard leading-edge flaps for the high-lift configuration is shown in figure 12. Stall of the wingtips was delayed to $\alpha \approx 26^{o}$ and flow over the remainder of the wing was fairly good through $\alpha = 28^{o}$. Sideslipping the high-lift configuration with all leading- and trailing-edge flaps deflected resulted in flow conditions which were markedly different than those exhibited by the clean wing. (Compare figures 10 and 13.) The retreating wing of the high-lift configuration was subject to some separated flow at $\alpha = 12^{o}$ and the retreating wingtip including the outboard flap was stalled at $\alpha = 16^{o}$. Installing a small canard on the model had no apparent effect on the wing flap pattern. (See figure 14.)

Longitudinal Characteristics

Basic configuration.- At the outset of the program tests were conducted on the clean configuration for a range of wind-tunnel speeds to determine whether there were appreciable effects of Reynolds number on the data. The effect of Reynolds number on the longitudinal characteristics of the clean wing configuration with vertical tails is shown in figure 15. There was no appreciable Reynolds number effect on the data, therefore most of the tests were conducted for a Reynolds number of 8.92×10^{6}.

Perhaps the most singificant point to be noted concerning the data presented in figure 15 is that the clean configuration exhibited static longitudinal instability (pitchup) for angles of attack greater than about $\alpha = 3^{o}$. The data also show that the variation of lift with angle of attack indicated an increase in lift-curve slope at moderate angles of attack due to vortex lift, and the lift-curve did not exhibit any

abrupt changes. A maximum value of lift-drag ratio of about 6 occurred near $\alpha = 3^{\circ}$.

Effect of vertical tails.- The effect of the vertical tails on the longitudinal characteristics of the clean wing configuration is shown in figure 16. These data indicate that a lift loss occurred at moderate to high angles of attack when the vertical tails were added to the model. The tuft studies of figures 8 and 9 seem to indicate the cause for the reduced lift. At moderate and high angles of attack, the flow outboard of the tails showed a large area of rough and separated flow. This flow condition would seem to indicate that the reduction in lift noted with the tails on was related to the constraining effect of the tails on the spanwise vortex flow. In general, the longitudinal stability characteristics, particularly the pitchup, were not affected by the tails.

Effect of leading- and trailing-edge flaps.- The effect of deflecting the trailing-edge flaps and outboard leading-edge flaps is shown in figure 17. Lift is seen to be increased significantly, as well as L/D; however, the configuration still exhibited the pitchup shown for the clean configuration in figure 15. Deflecting the inboard leading-edge flaps (fig. 18) produced a very significant effect in that the pitchup was delayed to about $\alpha = 18^{\circ}$ with only a very small loss of lift caused by the inboard leading-edge flap deflection at low angles of attack. It should be noted that deflection of the trailing-edge flaps in combination with the leading-edge flaps increased the untrimmed lift coefficient, at the estimated tail scrape angle of attack of 9.5°, from about 0.35 for the clean wing to about 0.50 for 30° trailing-edge flap deflection (see figs. 15 and 18). The effect of deflecting various leading-edge flaps for a fixed trailing edge is shown in figure 19. It should be noted that the inboard trailing-edge flap was only deflected 20°, which accounts for the apparently lower lift values than the data shown in figure 18. The most significant point shown by the data of figure 19 is that the inboard leading-edge flap segments 5, 6, and 7 must be deflected at least 60° to alleviate the pitchup at moderate and high angles of attack.

To determine the effect of outboard leading-edge flap deflection, the trailing-edge and inboard leading-edge flaps were deflected with and without outboard leading-edge flaps (segments 1, 2, and 3) with the results shown in figure 20. Deflecting the outboard leading-edge flaps reduced lift and, to a small extent, the longitudinal stability. For the relatively low wingtip flap loading (indicated by the tuft studies and by the very low control effectiveness of the outboard flap to be discussed later) the outboard leading-edge flaps were probably deflected too highly.

Effect of canard.- The results of tests wherein canards having areas of 0.02S and 0.025S were evaluated to determine the effectiveness of such surfaces to reduce longitudinal trim requirements are presented in figures 21 and 22. The data show that the canards provided substantial positive (favorable) increments of C_m over the angle-of-attack range. The canards produced no noticeable effect on lift, and a degradation in L/D.

Effect of thrust vectoring.- The effect of engine thrust with no thrust vectoring on the lift and pitch characteristics with the 0.02S canard deflected is shown to be negligible in figure 23. The effect of thrust vectoring is shown in figure 24. Directly comparable data were not obtained during the tests; i.e., canard on, $\delta_f = 20^o$ and 30^o with $T_c' = 0.10$ without thrust vectoring/ however, since thrust was shown in figure 23 to have negligible effects on lift and pitch, it may be assumed that the effects shown in figure 24 are mainly attributable to thrust vectoring. The effect of deflecting the engine nozzle 30^o is shown in figure 24 to increase lift slightly, in the high angle-of-attack range, and to slightly increase the longitudinal stability. The rather minor effects of thrust vectoring for the present configuration can be explained by a number of reasons. The nozzle deflection technique of the subject tests (only deflecting the upper half of the nozzle) was very poor from the standpoint of efficiently turning the exhaust flow. Also, the nozzle area was larger than required, which resulted in relatively low exhaust velocities and probably poor turning of the exhaust flow. It is expected

that a better nozzle deflection arrangement would provide substantial gains in lift with nozzle deflection.

Longitudinal control effectiveness.- The longitudinal control effectiveness of the trailing-edge flaps is shown in figures 25 and 26. All combinations of flaps were quite effective in providing longitudinal trim (with attendant reduction in lift) with the exception of the outboard flaps alone (fig. 25(d)). These outboard flaps were relatively ineffective as might be expected based on the tuft studies of figure 11 which show the flow over the outboard flap to be fairly poor. As expected, the data of figure 26 show that the presence of the canard had no appreciable effect on the longitudinal control effectiveness.

Effects of sideslip.- The effects of sideslip on the longitudinal characteristics of the model are shown in figures 27 to 29. The data show that sideslip tended to make the pitchup characteristics of both the clean and high-lift configurations more severe.

Lateral-Directional Stability Characteristics

The lateral-directional stability characteristics of the model are presented in figures 31 to 38. An analysis of lateral-directional data obtained for the clean configuration over the range of Reynolds number previously discussed for the longitudinal data indicated that the effects of Reynolds number were also negligible in the lateral-directional tests. As a result, most of the tests were conducted at a value of Reynolds number of 8.92×10^6 (the same value used for the longitudinal tests).

The variations of side force, rolling-moment, and yawing-moment coefficients with sideslip for the clean configuration, the high-lift configuration, and the high-lift configuration with canard are presented in figures 31, 32, and 33. The data show that the variation of C_ℓ with β was generally linear for angles of attack up to about $\alpha = 20^\circ$; whereas the variation of C_n with β became nonlinear near $\alpha = 8^\circ$ with increasing nonlinearity at higher angles of attack. In addition, the data

show large yawing and rolling moment asymmetries for angles of attack greater than $\alpha = 20^{\circ}$. These asymmetric moments, which are believed to be caused by asymmetric vortex shedding off the highly swept nose, would have a significant effect on the lateral-directional control of the configuration at high angles of attack, as will be discussed in the next section. As shown in figure 34, the magnitudes and directions of the C_n and C_ℓ asymmetries varied over the range of Reynolds number tested.

The lateral-directional stability characteristics of the model are summarized in figures 35 to 38 in terms of the side-force derivative C_{Y_β}, the directional stability derivative C_{n_β}, and the effective dihedral derivative C_{ℓ_β}. The magnitudes of the derivatives were determined from values of the respective coefficients at values of β of $\pm 5^{\circ}$.

The data of figure 35 show that the clean configuration was directionally stable at low angles of attack, and the level of directional stability increased markedly as angle of attack was increased such that the configuration was extremely stable at high angles of attack. It should be noted that the marked increase in C_{n_β} at high angles of attack was produced in conjunction with a large positive increment of C_{Y_β}. An analysis of the relative signs of the two derivatives indicates that the aerodynamic stabilizing moment was produced forward of the center-of-gravity position. Past investigations have shown that the foregoing characteristics may be related to the aerodynamic effects of a pair of strong vortices shed off the highly swept, flat nose of the model (see refs. 8 through 12).

The data of figure 35 also show that the magnitude of C_{ℓ_β} increased with increasing α up to $\alpha = 12^{\circ}$. Above this angle, the value of the derivative decreased rapidly. This decrease in C_{ℓ_β} is related to the advancing wing panel stall discussed in the section on flow visualization.

As previously noted, variations in Reynolds number had no significant effect on the lateral-directional characteristics.

The effect of the vertical tails on the lateral-directional stability derivatives of the clean configuration is presented in figure 36. The data show that the tail contribution to C_{n_β} was essentially constant over the angle-of-attack range, and that the tails had a significant effect on the magnitude of C_{ℓ_β}.

Shown in figure 37 is a comparison of the lateral-directional derivatives from the clean and high-lift configurations; these data show essentially similar trends although the high-lift configuration did exhibit less stable values of C_{n_β} at extremely high angles of attack.

Presented in figure 38 is the effect of the canard on the derivatives for the high-lift configuration. The data show that although the canard caused a large reduction in C_{n_β} at angles of attack above $\alpha = 4^\circ$, the configuration still had a high level of directional stability at all angles of attack.

Lateral-Directional Control Characteristics

In the present investigation, the outboard trailing-edge flaps (trailing-edge segment 3) were evaluated as a possible source of roll control. Presented in figure 39 are the variations of C_Y, C_n, and C_ℓ with deflections of the left-hand outboard flap. The data show that deflections of $\pm 30^\circ$ of the outboard surface produced an increment of C_ℓ of only about 0.01. This magnitude of roll control effectiveness is generally similar to values obtained from the deflection of outboard surfaces on other highly swept configurations previously tested (see refs. 13 and 14). An evaluation of roll control requirements for satisfactory handling qualities indicates that this level of control effectiveness may be insufficient for some operational conditions. For example, in terms of the roll control required to trim the rolling moments resulting from sideslip, an examination of the effective dihedral characteristics of the present model (see fig. 38) shows that a 10° sideslip angle would require a value of C_ℓ of 0.03 for roll trim near an α of 10°. On this

basis, it appears that additional means of roll control would be required for satisfactory operation in the landing and takeoff modes where cross-winds could produce sideslip angles of this magnitude. It is possible that differential deflection of full-span trailing-edge flaps or various combinations of the trailing-edge flaps could produce adequate roll control; however, no data of this type were obtained for the present model.

Presented in figure 40 are the variations of C_Y, C_n, and C_ℓ with deflections of the twin rudders. The data show that the rudder effectiveness decreases with increasing angle of attack. At low angles of attack, rudder deflections of $\pm 20^\circ$ produced a value of C_n of about 0.03. This control effectiveness is generally similar to that shown in references 13 and 14 for configurations having geometric characteristics generally similar to those of the present model. An examination of the directional stability data for the present model (fig. 38) indicates that a value of C_n of 0.03 is adequate for trimming the yawing moments resulting from about 15° of sideslip. It should also be noted that at extremely high angles of attack the asymmetric yawing moments were much larger than the yaw control provided by the rudders.

CONCLUDING REMARKS

Force tests of a 1/10-scale advanced blended-arrow supersonic transport model in the Langley full-scale tunnel show the following results:

1. The clean configuration exhibited static longitudinal instability (pitchup) at an angle of attack of about 3°; however, deflecting inboard leading-edge flaps delayed the pitchup to an angle of attack of about 18°.

2. Deflecting full-span trailing-edge flaps and leading-edge flaps increased the lift coefficient from a value of about 0.35 for the clean configuration to a value of about 0.50 (untrimmed) at an angle of attack of 9.5° (estimated tail scrape angle).

3. The model exhibited satisfactory lateral-directional characteristics for angles of attack up to about $\alpha = 16^{o}$. At higher angles of attack the directional stability increased markedly; however, the effective dihedral decreased to nearly zero near $\alpha = 24^{o}$.

4. The deflection of leading- and trailing-edge flaps and the addition of a canard for longitudinal trim reduced the level of directional stability at high angles of attack.

5. Outboard trailing-edge flaps were relatively ineffective for roll control; particularly for roll trim during takeoff and landing in a crosswind.

REFERENCES

1. Carlson, Harry W.; Barger, Raymond L.; and Mack, Robert J.: Application of Sonic-Boom Minimization Concepts in Supersonic Transport Design. NASA TN D-7218, June 1973.

2. Corson, Blake W., Jr.; Capone, Francis J.; and Putman, Lawrence E.: Lift Induced on a Sweptwing by a Two-Dimensional Partial-Span Deflected Jet at Mach Numbers from 0.20 to 1.30. NASA TM X-2309, 1971.

3. Capone, Francis J.: Exploratory Investigation of Lift Induced on a Sweptwing by a Two-Dimensional, Partial Span, Deflected Jet at Mach Numbers from 0.20 to 1.30. NASA TM X-2529, 1971.

4. Robins, Warner A.; Morris, Odell A.; and Harris, Roy V., Jr.: Recent Research Results in the Aerodynamics of Supersonic Vehicles. Journal of Aircraft, vol. 3, No. 6, November-December 1966.

5. Baals, Donald D.; Robins, Warner A.; and Harris, Roy V., Jr.: Aerodynamic Design Integration of Supersonic Aircraft. Journal of Aircraft, vol. 7, No. 5, September-October 1970. (pp. 385-394.)

6. Mechtly, E. A.: The International System of Units - Physical Constants and Conversion Factors (Second Revision). NASA SP-7012, 1973.

7. Heyson, Harry H.: Use of Superposition in Digital Computers to Obtain Wind-Tunnel Interference Factors for Arbitrary Configurations, With Particular Reference to V/STOL Models. NASA TR R-302, 1969.

8. Grafton, Sue B.; Chambers, Joseph R.; and Coe, Paul L., Jr.: Wind-Tunnel Free-Flight Investigation of a Model of a Spin-Resistant Fighter Configuration. NASA TN D-7716, 1974.

9. Johnson, Joseph L.: Damping in Yaw and Static Directional Stability of a Canard Airplane Model and of Several Models Having Fuselages of Relatively Flat Cross Section. NACA RM L50H30a, 1950.

10. Paulson, John W.; and Johnson, Joseph L., Jr.: Free-Flight-Tunnel Investigation of the Low-Speed Stability and Control Characteristics of a Model Having a Fuselage of Relatively Flat Cross Section. NACA RM L52L22, 1953.

11. Bates, William R.: Static Stability of Fuselage Having a Relatively Flat Cross Section. NACA TN 3429, 1955. (Supersedes NACA RM L9I06a.)

12. Spencer, Bernard, Jr.; and Phillips, W. Pelham: Effects of Cross-Section Shape on the Low-Speed Aerodynamic Characteristics of a Low-Wave-Drag Hypersonic Body. NASA TN D-1963, 1963.

13. Henderson, William P.: Low-Speed Aerodynamic Characteristics of a Supersonic Transport Model With a Highly Swept, Twisted and Cambered, Fixed Wing. NASA TM X-1249, July 1966.

14. Ray, Edward J.; and Henderson, William P.: Low-Speed Aerodynamic Characteristics of a Highly Swept Supersonic Transport Model With Auxiliary Canard and High-Lift Devices. NASA TM X-1694, November 1968.

National Aeronautics and Space Administration
Langley Research Center, Hampton, Va.
March 11, 1975

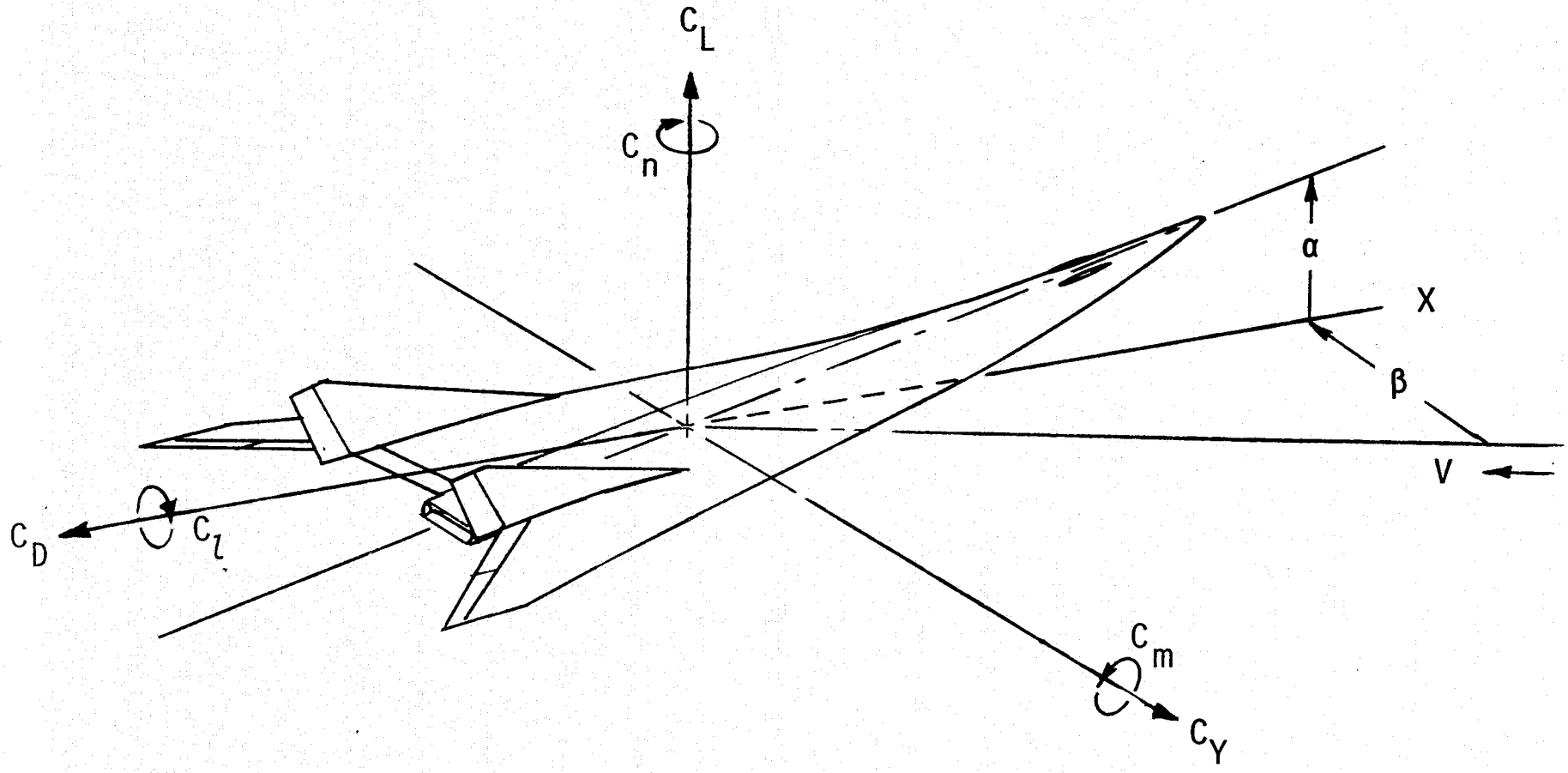

Figure 1. - System of stability axes and positive sense of angles, forces, and moments.

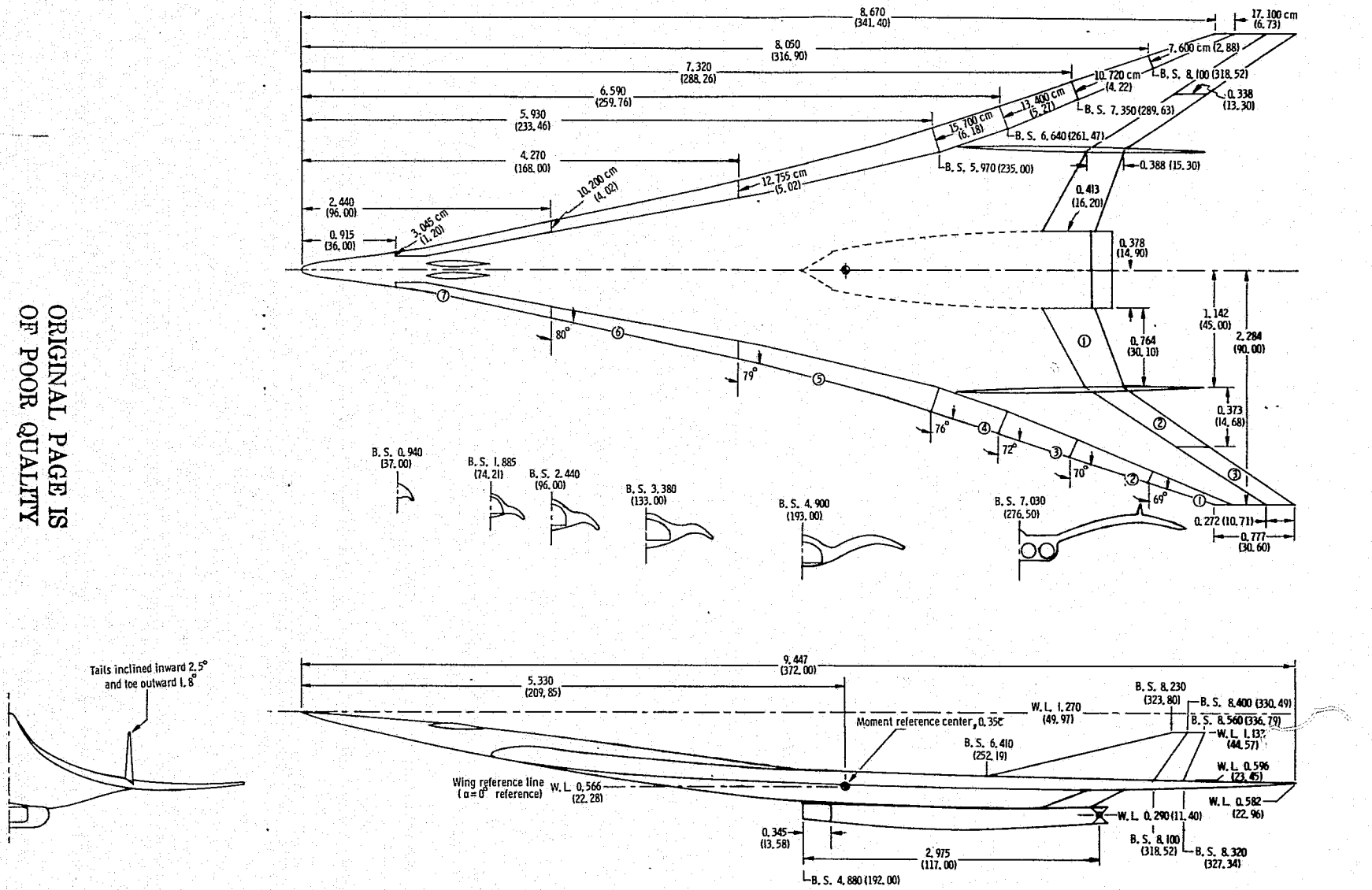

Figure 2.- Geometric characteristics of 1/10-scale arrow-wing model. All dimensions in meters unless noted as cm. (Inches noted in parenthesis.)

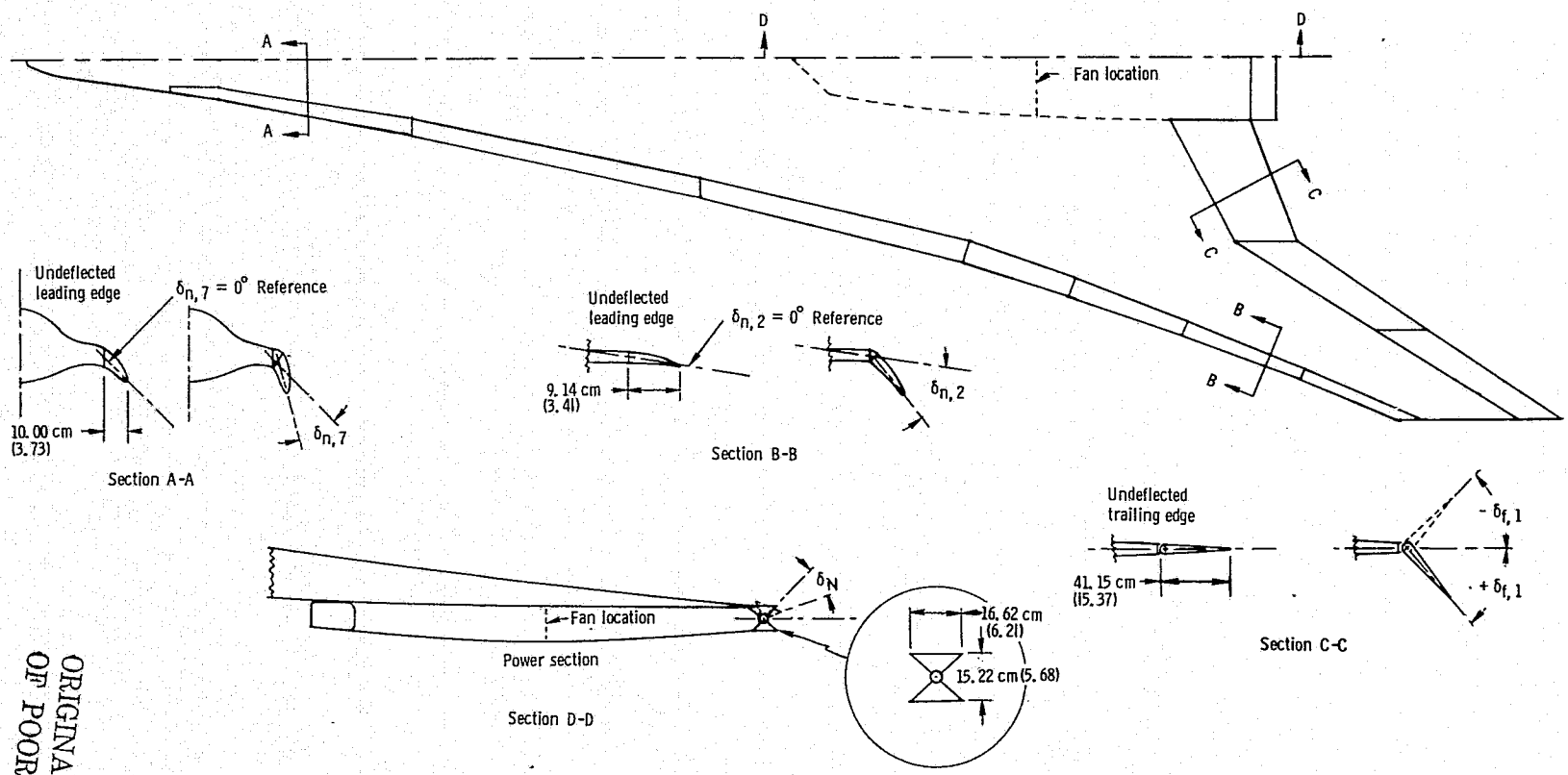

Figure 3.- Schematic arrangements of leading- and trailing-edge flaps and engine exhaust nozzle. (Components not to scale.) Dimensions in cm and (inches).

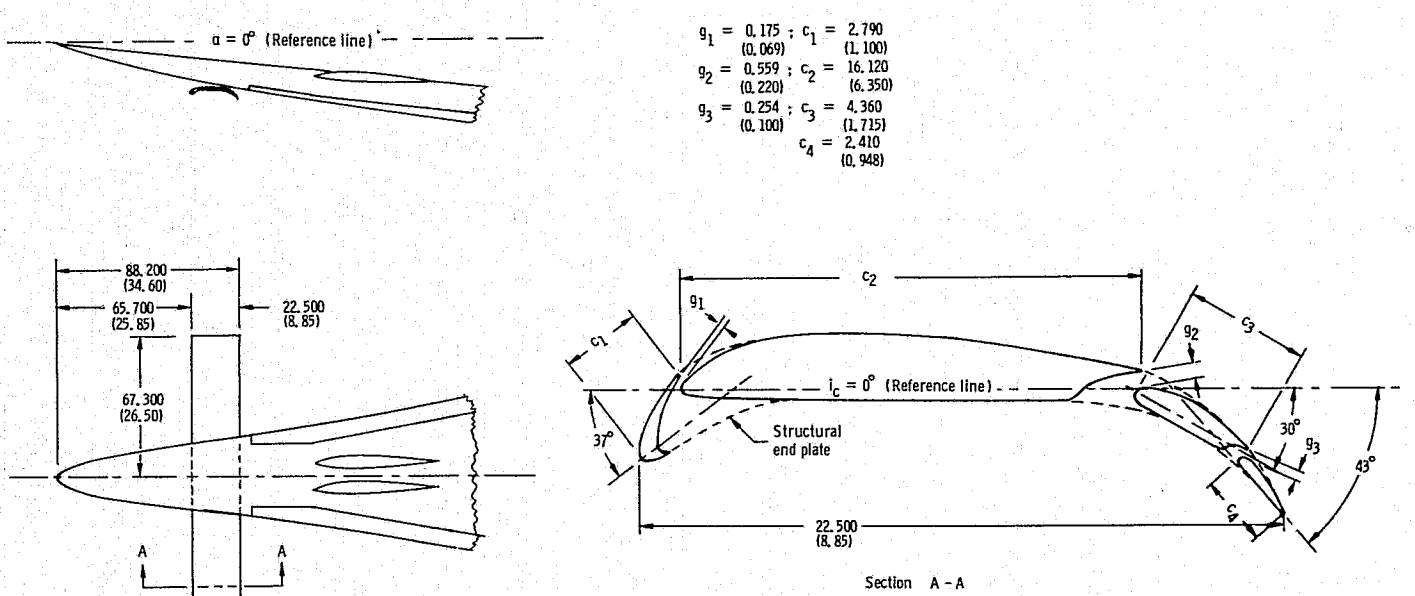

Figure 4.- Geometric characteristics and location of canard. Dimensions in cm. and (inches).

NASA
L-73-7547

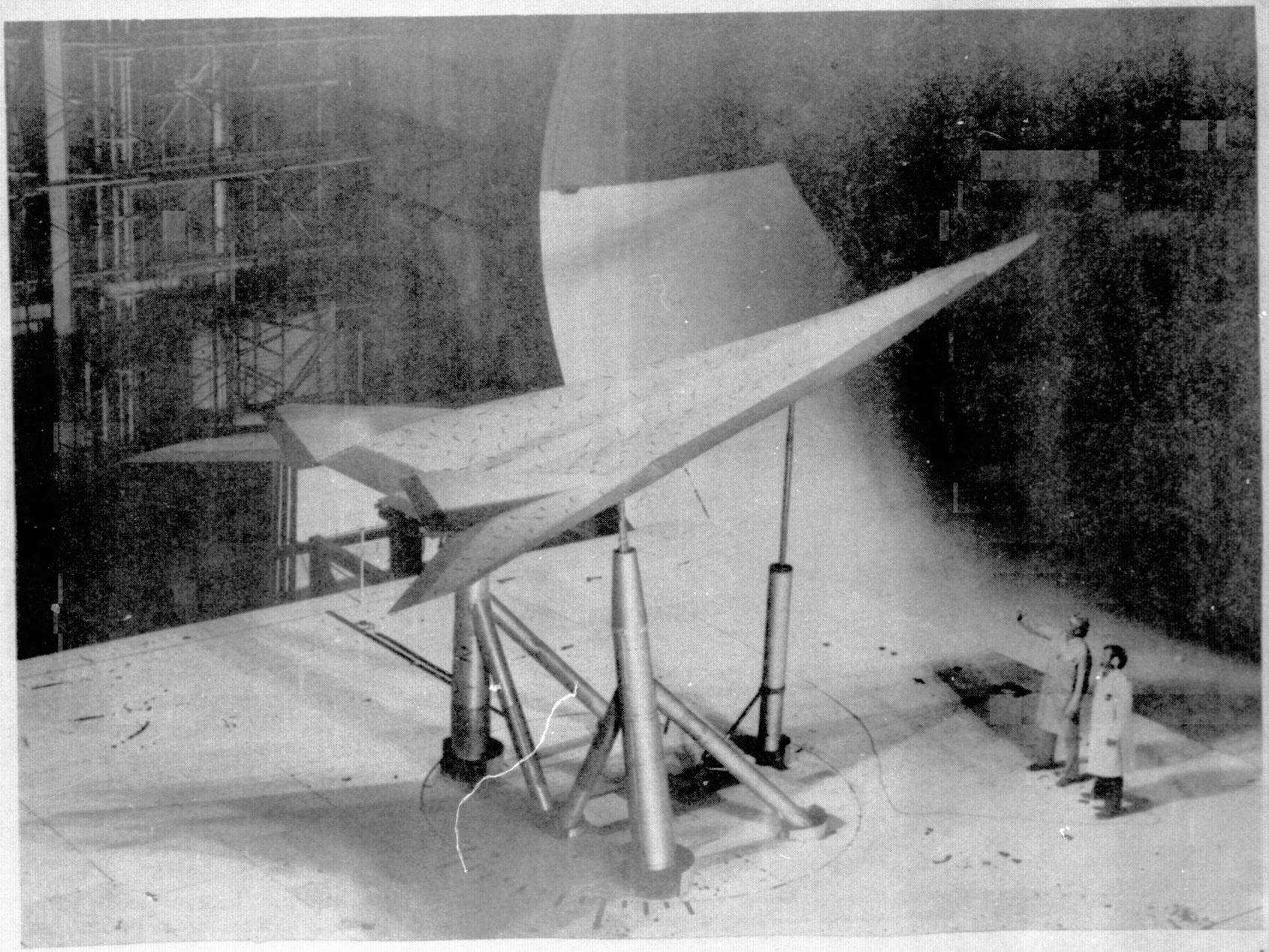

Figure 5. - Three-quarter rear view of 1/10-scale model mounted for tests in the Langley full-scale tunnel.

NASA
L-73-8616

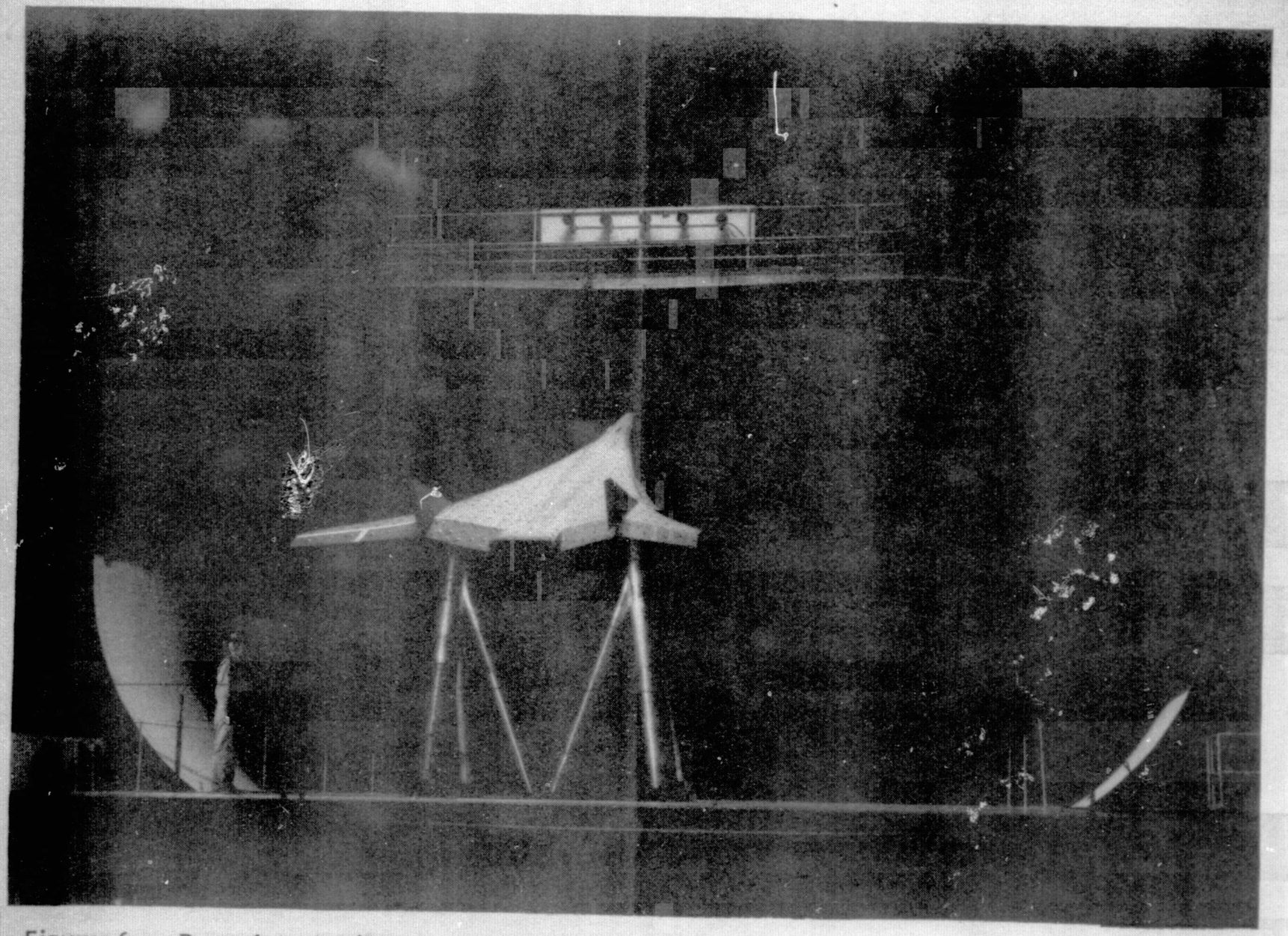

Figure 6. - Rear view of 1/10-scale model mounted for tests in the Langley full-scale tunnel.

NASA
L-73-8617

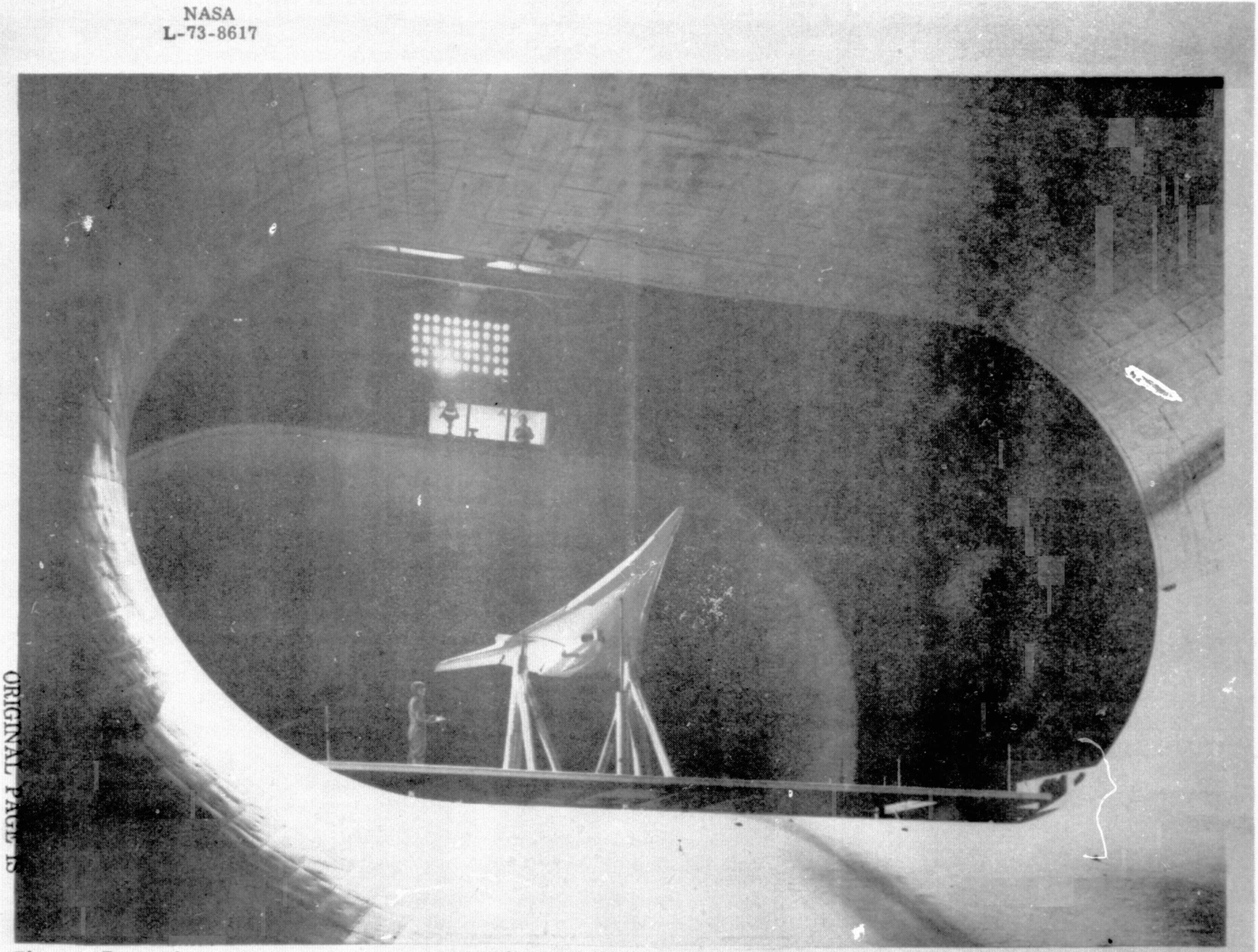

Figure 7.- Three-quarter front view of 1/10-scale model mounted for tests in the Langley full-scale tunnel.

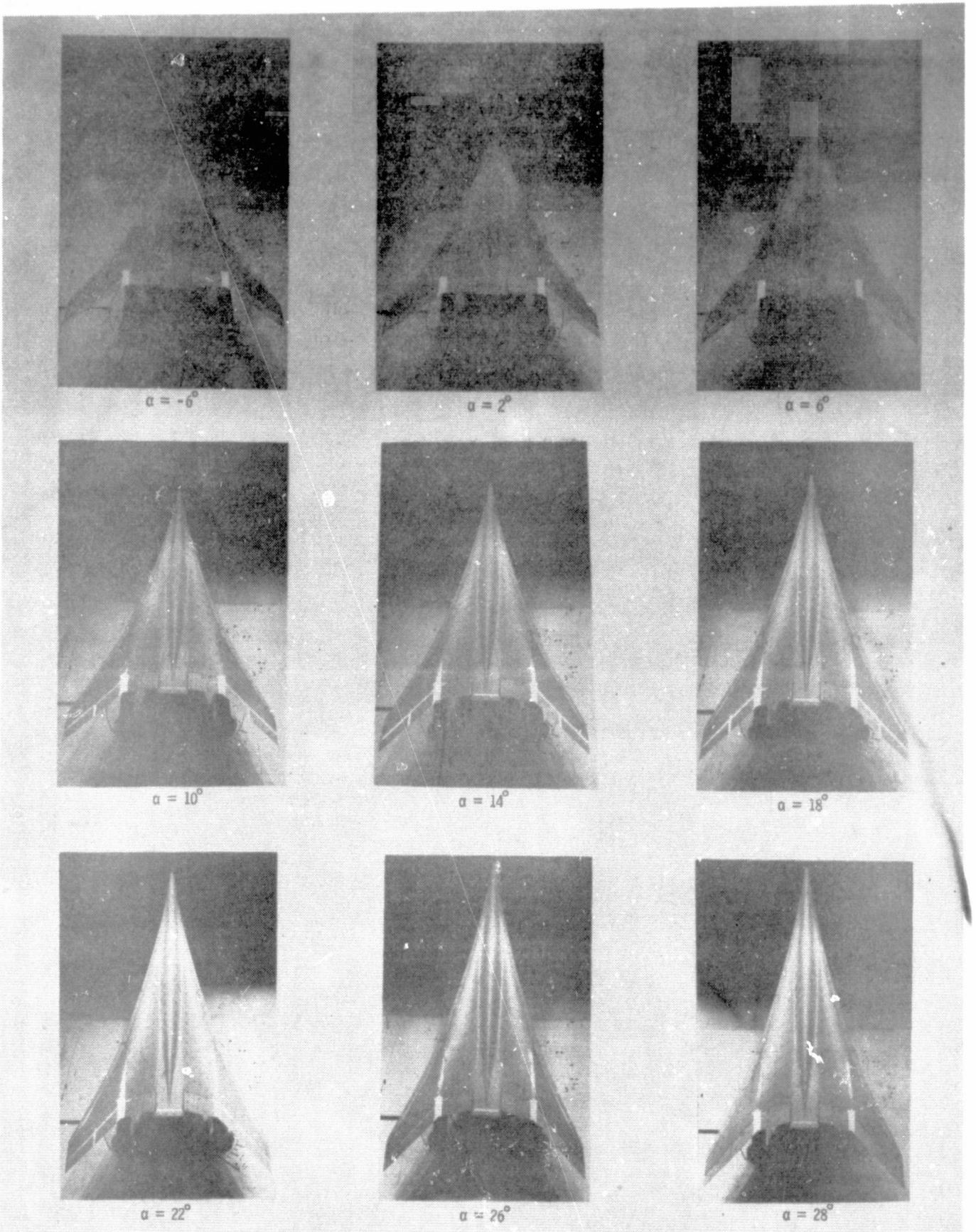

Figure 8.- Tuft studies of clean wing at $\beta = 0°$. $\delta_f = 0$, $\delta_n = 0$, $T_c' = 0$.
Vertical tails off.

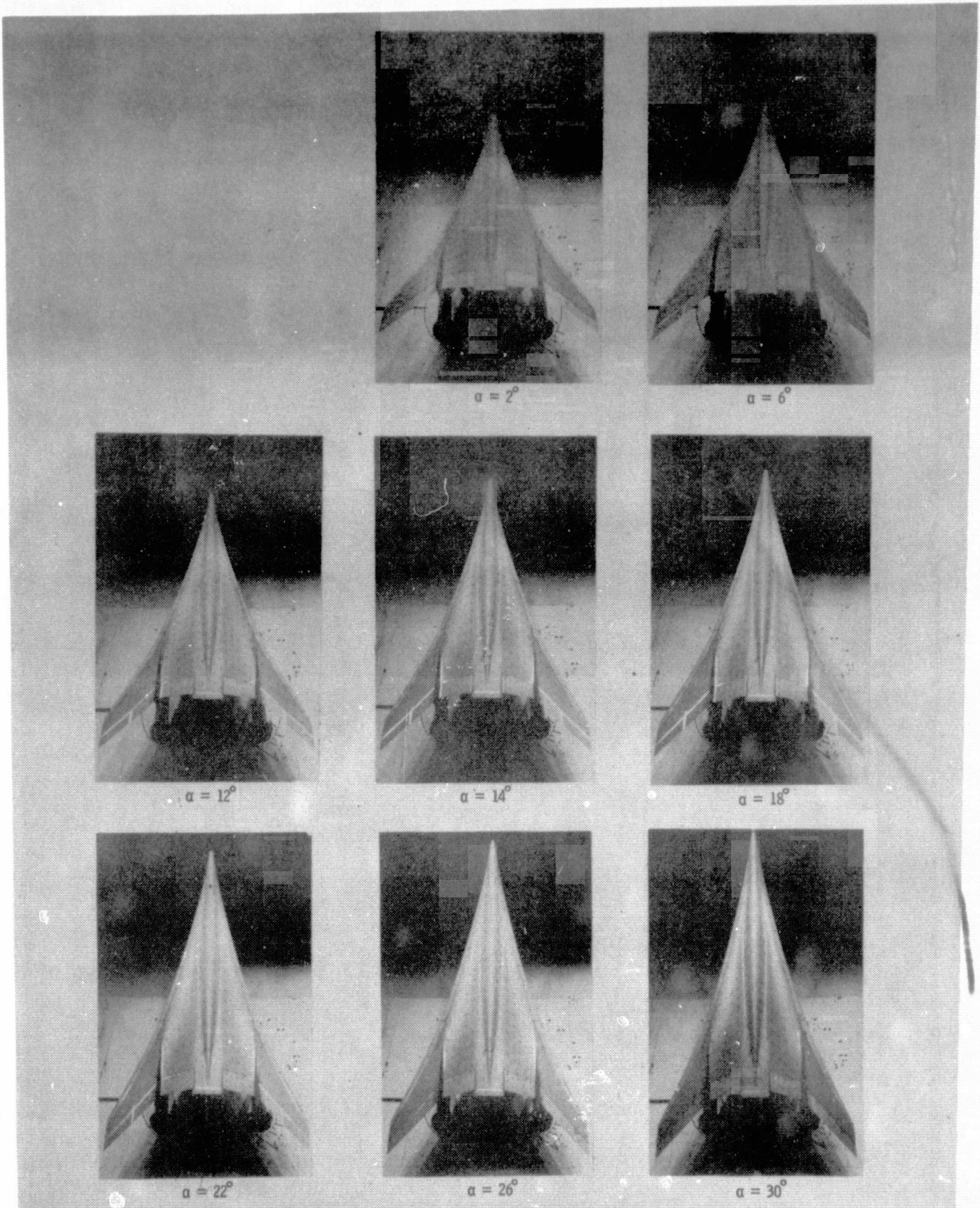

Figure 9.- Tuft studies of clean wing at $\beta = 0°$, $\delta_f = 0°$, $\delta_n = 0°$, $T_c' = 0$. Vertical tails on.

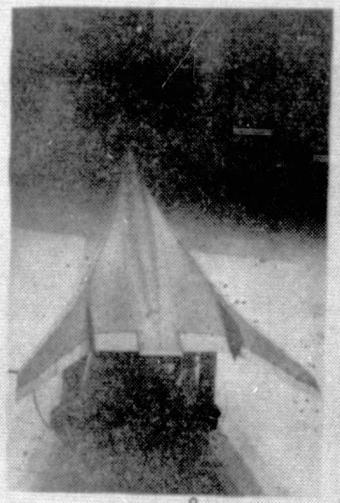

$\alpha = -6^\circ$

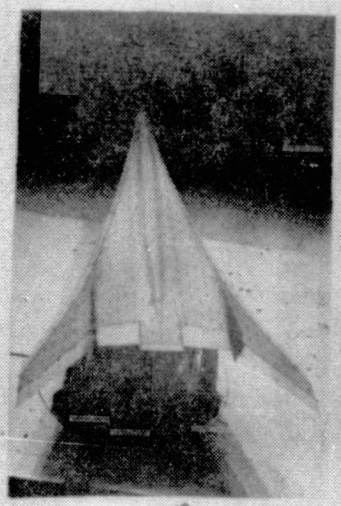

$\alpha = 2^\circ$

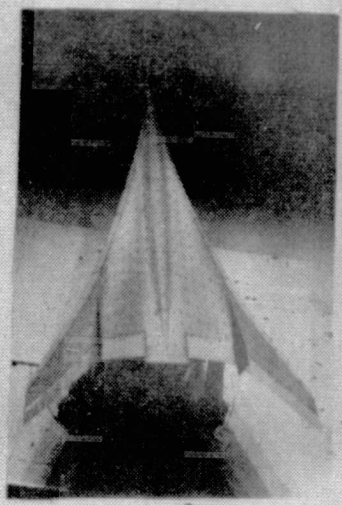

$\alpha = 6^\circ$

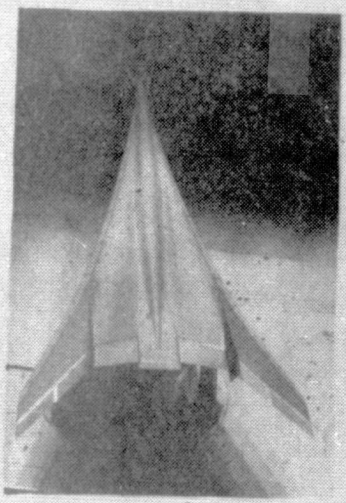

$\alpha = 10^\circ$

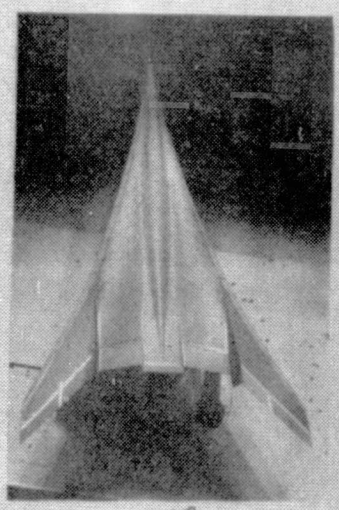

$\alpha = 14^\circ$

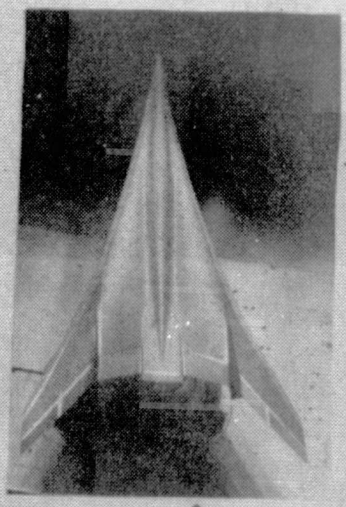

$\alpha = 18^\circ$

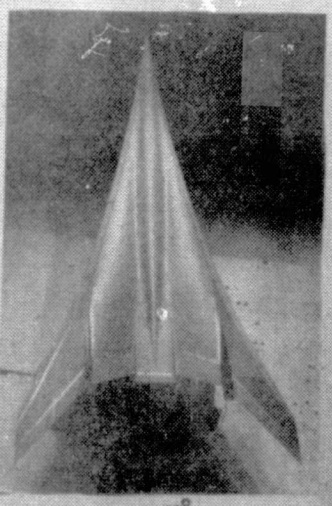

$\alpha = 22^\circ$

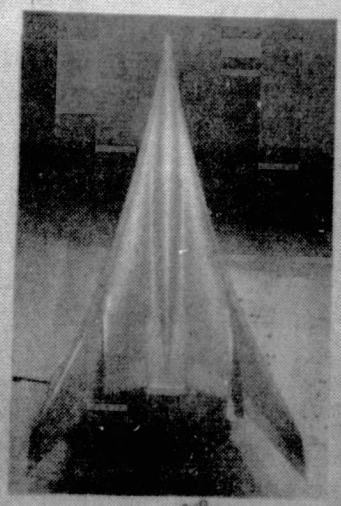

$\alpha = 26^\circ$

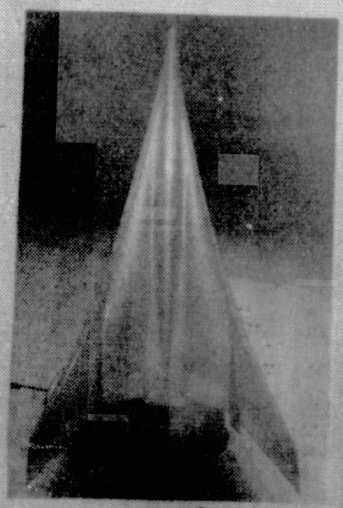

$\alpha = 30^\circ$

Figure 10.- Tuft studies of clean wing at $\beta = 10^\circ$. $\delta_f = 0^\circ$, $\delta_n = 0^\circ$, $T_c' = 0$. Vertical tails on.

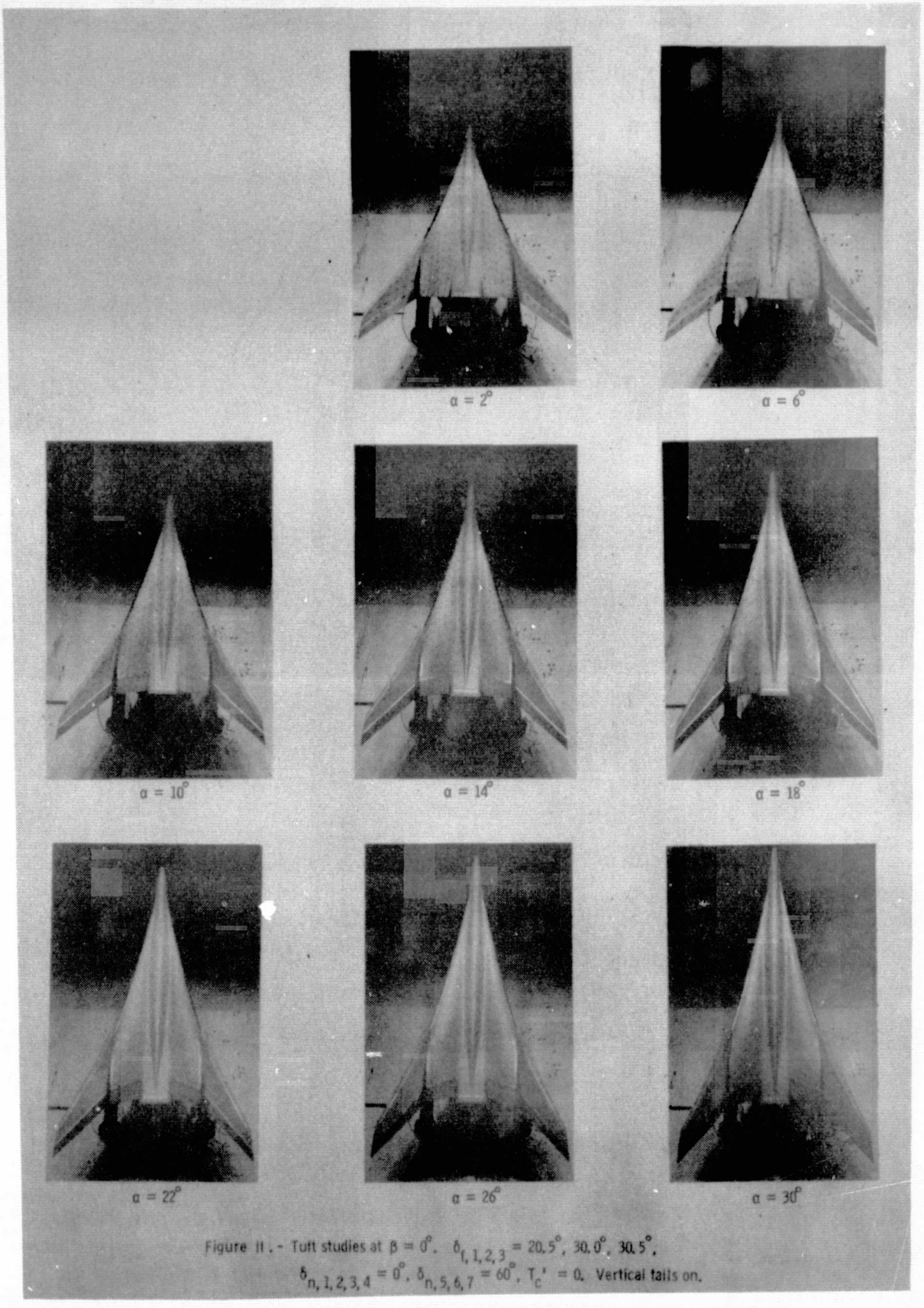

Figure 11.- Tuft studies at $\beta = 0°$. $\delta_{f,1,2,3} = 20.5°, 30.0°, 30.5°$, $\delta_{n,1,2,3,4} = 0°$, $\delta_{n,5,6,7} = 60°$, $T_c' = 0$. Vertical tails on.

$\alpha = -6^\circ$

$\alpha = 2^\circ$

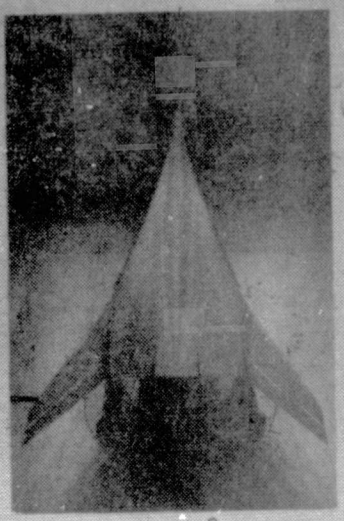

$\alpha = 6^\circ$

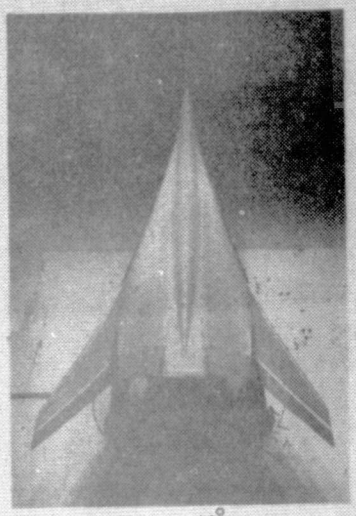

$\alpha = 12^\circ$

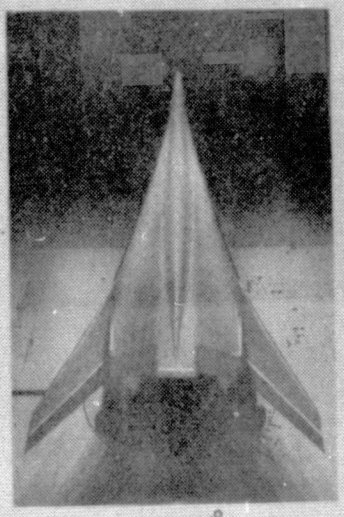

$\alpha = 14^\circ$

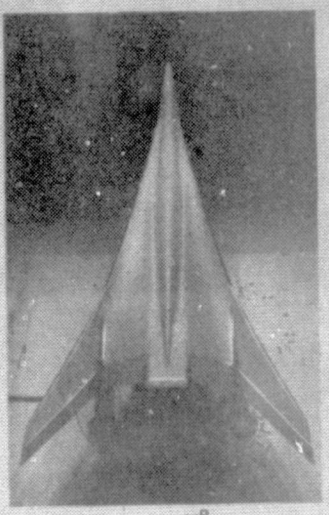

$\alpha = 18^\circ$

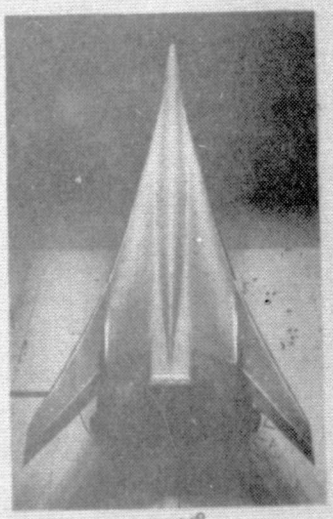

$\alpha = 22^\circ$

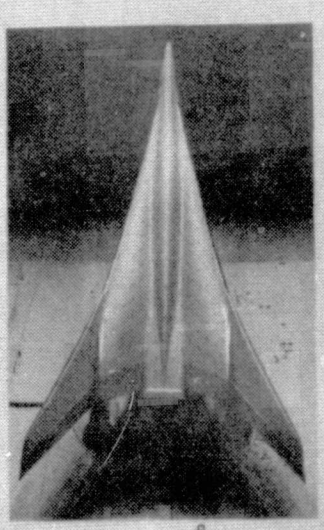

$\alpha = 26^\circ$

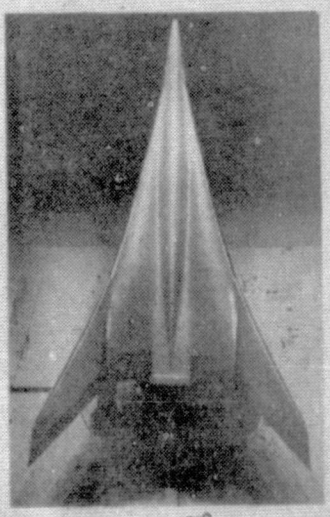

$\alpha = 28^\circ$

Figure 12.- Tuft studies at $\beta = 0^\circ$. $\delta_{f,1,2,3} = 20.5^\circ, 30.0^\circ, 30.5^\circ$, $\delta_{n,1,2,3,4} = 45^\circ$, $\delta_{n,5,6,7} = 60^\circ$, $T_c' = 0$. Vertical tails on.

$\alpha = 12^\circ$

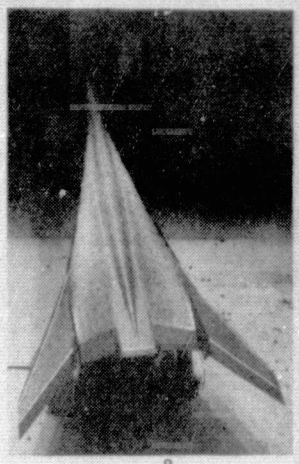

$\alpha = 14^\circ$

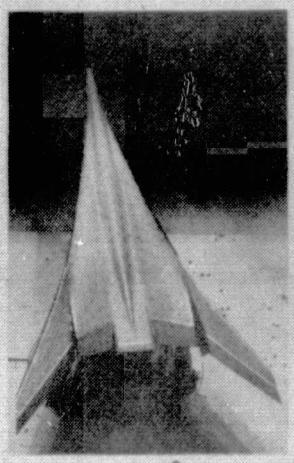

$\alpha = 16^\circ$

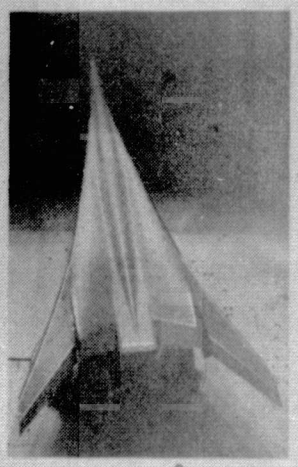

$\alpha = 18^\circ$

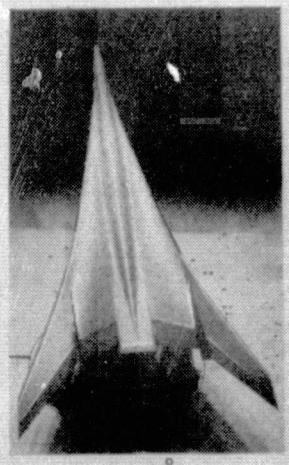

$\alpha = 22^\circ$

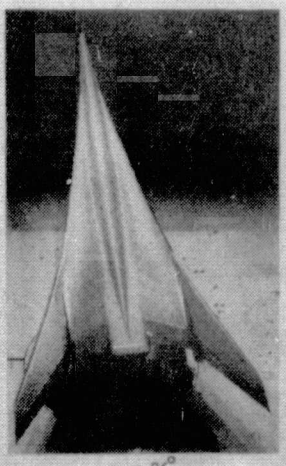

$\alpha = 26^\circ$

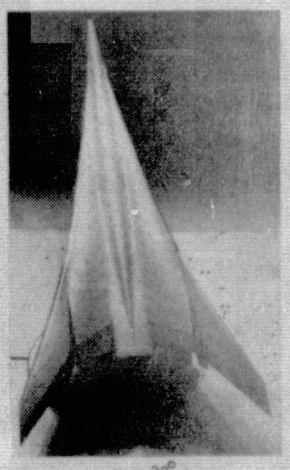

$\alpha = 30^\circ$

Figure 13.- Tuft studies at $\beta = 10^\circ$. $\delta_{f,1,2,3} = 20.5^\circ, 30.0^\circ, 30.5^\circ$, $\delta_{n,1,2,3,4} = 45^\circ$, $\delta_{n,5,6,7} = 60^\circ$. $T_c' = 0$. Vertical tails on.

$\alpha = -6^\circ$

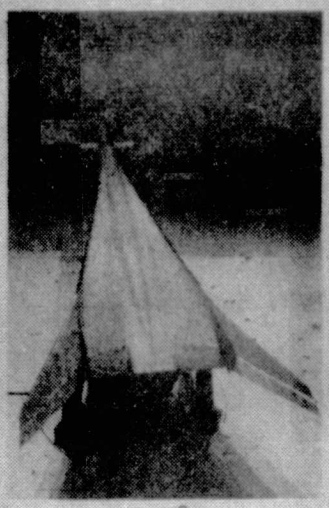

$\alpha = 2^\circ$

$\alpha = 6^\circ$

$\alpha = 10^\circ$

$\alpha = 14^\circ$

$\alpha = 18^\circ$

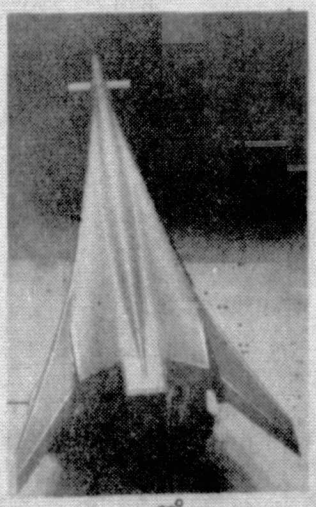

$\alpha = 22^\circ$

$\alpha = 26^\circ$

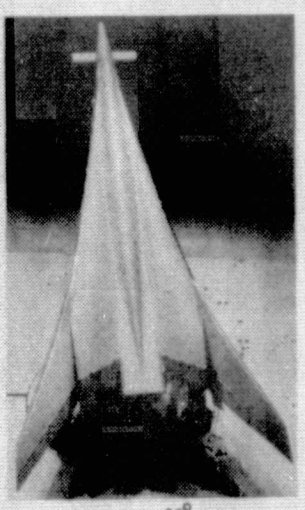

$\alpha = 30^\circ$

Figure 14.- Tuft studies with canard on. $\beta = 10^\circ$. $\delta_{f,1,2,3} = 30.0^\circ, 30.0^\circ, 30.5^\circ$, $\delta_{n,1,2,3,4} = 45^\circ$, $\delta_{n,5,6,7} = 60^\circ$, $T_c' = 0$. Vertical tails on.

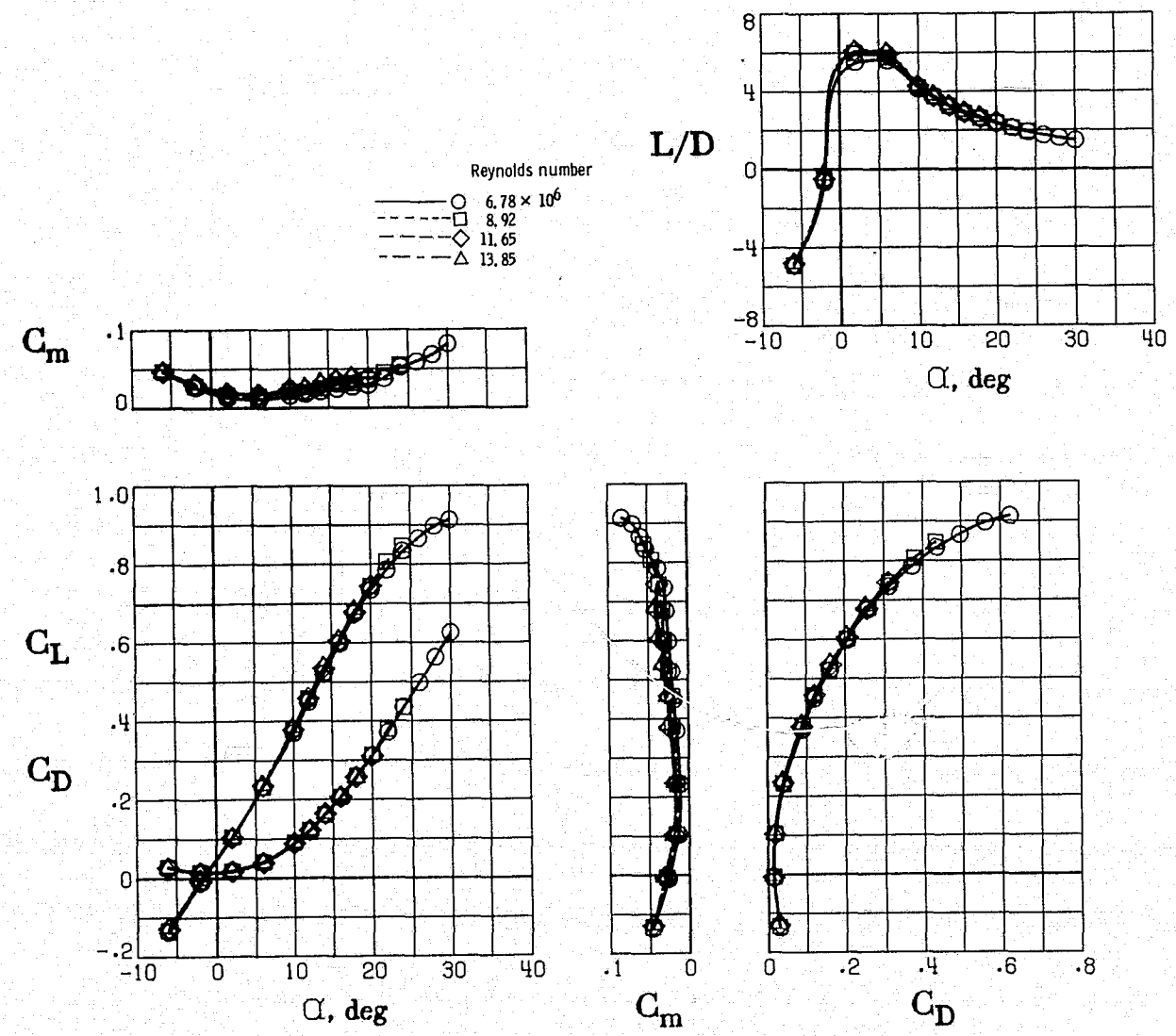

Figure 15.- Effect of Reynolds number. Vertical tails on. $\delta_f = 0°$, $\delta_n = 0°$, $\beta = 0°$, $T_c' = 0$.

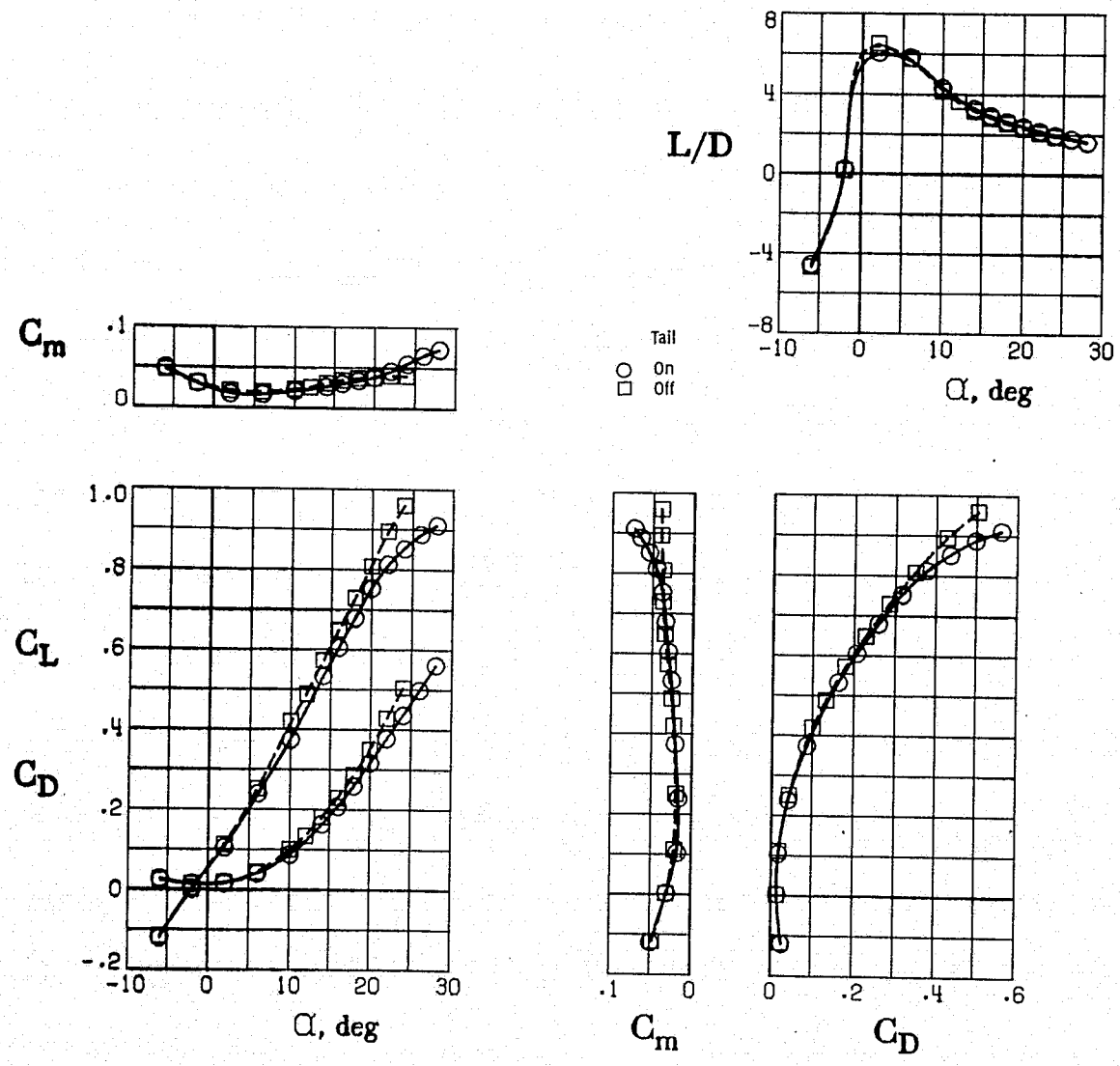

Figure 16. - Effect of vertical tails, $\delta_f = 0°$, $\delta_n = 0°$, $\beta = 0°$, $T_c' = 0$.

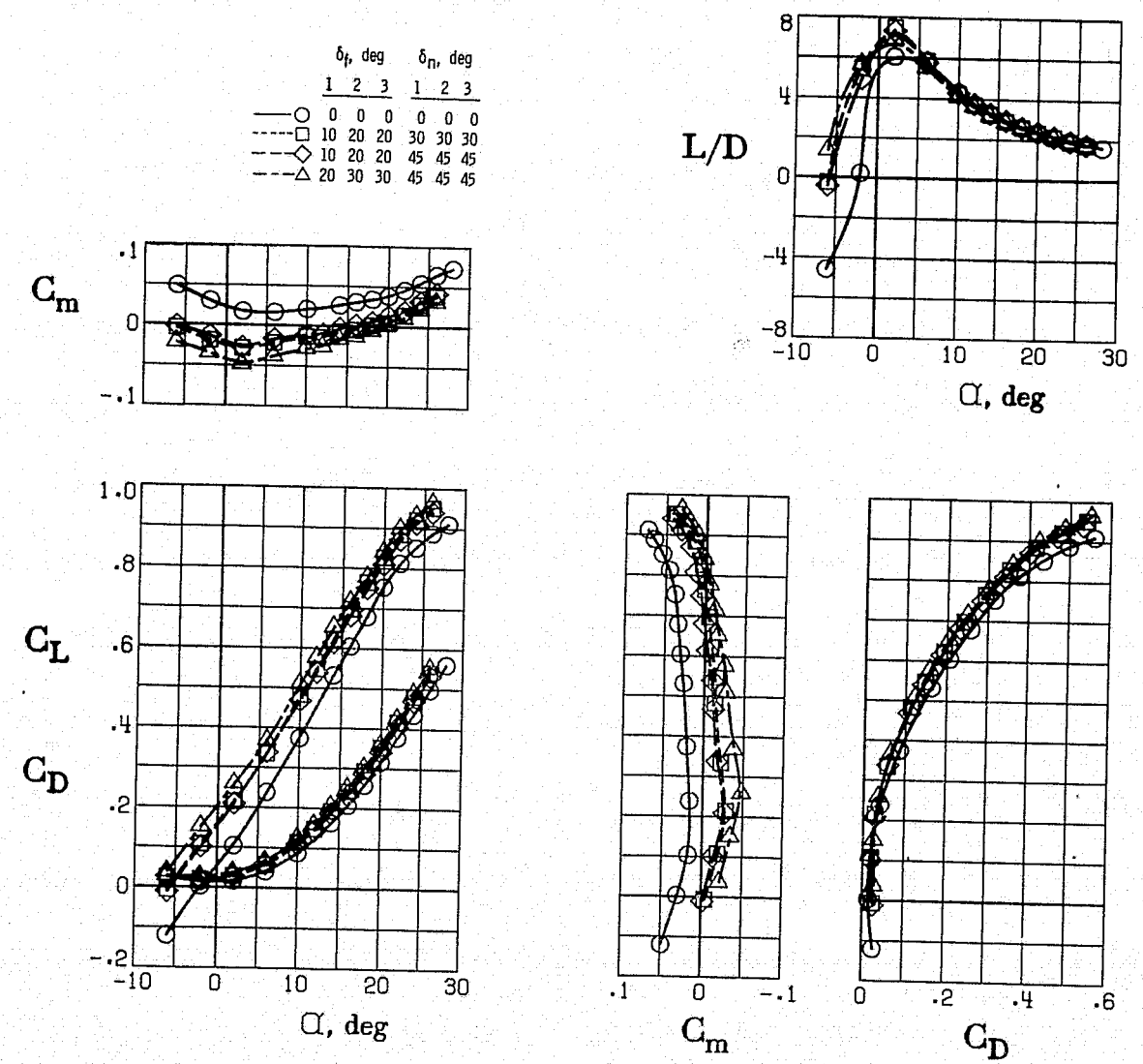

Figure 17. - Effect of wing L.E. flap and T.E. flap deflection. $\delta_{n,4,5,6,7} = 0°$, $\beta = 0°$, $T_c' = 0$.

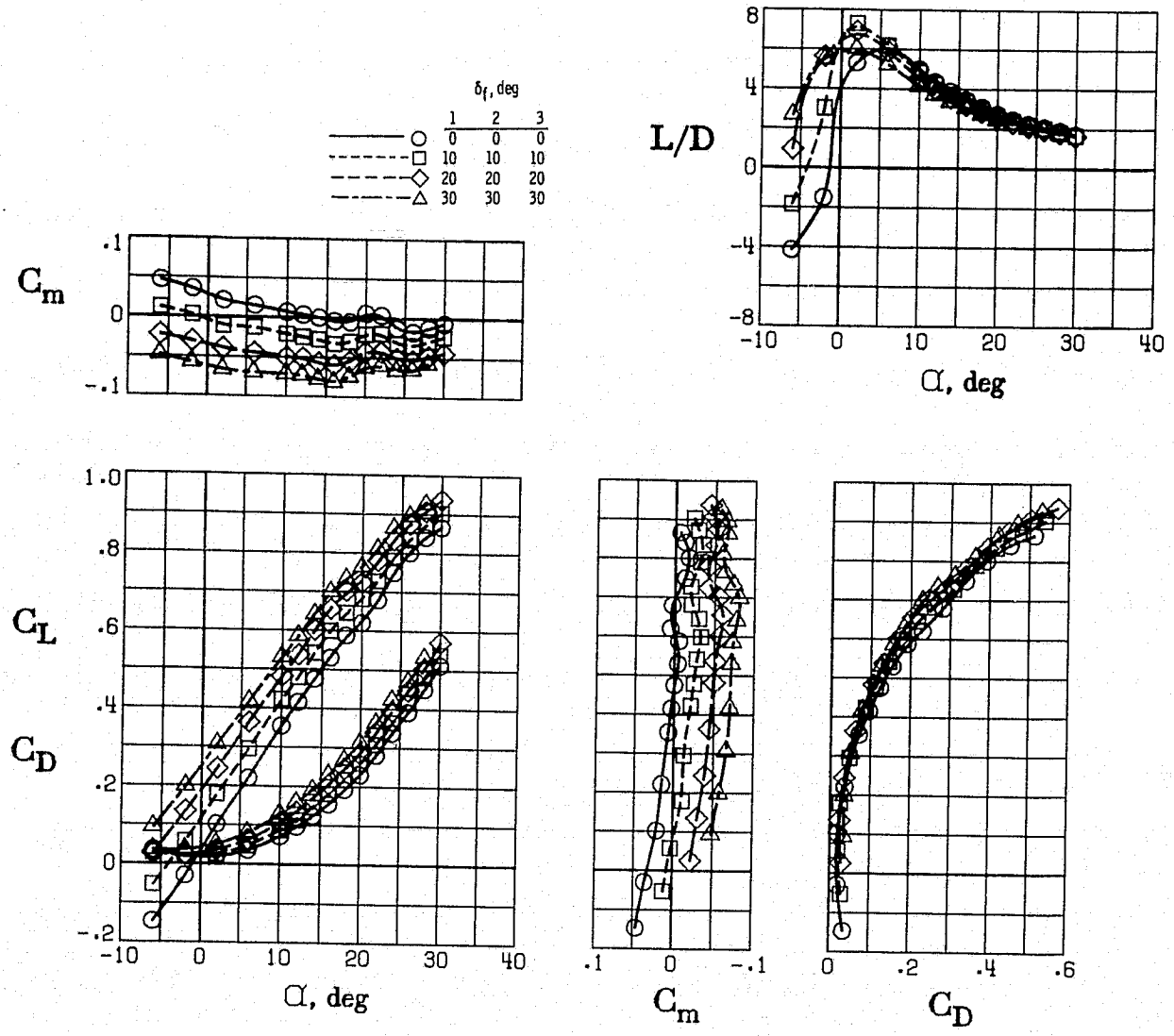

Figure 18.- Effect of full-span flap deflection. $\delta_{n,1,2,3,4} = 45°$, $\delta_{n,5,6,7} = 60°$, $\beta = 0°$, $T_c' = 0$.

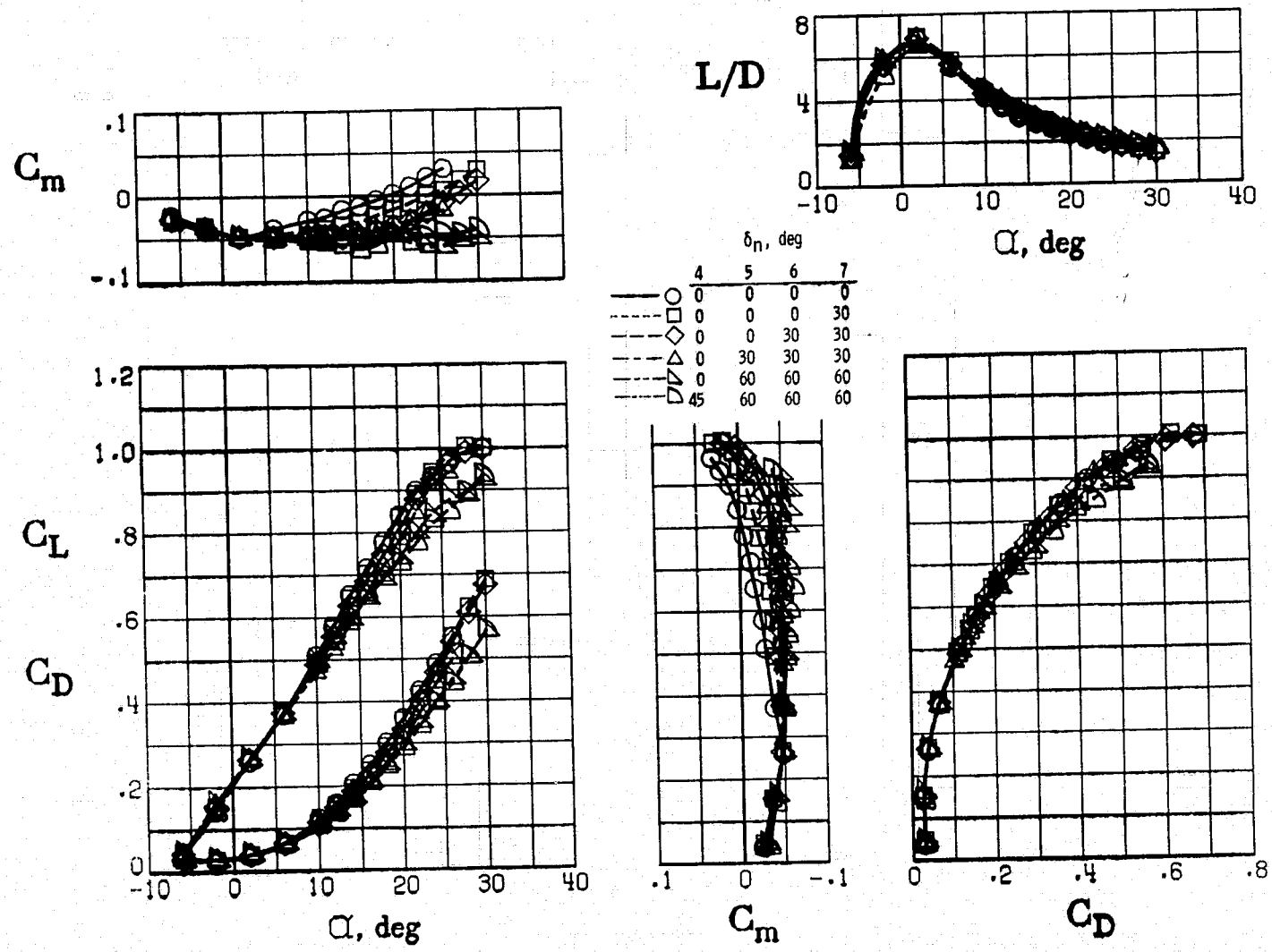

Figure 19.- Effect of wing L.E. flap deflection. $\delta_{f,1,2,3} = 20°, 30°, 30°$, $\delta_{n,1,2,3} = 45°$, $\beta = 0°$, $T_c' = 0$.

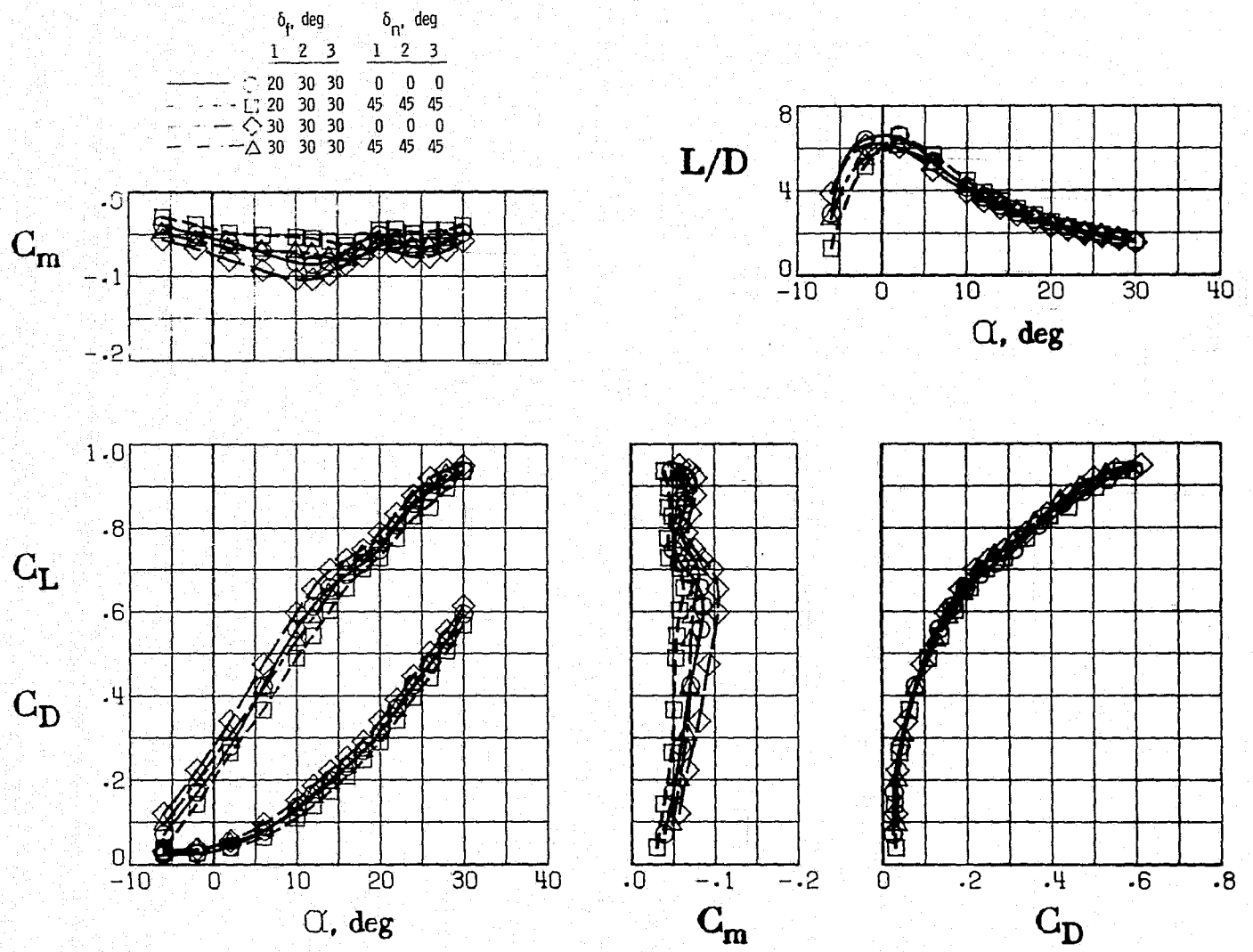

Figure 20. - Effect of outboard L.E. flap deflection. $\delta_{n,5,6,7} = 60°$, $\beta = 0°$, $T_c' = 0$.

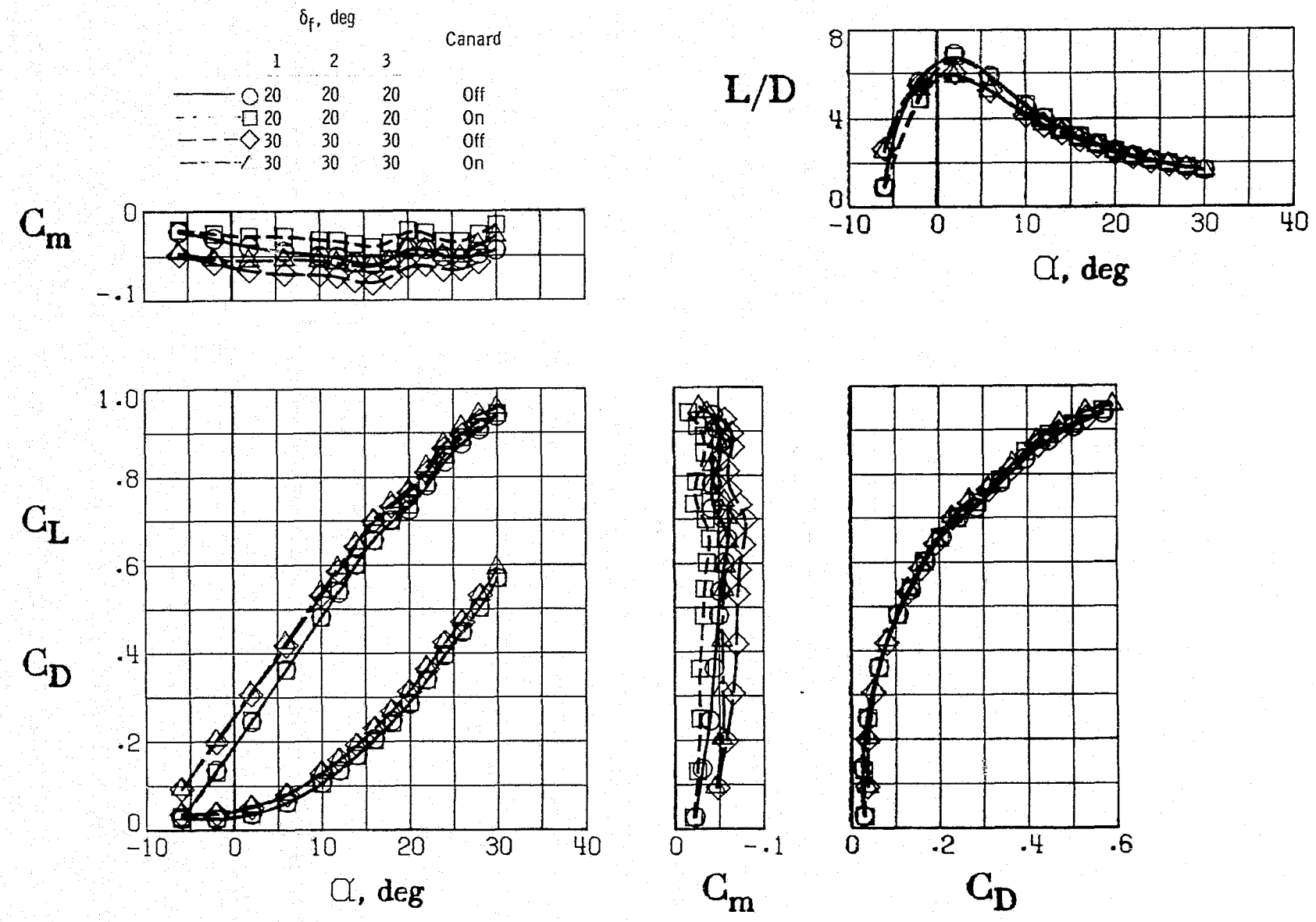

Figure 21. - Effect of deflecting a 0.020S canard. $\delta_{n,1,2,3,4} = 45°$, $\delta_{n,5,6,7} = 60°$, $\beta = 0°$, $T_c' = 0$.

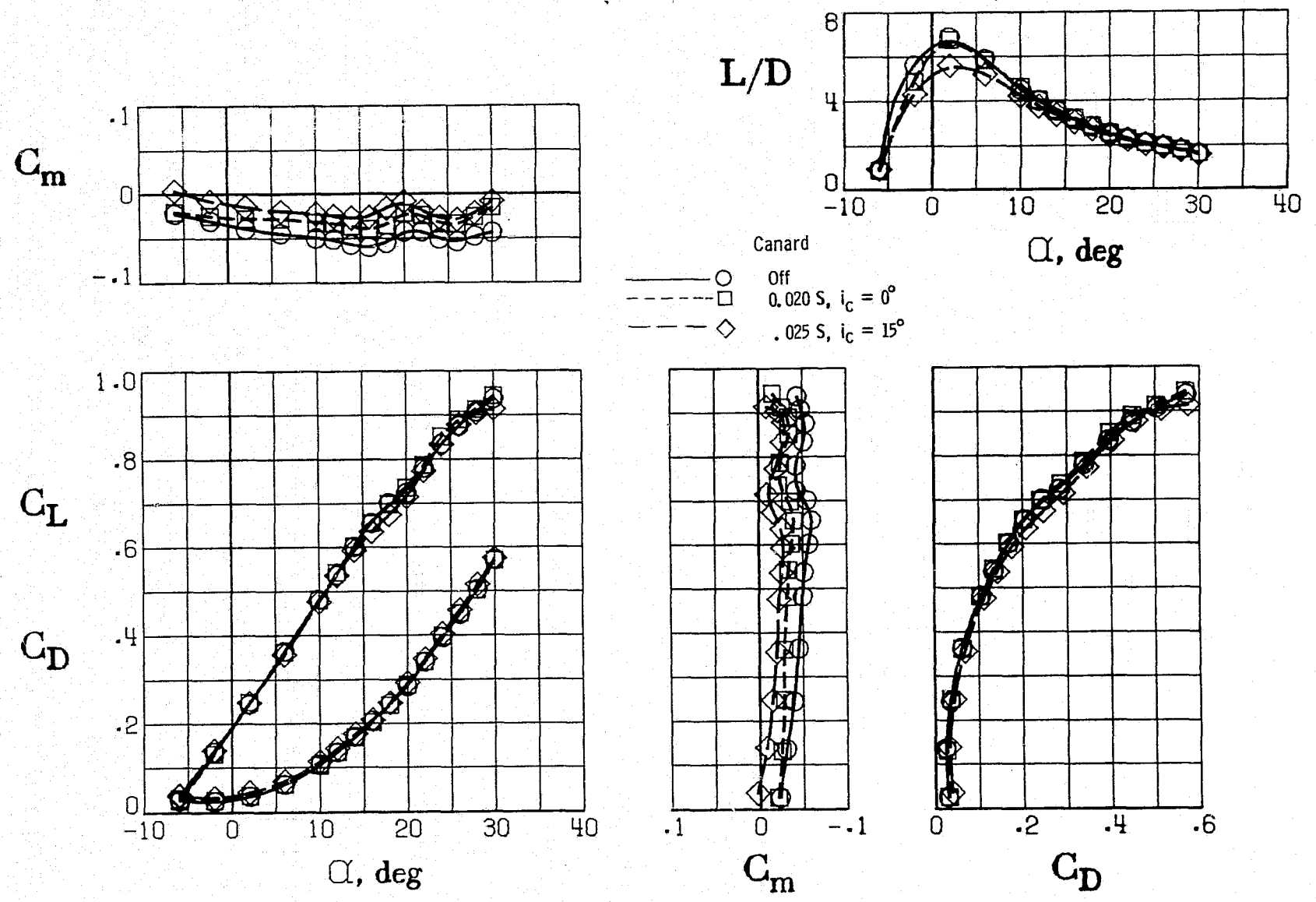

(a) $\delta_{f, 1, 2, 3} = 20°$.

Figure 22. - Effect of increasing canard area and canard incidence. $\delta_{n, 1, 2, 3, 4} = 45°$, $\delta_{n, 5, 6, 7} = 60°$, $\beta = 0°$, $T_c' = 0$.

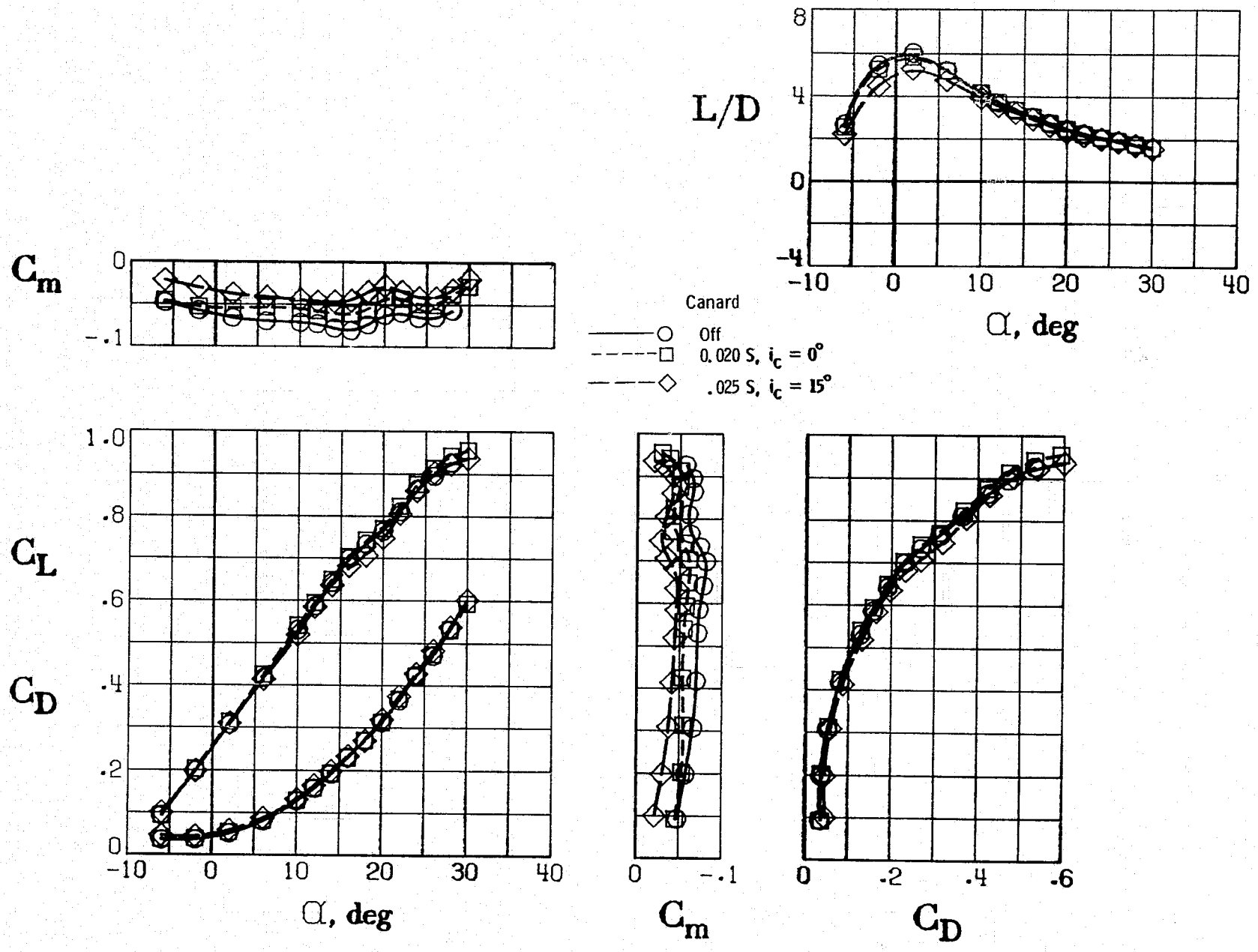

(b) $\delta_{f,1,2,3} = 30°$

Figure 22. - Concluded.

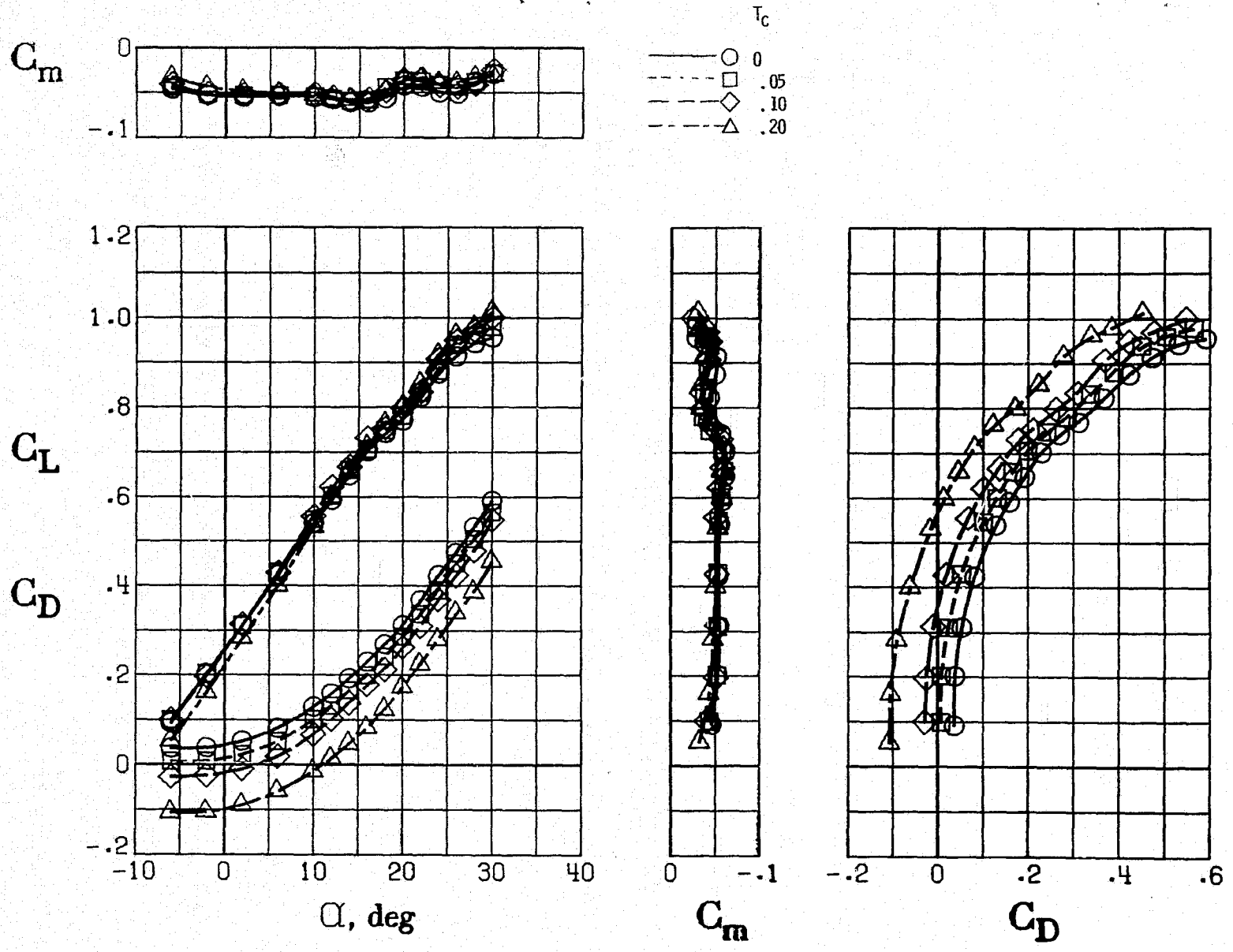

Figure 23. - Effect of engine thrust. $\delta_{f,1,2,3} = 30°$, $\delta_{n,1,2,3,4} = 45°$, $\delta_{n,5,6,7} = 60°$, 0.020S canard, $\beta = 0°$.

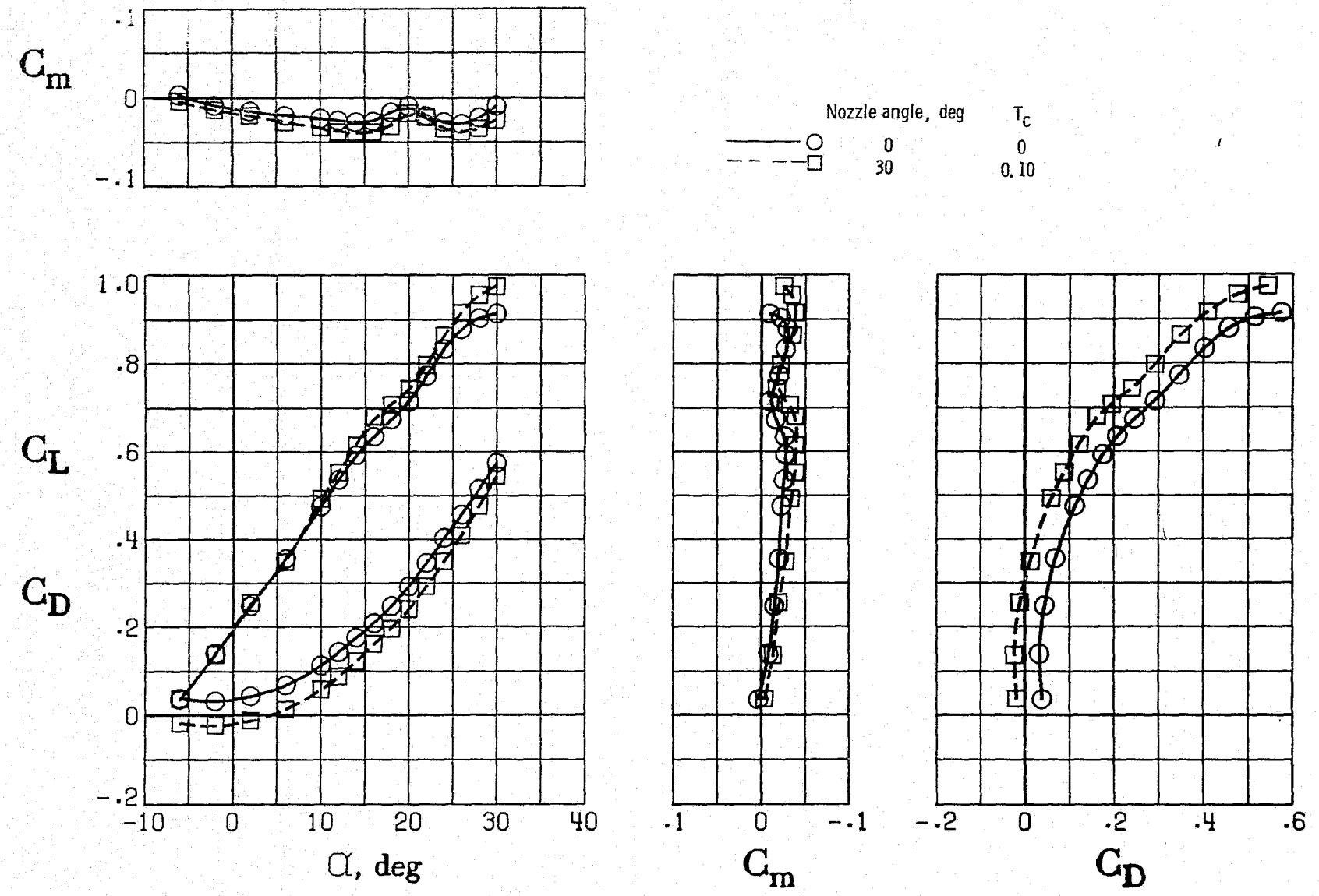

(a) $\delta_{f,1,2,3} = 20^\circ$

Figure 24. - Effect of thrust vectoring. $\delta_{n,\ 1,2,3,4} = 45^\circ$, $\delta_{n,\ 5,6,7} = 60^\circ$, 0.020 S canard, $\beta = 0^\circ$.

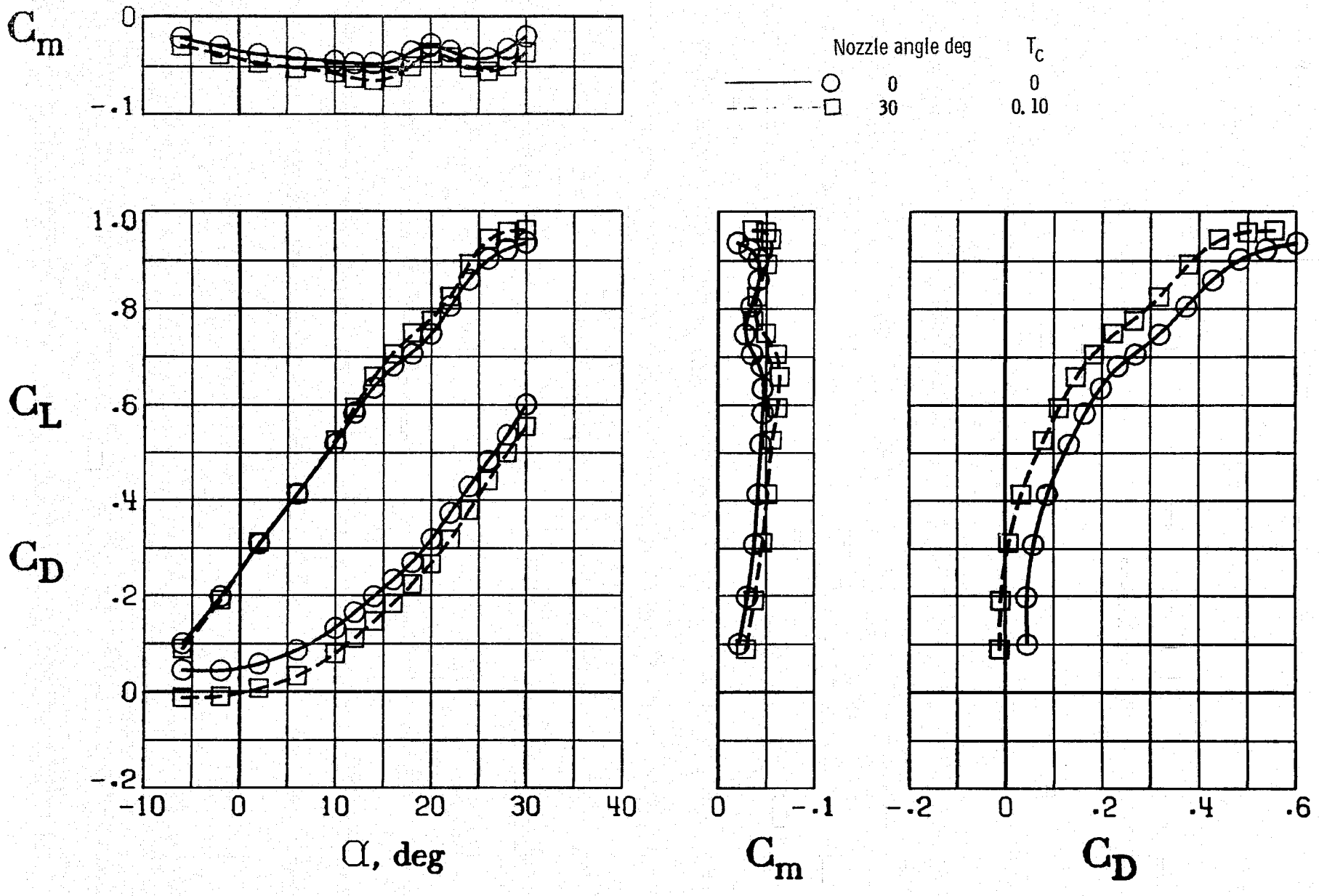

(b) $\delta_{f,1,2,3} = 30°$

Figure 24. - Concluded.

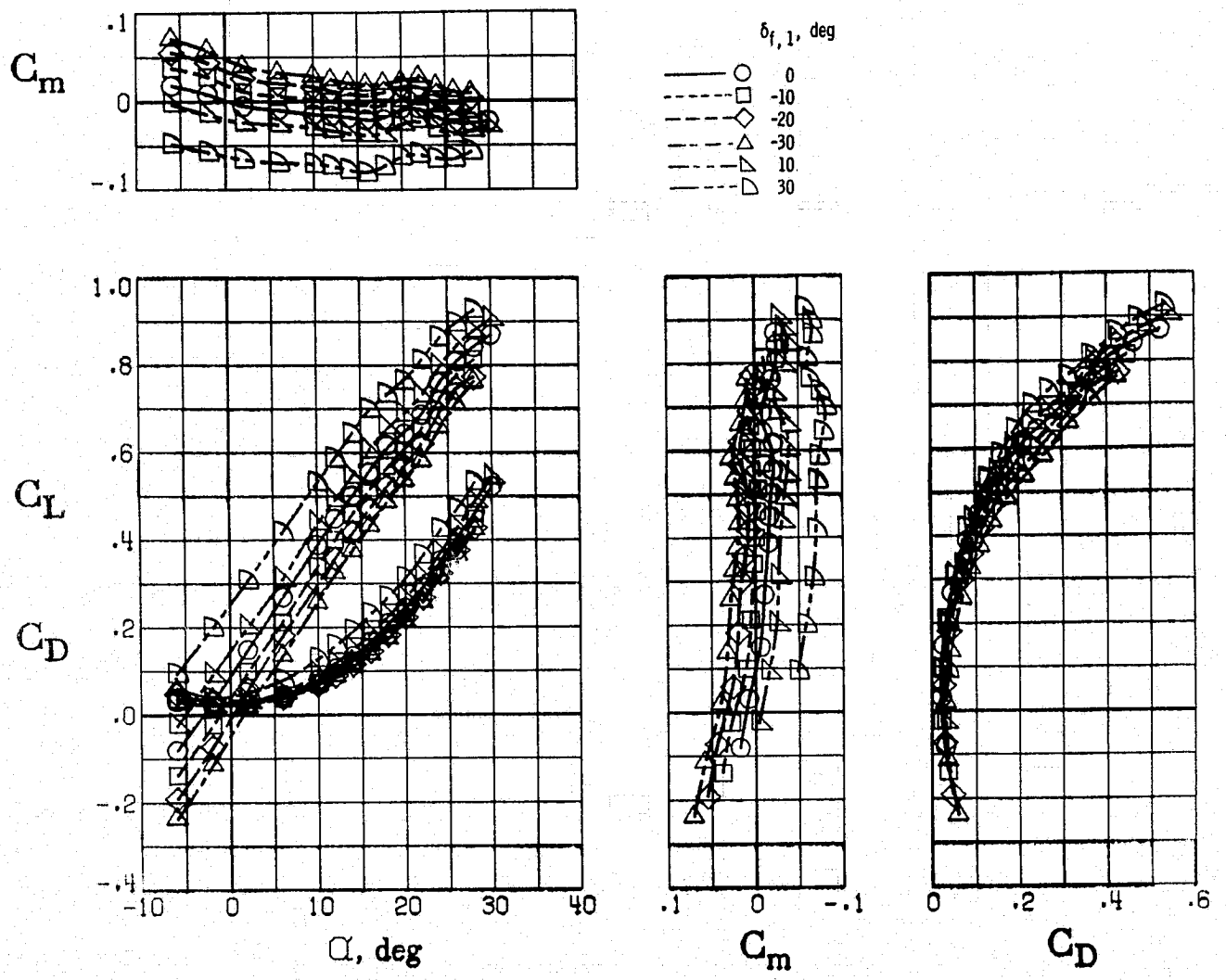

(a) $\delta_{f,2,3} = 30°$ (Inboard flap variable)

Figure 25.- Longitudinal control effectiveness. $\delta_{n,1,2,3,4} = 45°$, $\delta_{n,5,6,7} = 60°$, $\beta = 0°$, $T_c' = 0$.

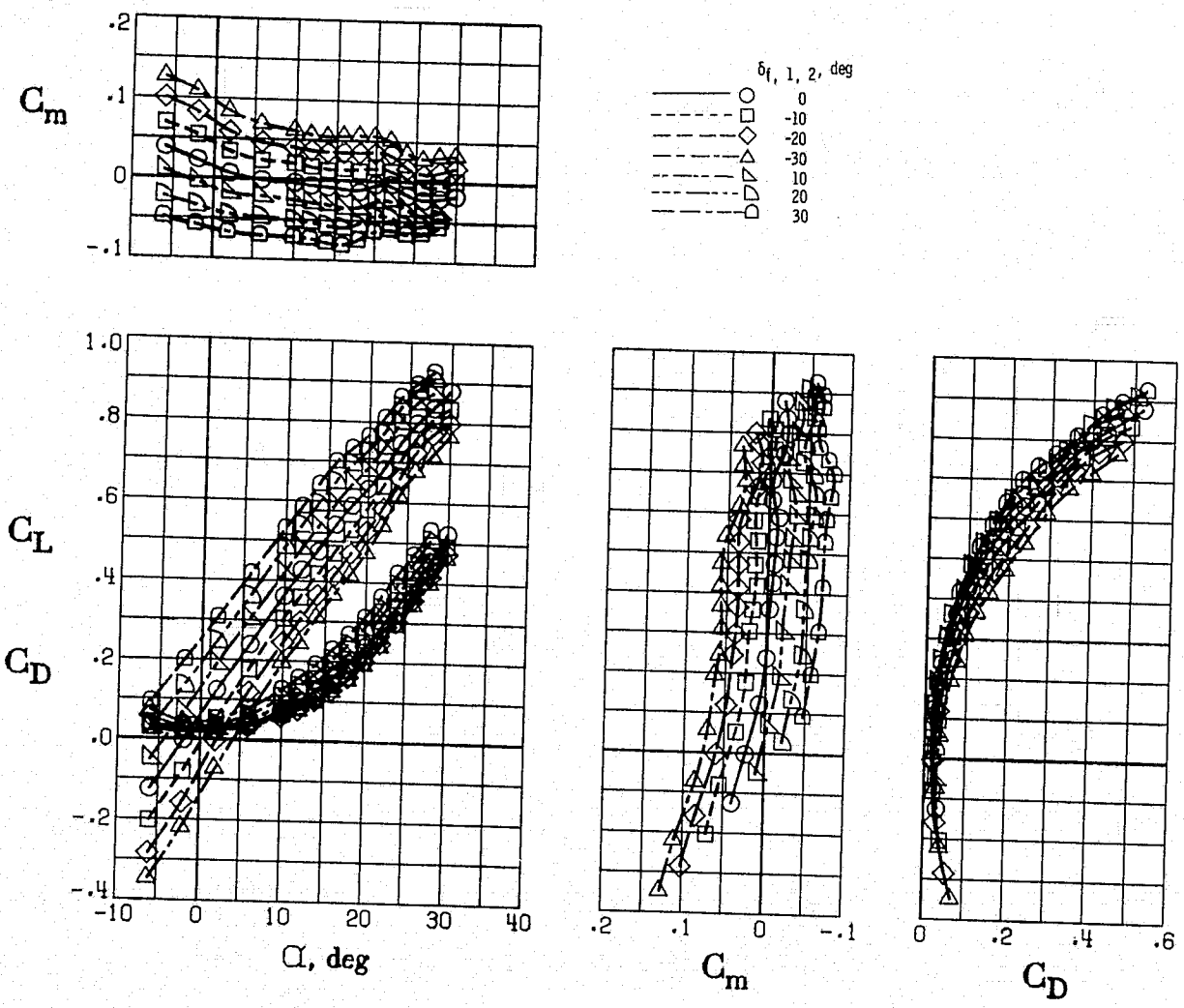

(b) $\delta_{f,3} = 30°$ (Inboard and center flap variable)

Figure 25. - Continued.

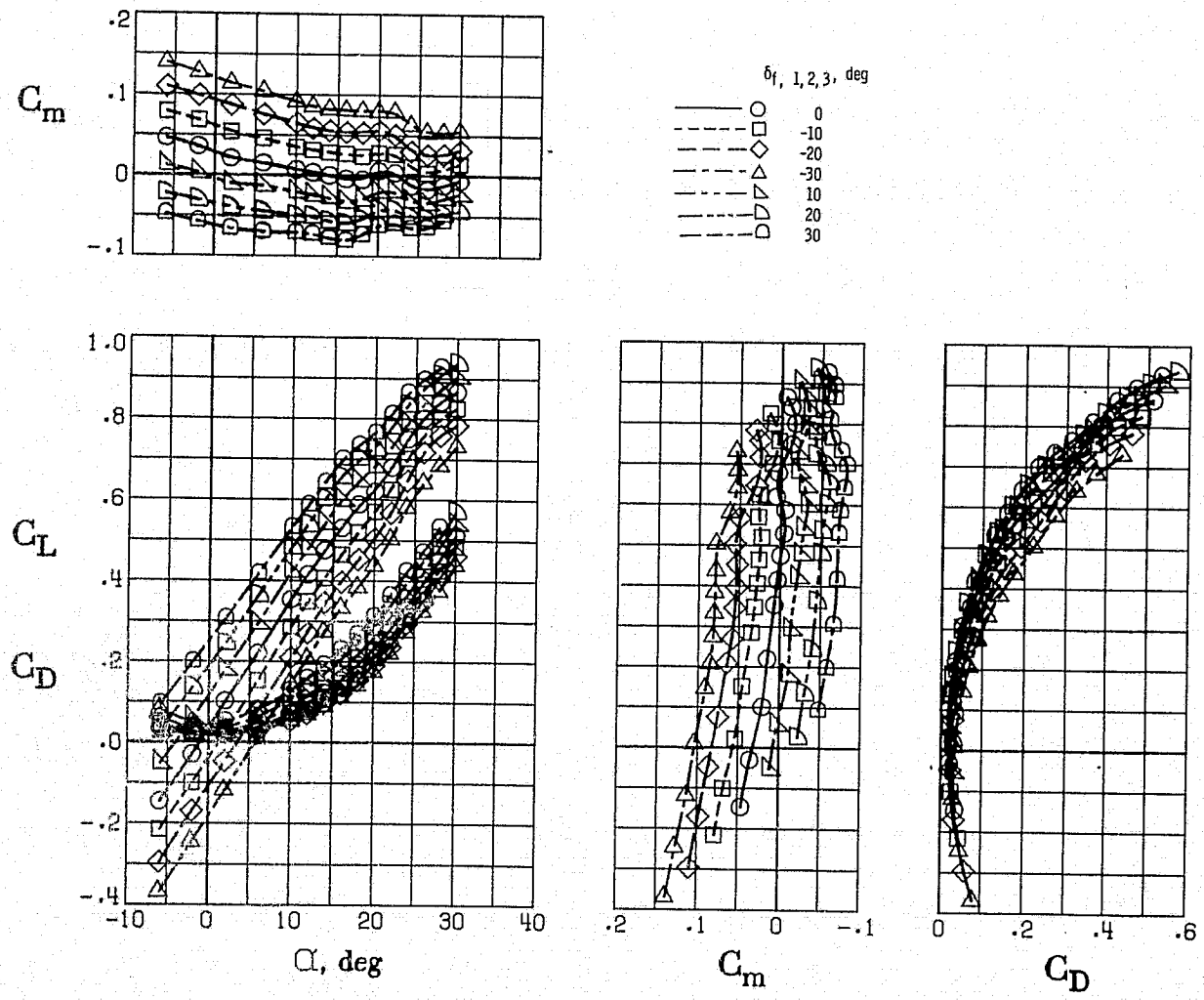

(c) Inboard, center, and outboard flap variable

Figure 25.- Continued.

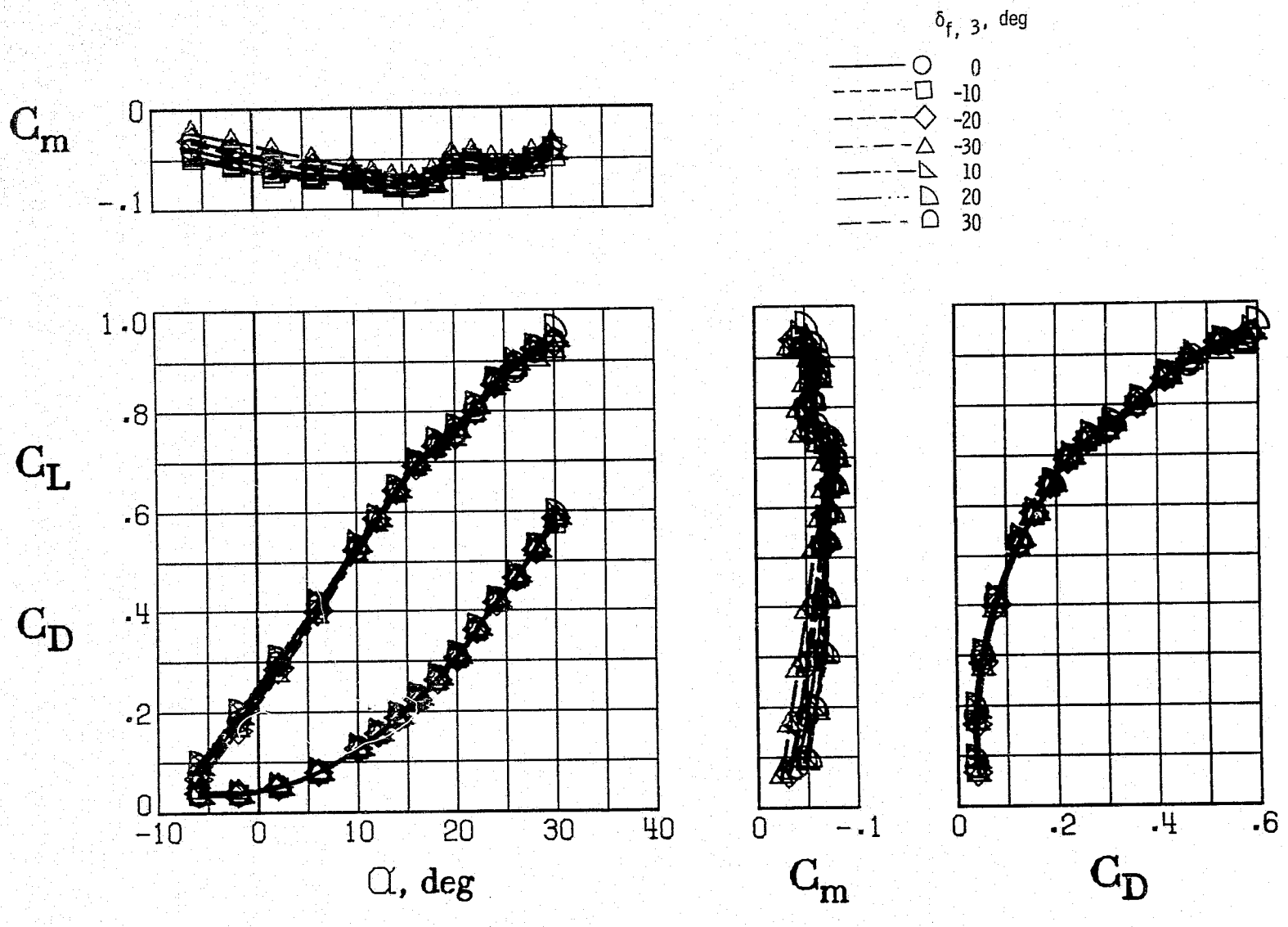

(d) $\delta_{f,1,2} = 30°$ (Outboard flap variable)

Figure 25. - Concluded.

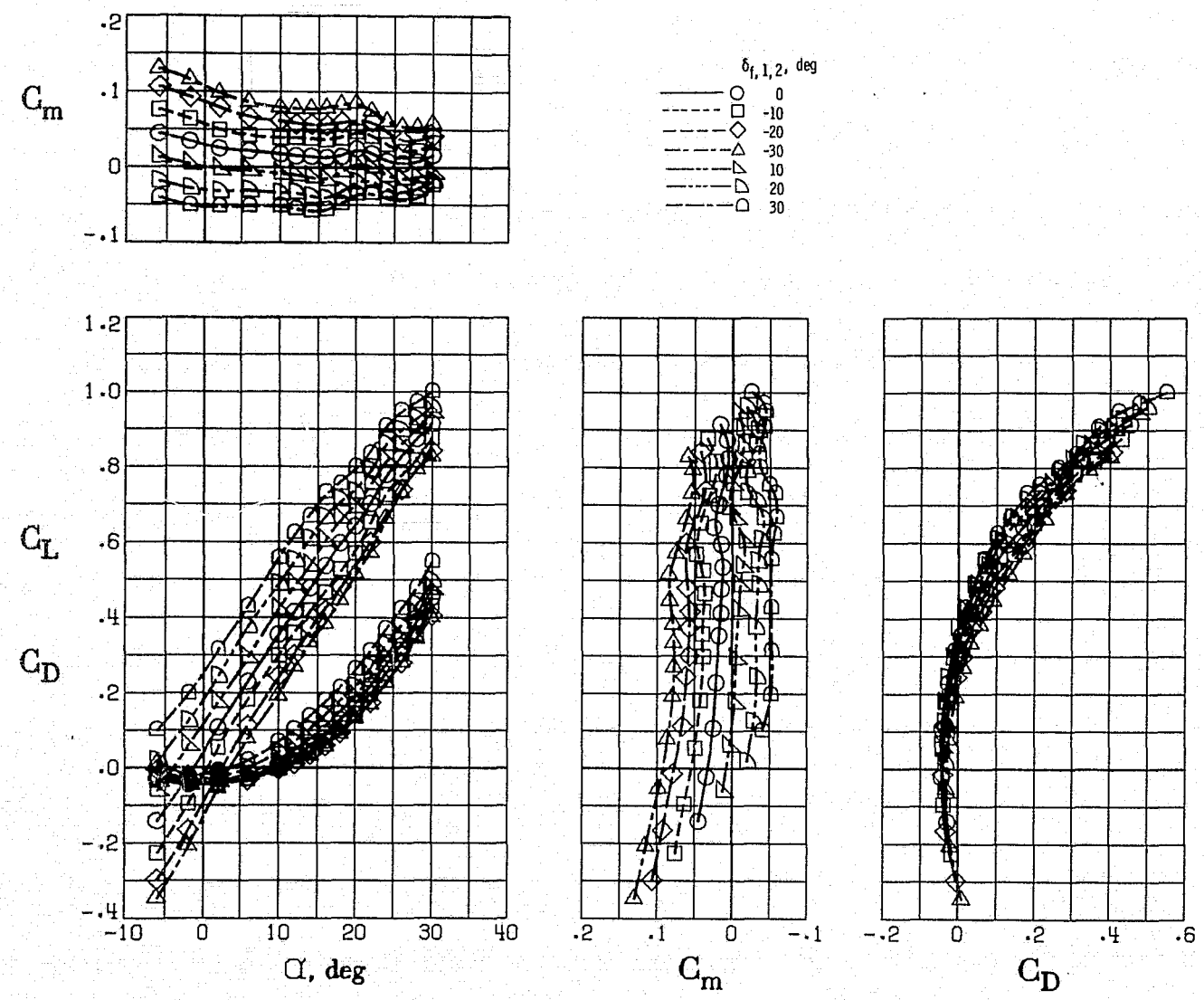

Figure 26. - Longitudinal control effectiveness with 0.020S canard, and with engines operating. $\delta_{f,3} = 30^\circ$, $\delta_{n,1,2,3,4} = 45^\circ$, $\delta_{n,5,6,7} = 60^\circ$, $\beta = 0^\circ$, $T_c' = 0.10$.

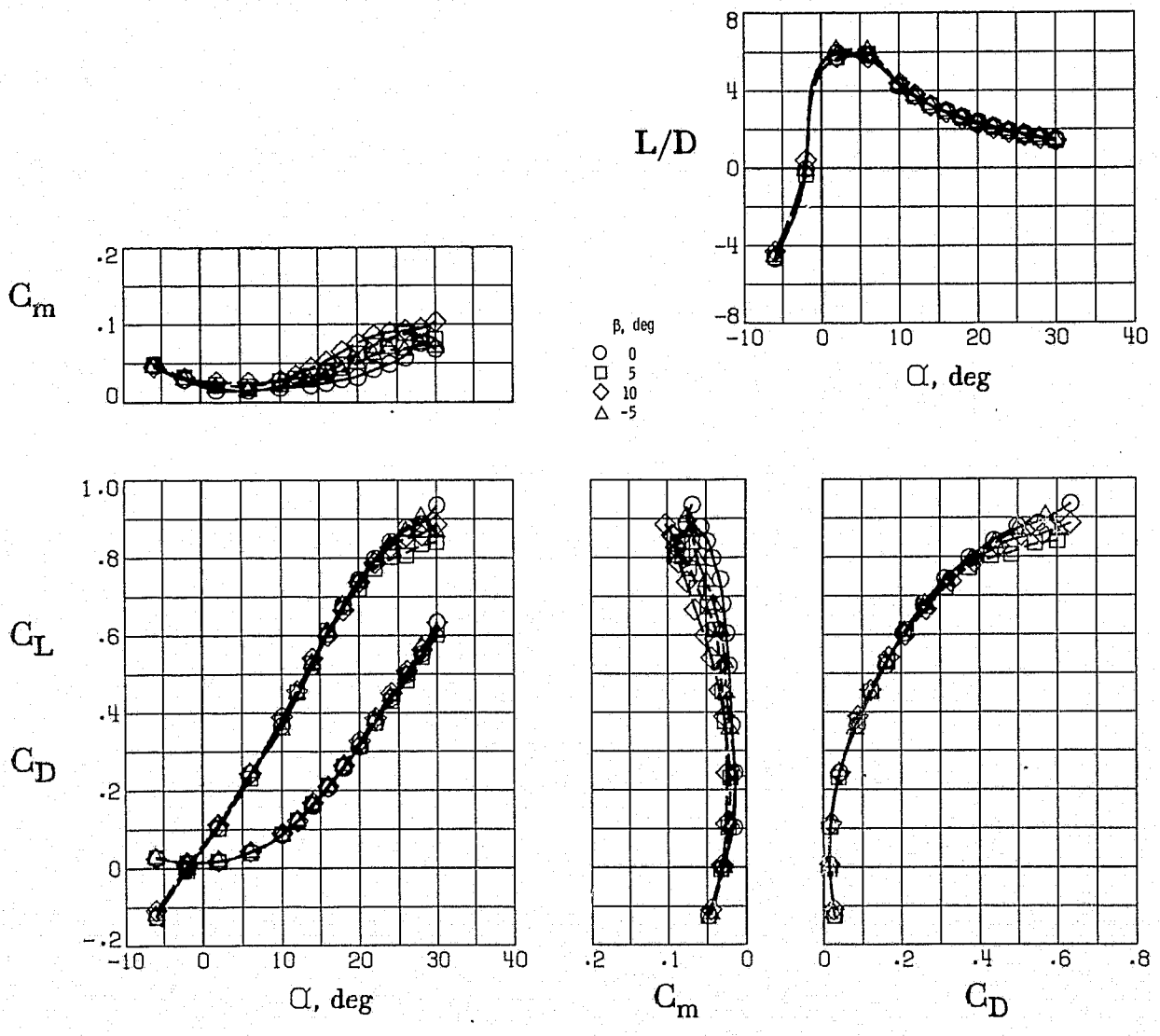

(a) Reynolds number = 6.78×10^6.

Figure 27.- Effect of sideslip. $\delta_f = 0°$, $\delta_n = 0°$, $T_c' = 0$.

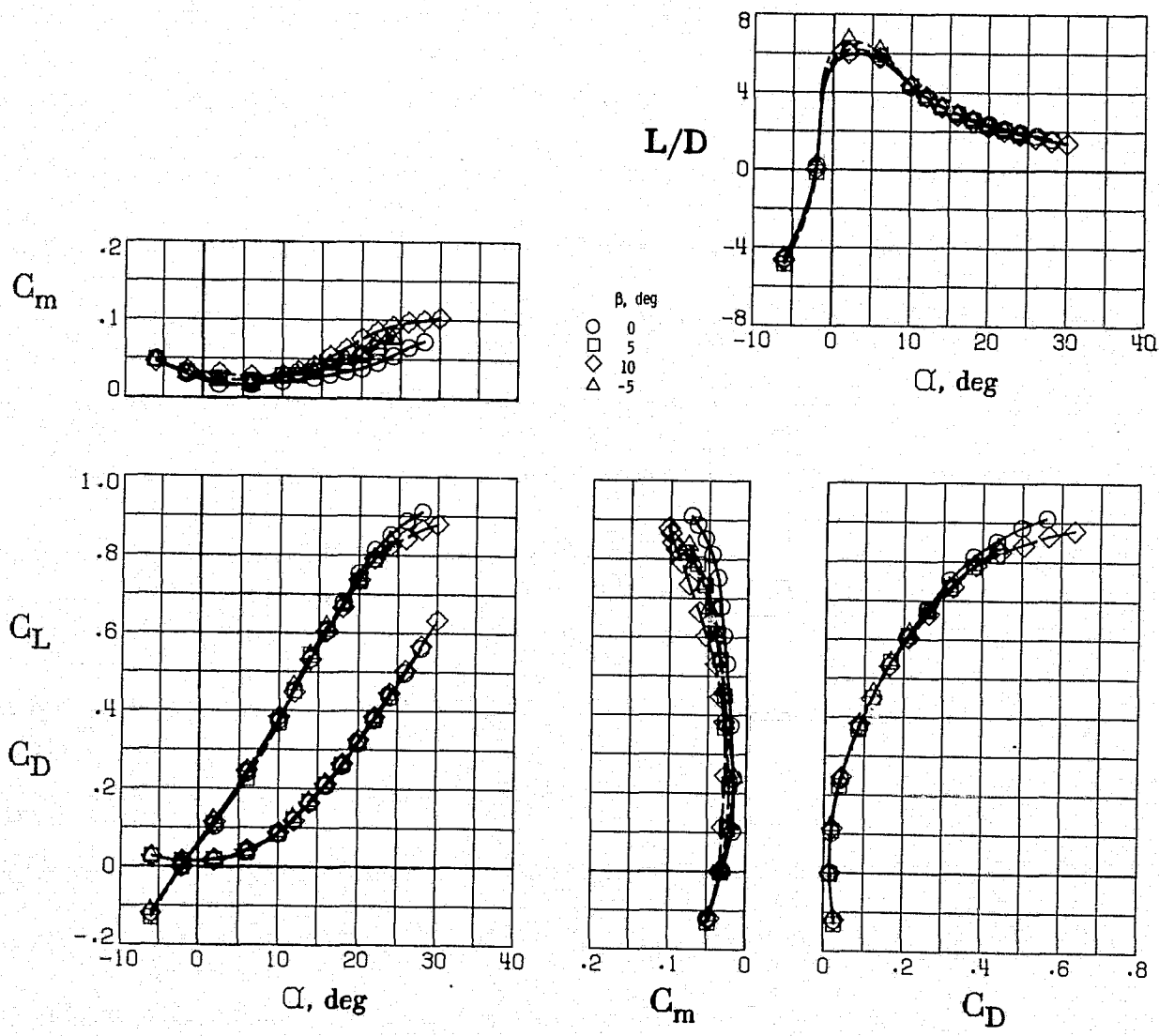

(b) Reynolds number = 8.92 × 10^6.

Figure 27. - Continued.

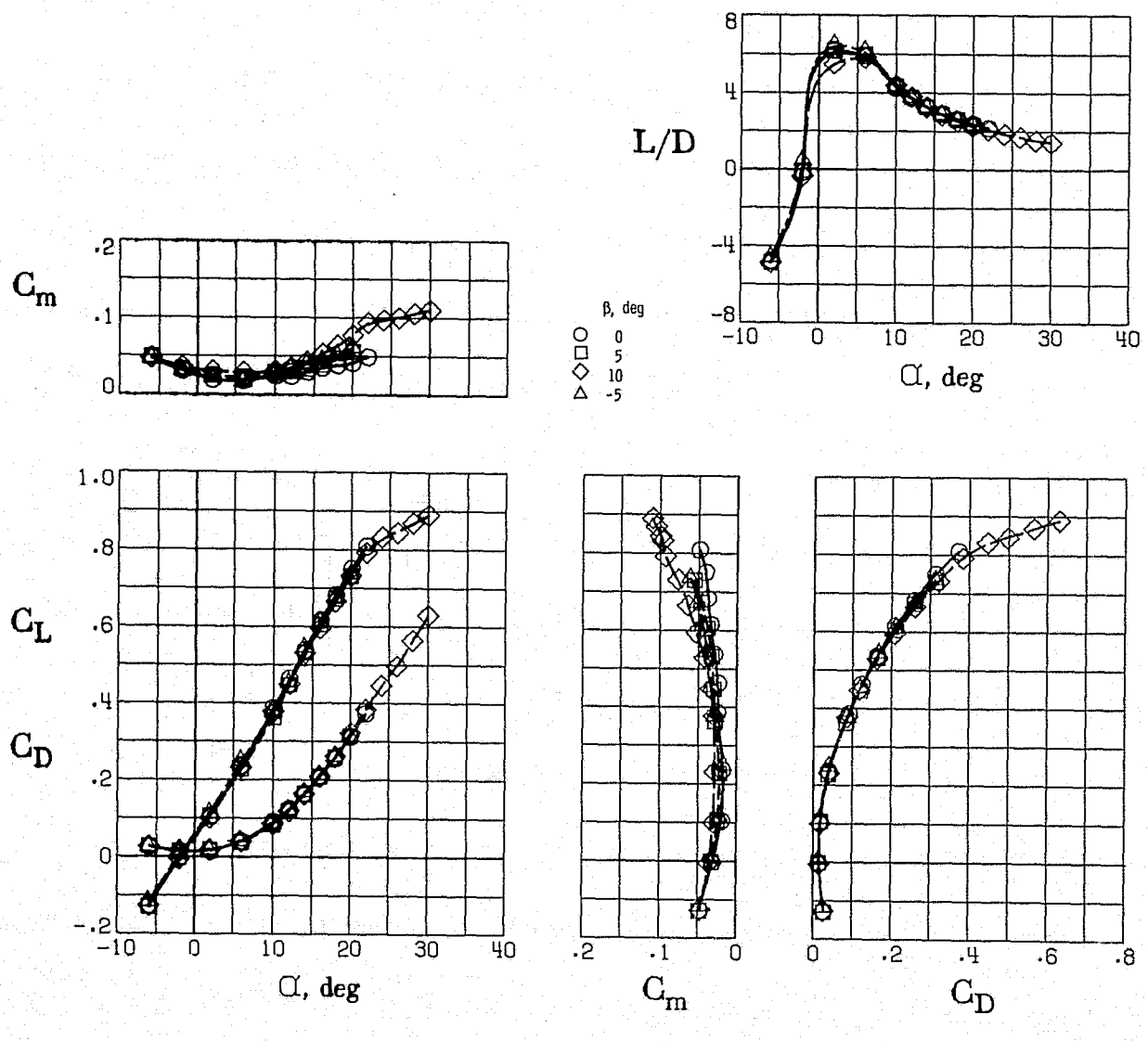

(c) Reynolds number = 11.65×10^6.

Figure 27.- Continued.

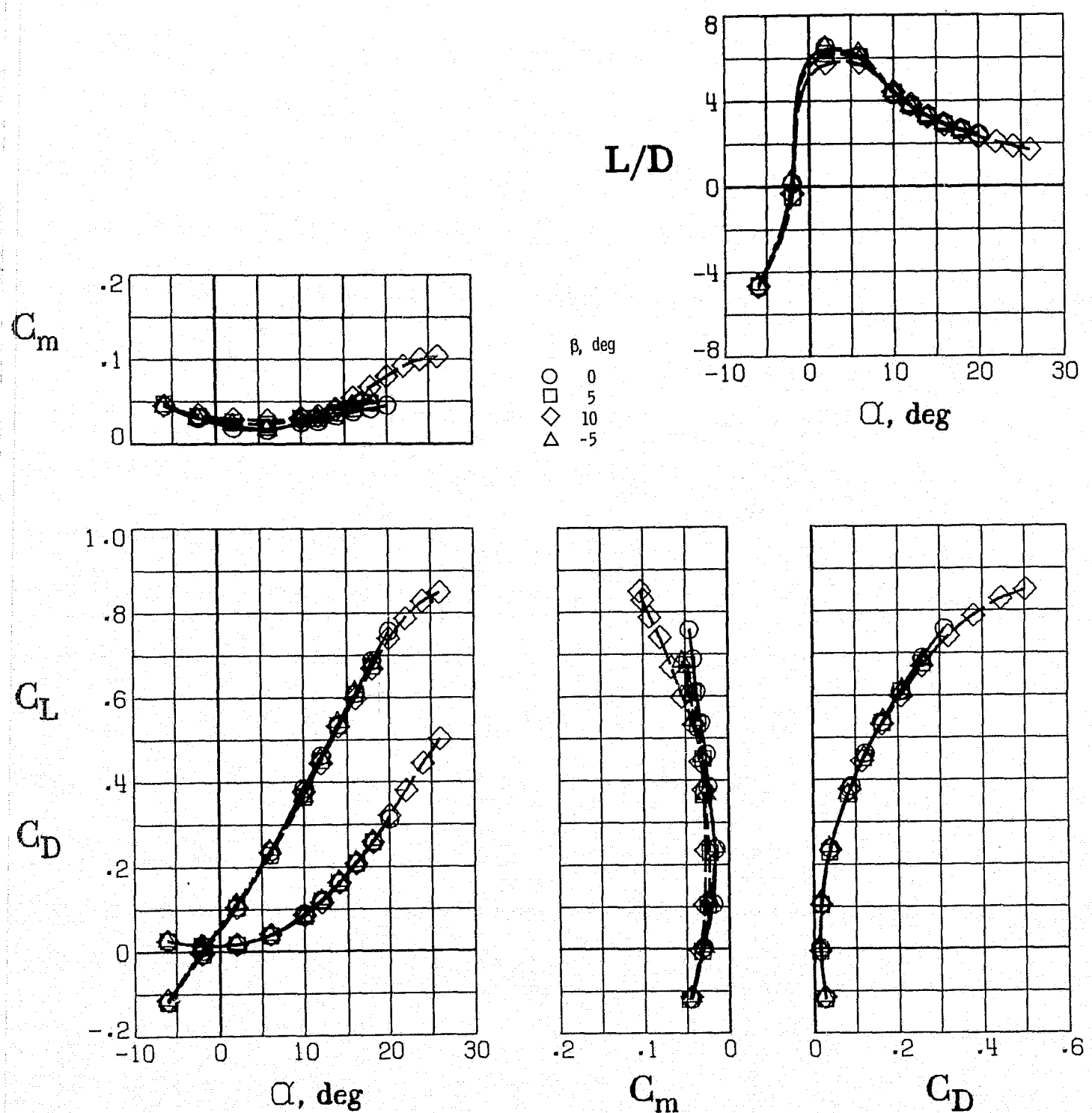

(d) Reynolds number = 13.85×10^6.

Figure 27. - Concluded.

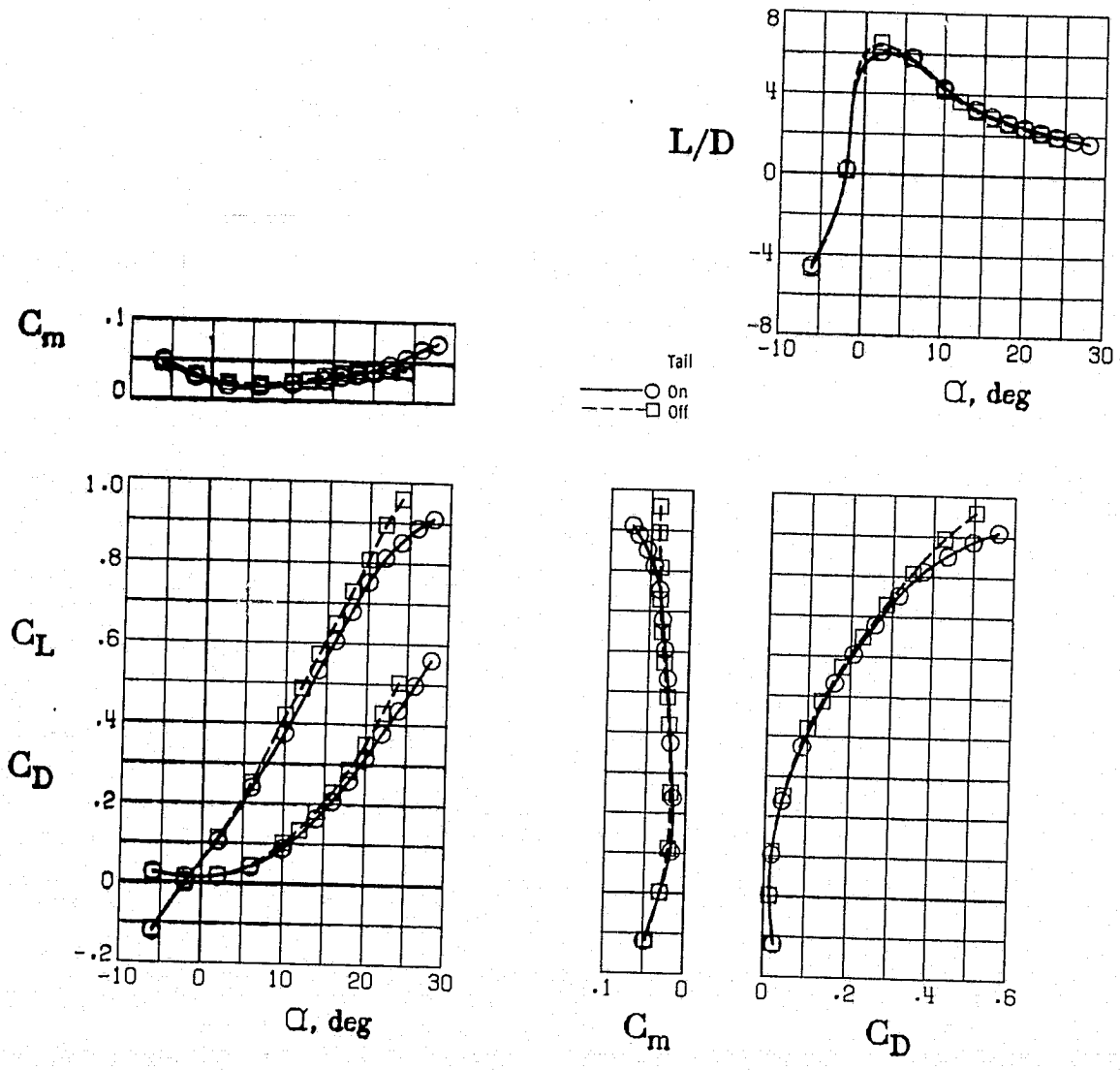

(a) $\beta = 0°$.

Figure 28.- Effect of vertical tails. $\delta_f = 0°$, $\delta_n = 0°$, $T_c' = 0$.

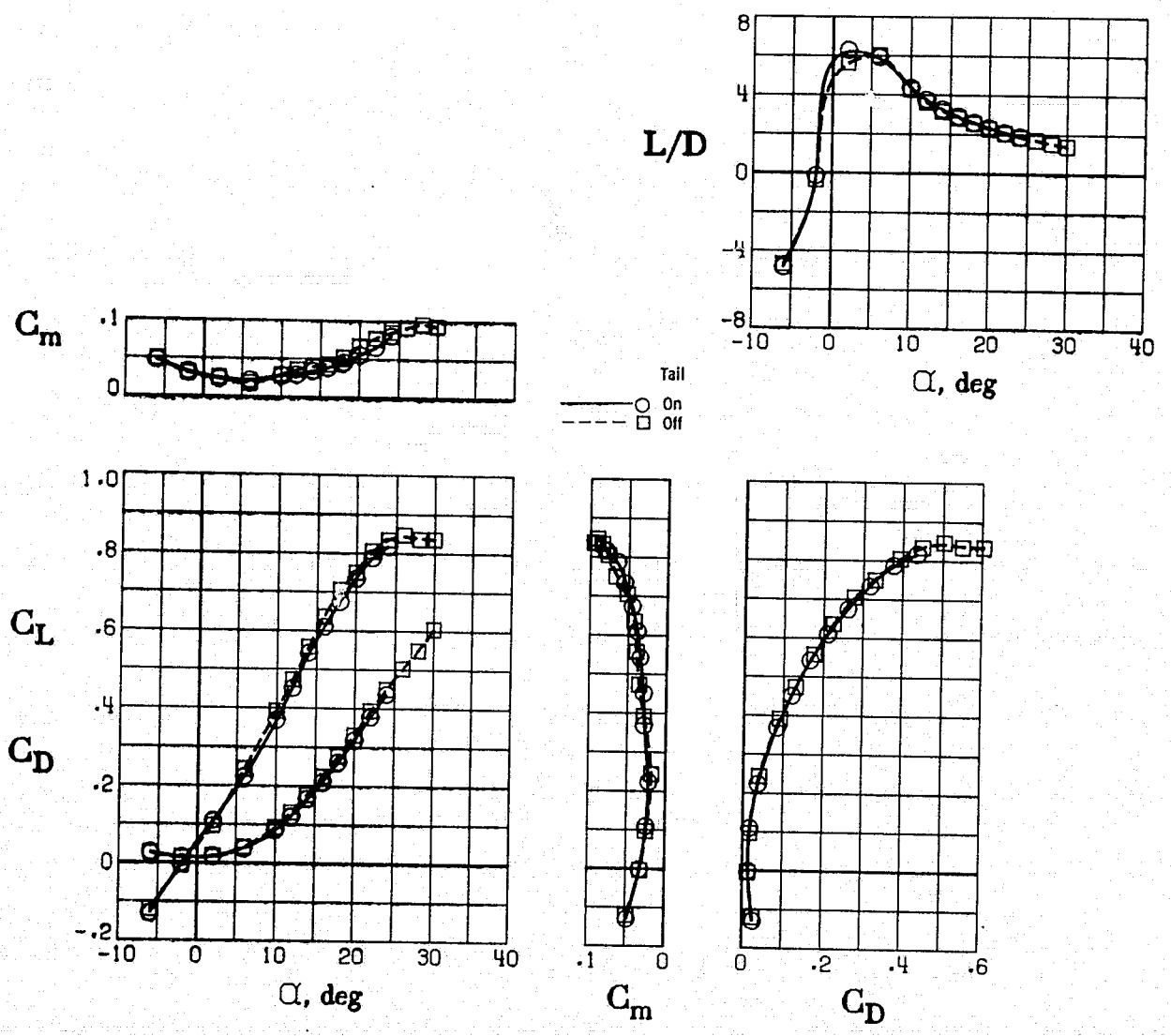

(b) $\beta = 5°$.

Figure 28. - Continued.

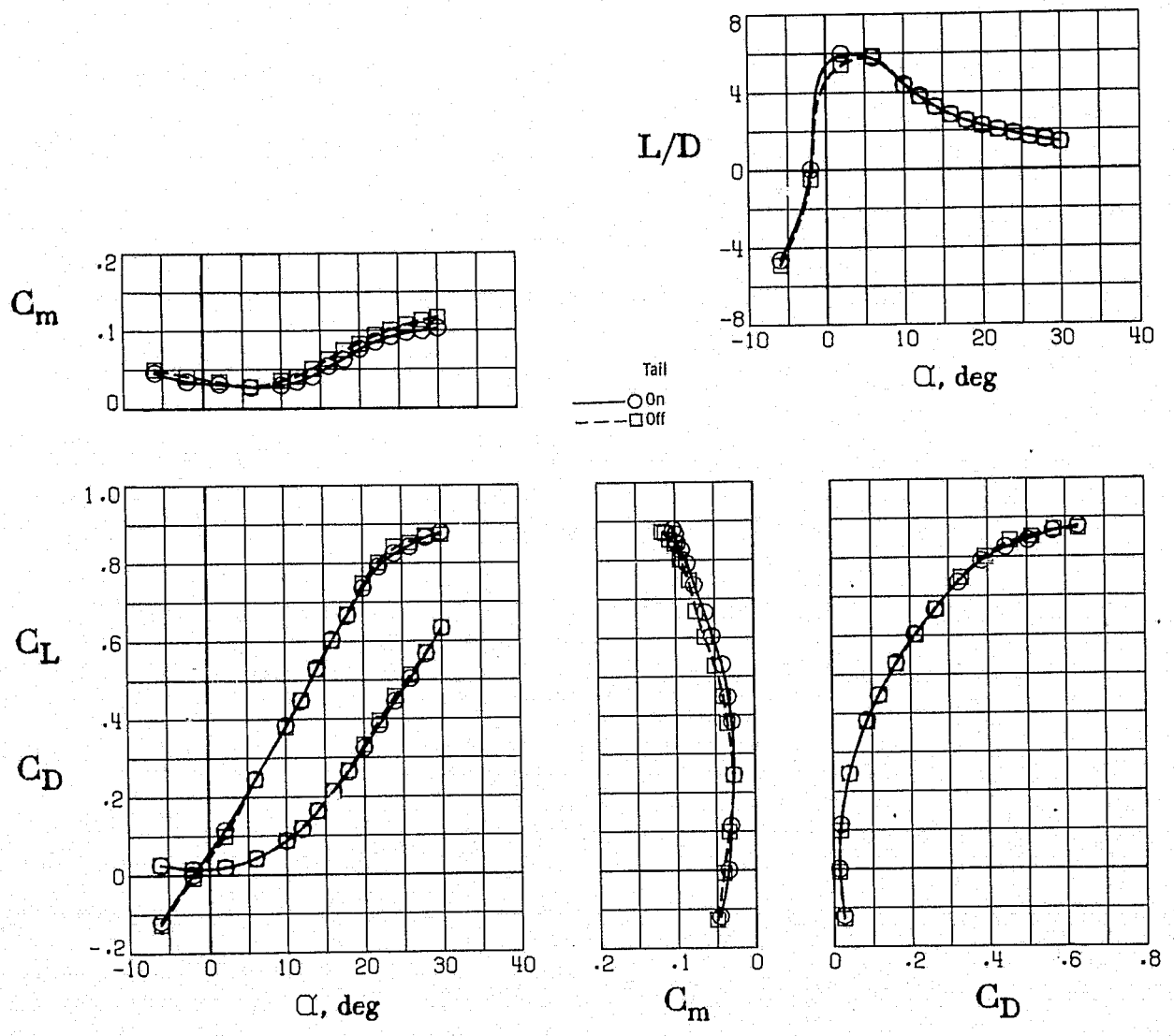

(c) $\beta = 10°$.

Figure 28.- Continued.

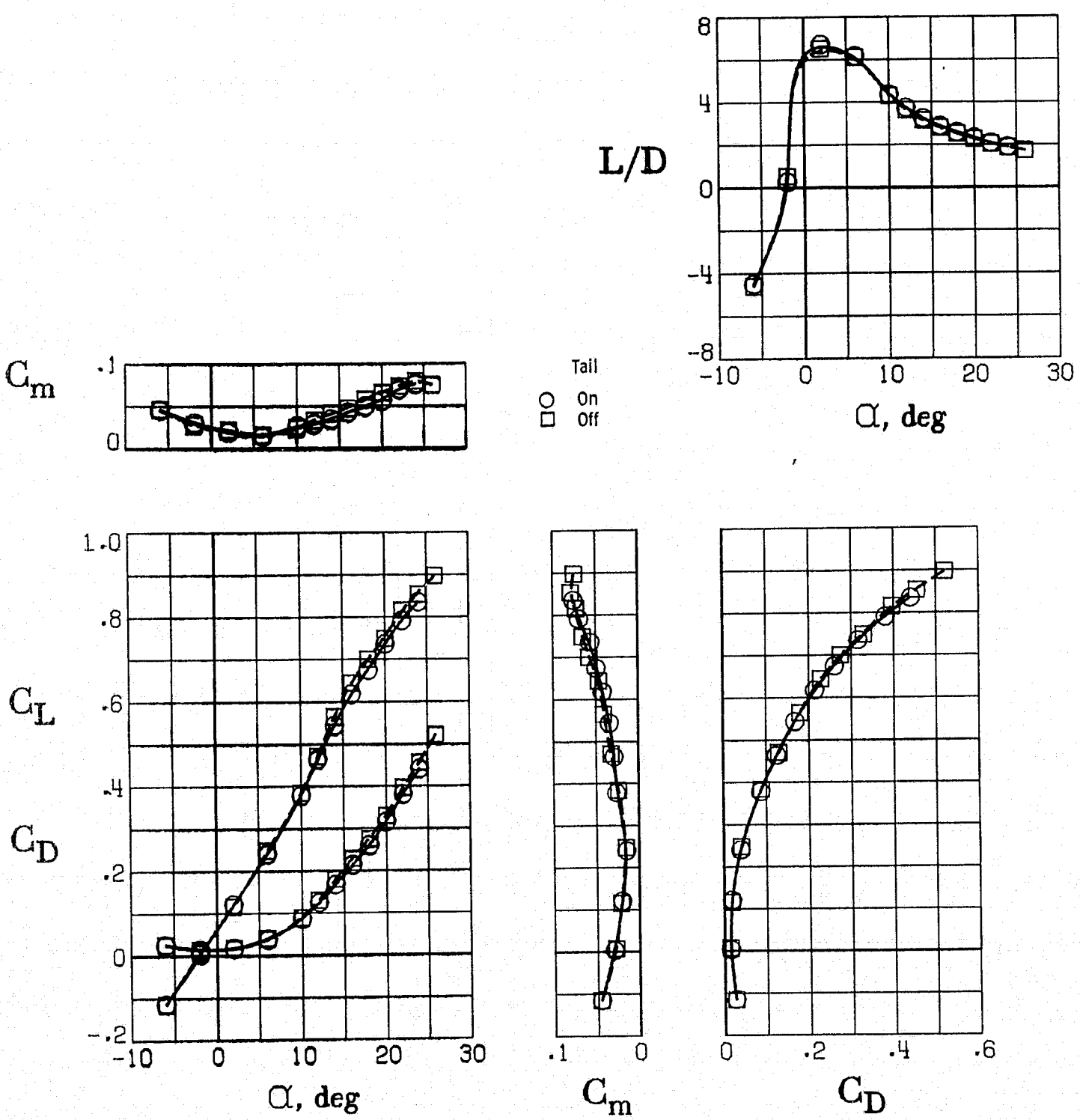

(d) $\beta = -5°$.

Figure 28. - Concluded.

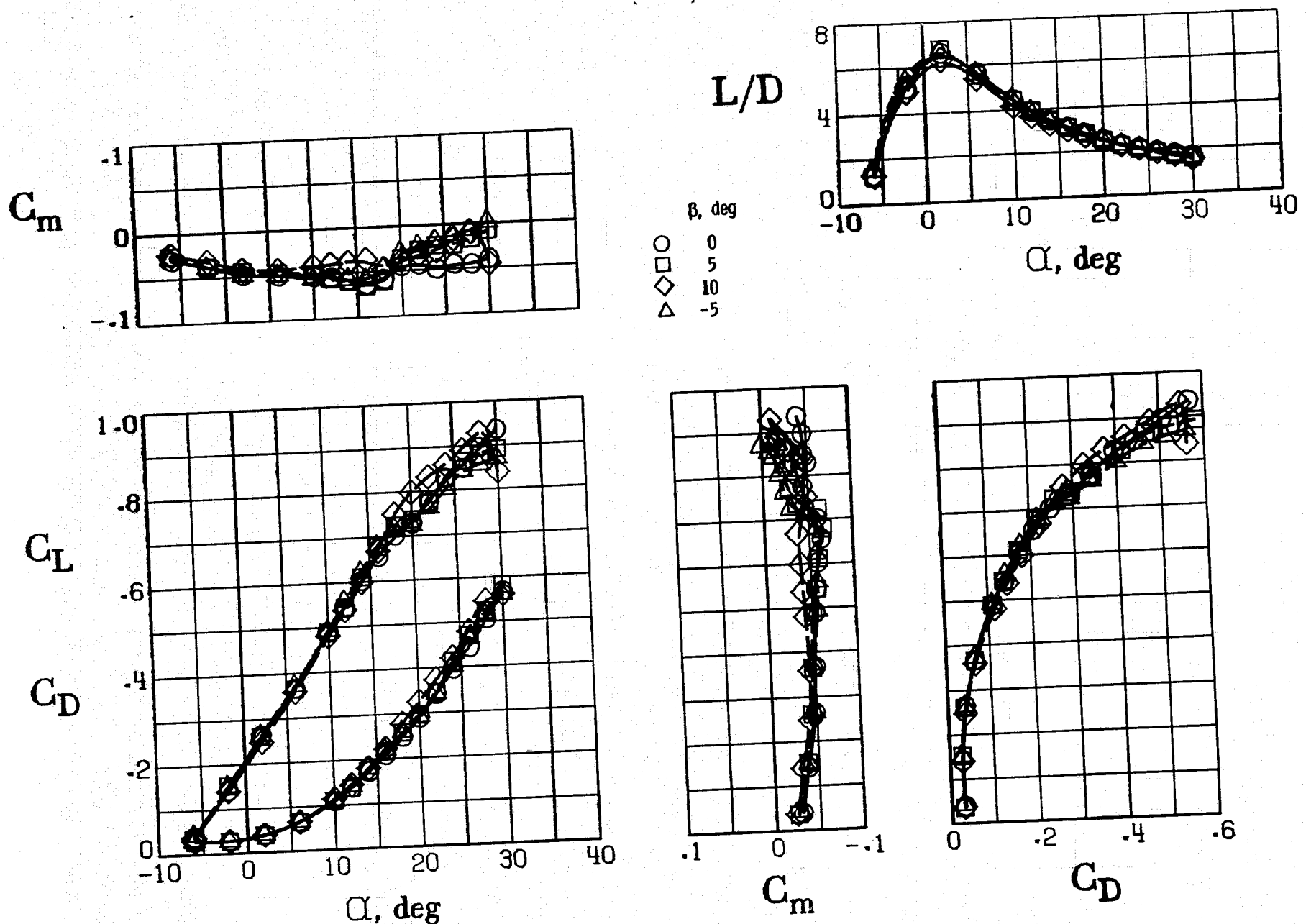

Figure 29. - Effect of sideslip. $\delta_{f,\ 1,2,3} = 20°,\ 30°, 30°,\ \delta_{n,\ 1,2,3,4} = 45°,\ \delta_{n,\ 5,6,5} = 60°,\ T_c' = 0.$

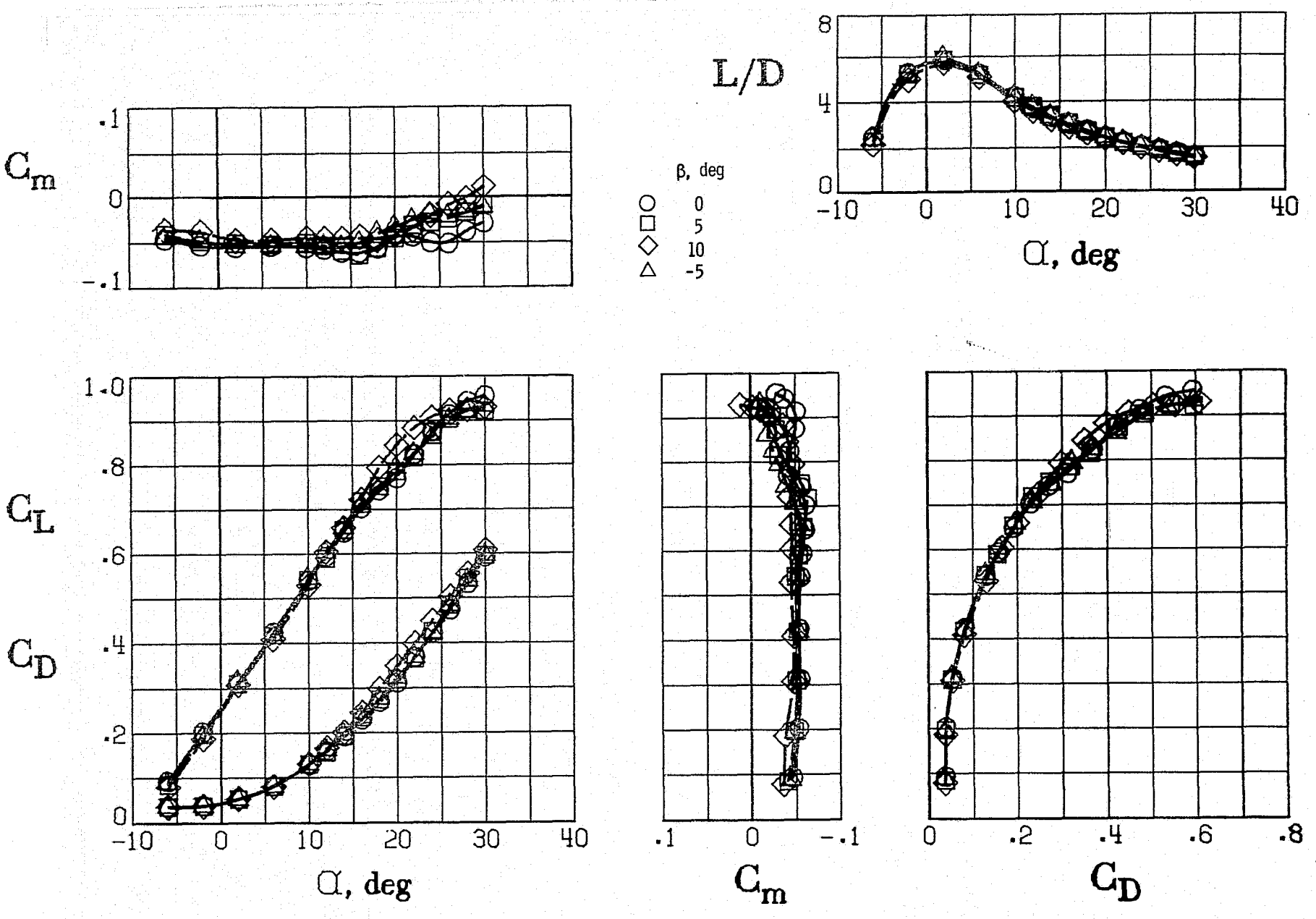

Figure 30. - Effect of sideslip with a 0.020 S canard. $\delta_{f,1,2,3} = 30°$, $\delta_{n,1,2,3,4} = 45°$, $\delta_{n,5,6,7} = 60°$, $T_c' = 0$.

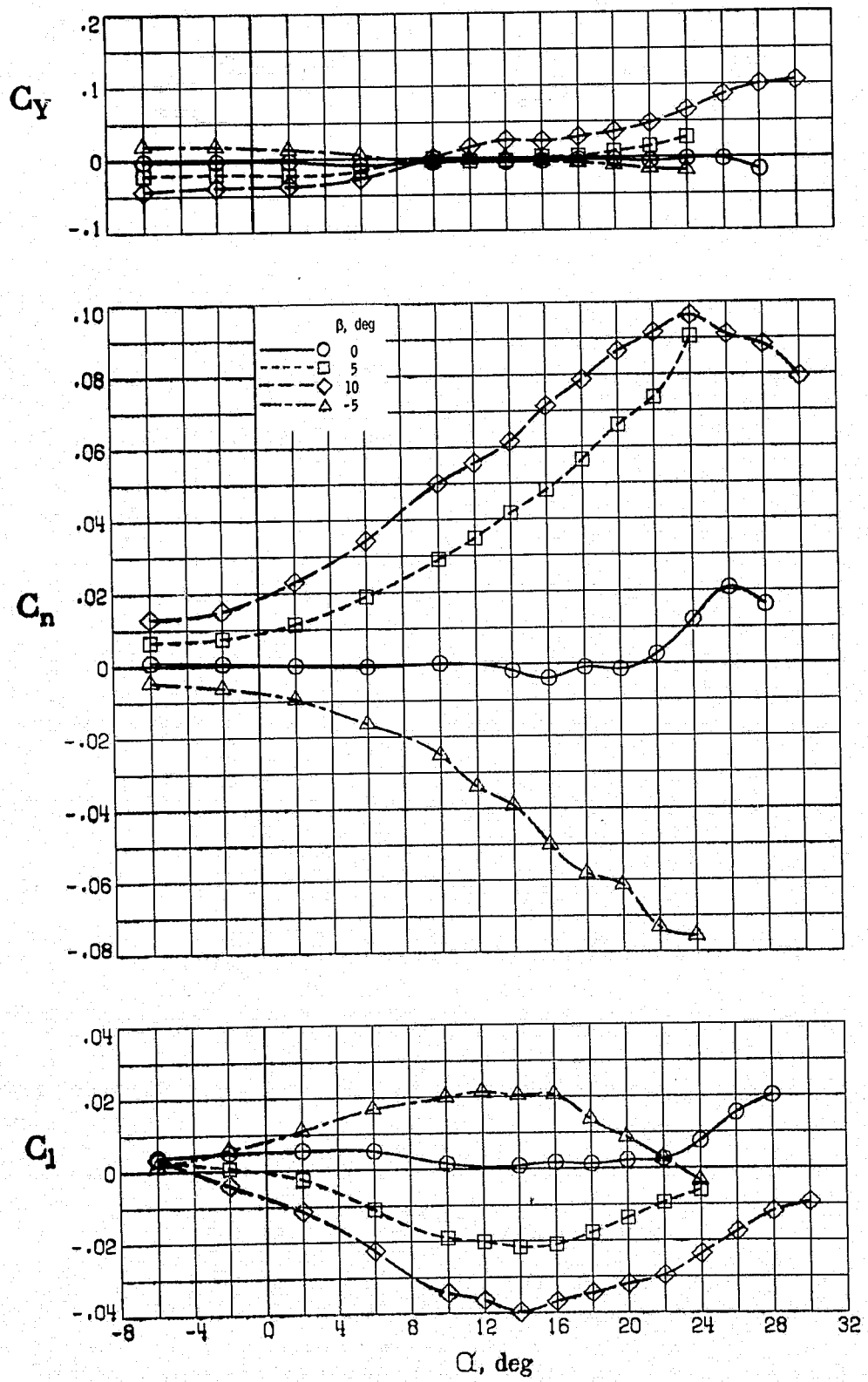

Figure 31. - Effect of sideslip on the lateral-directional characteristics of the clean wing with vertical tails. $T_C' = 0$.

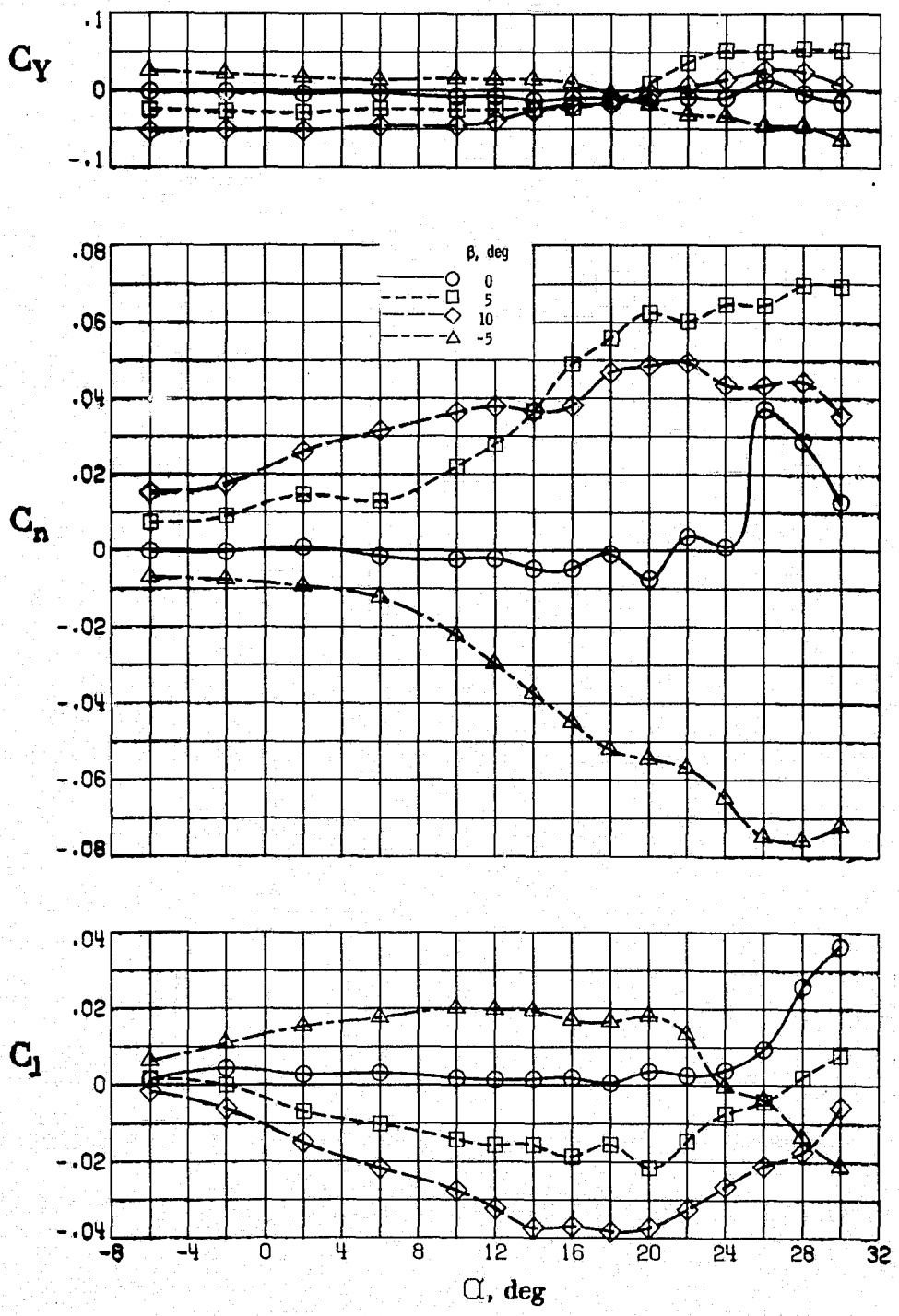

Figure 32. - Effect of sideslip on the lateral - directional characteristics. Vertical tails, $\delta_{f,1,2,3} = 20°, 30°, 30°$, $\delta_{n,1,2,3,4} = 45°$, $\delta_{n,5,6,7} = 60°$, $T_c' = 0$.

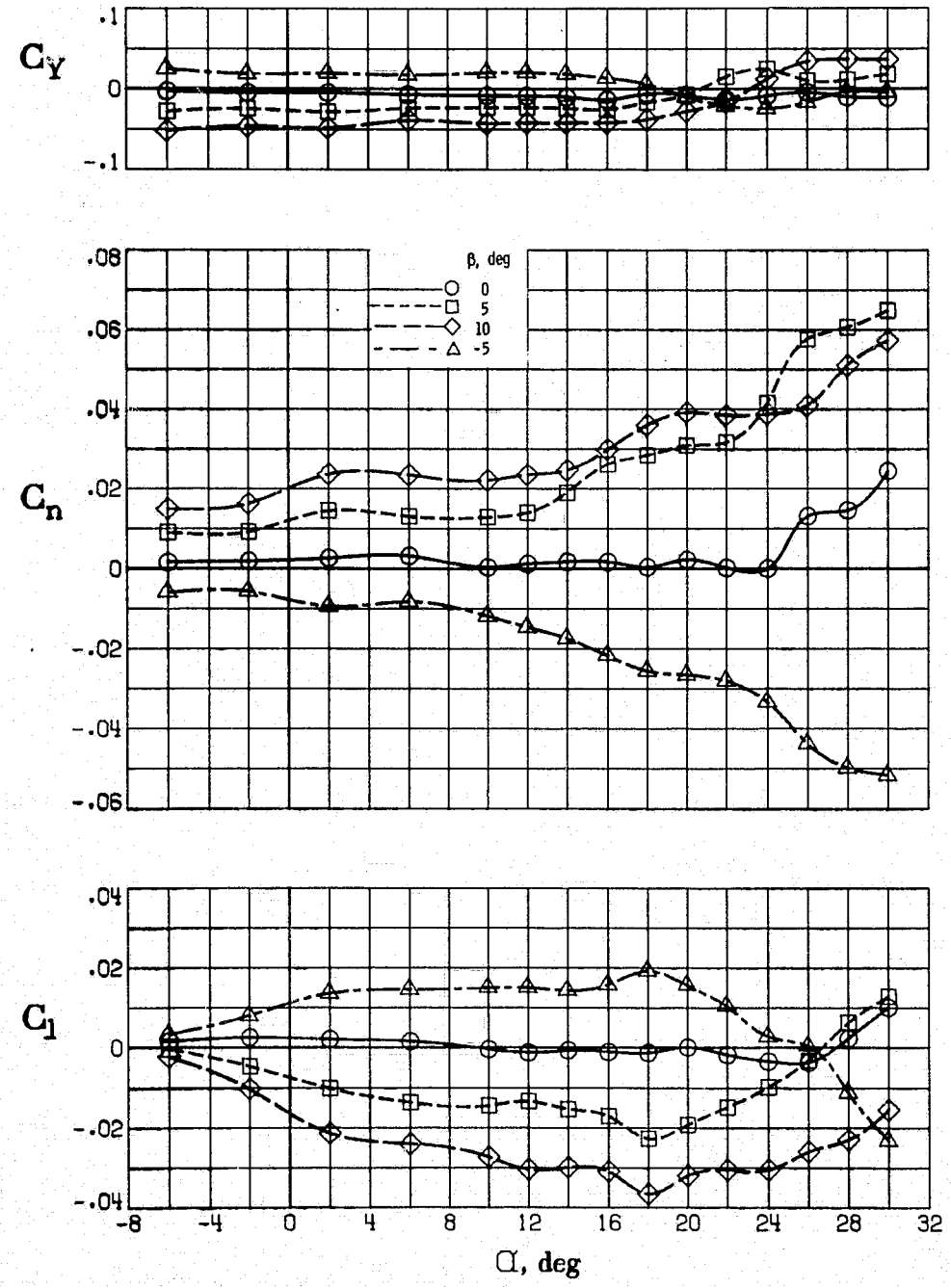

Figure 33. - Effect of sideslip on the lateral - directional characteristics with a 0.020 S canard and vertical tails. $\delta_{f,1,2,3} = 30°$, $\delta_{n,1,2,3,4} = 45°$, $\delta_{n,5,6,7} = 60°$, $T_c = 0$.

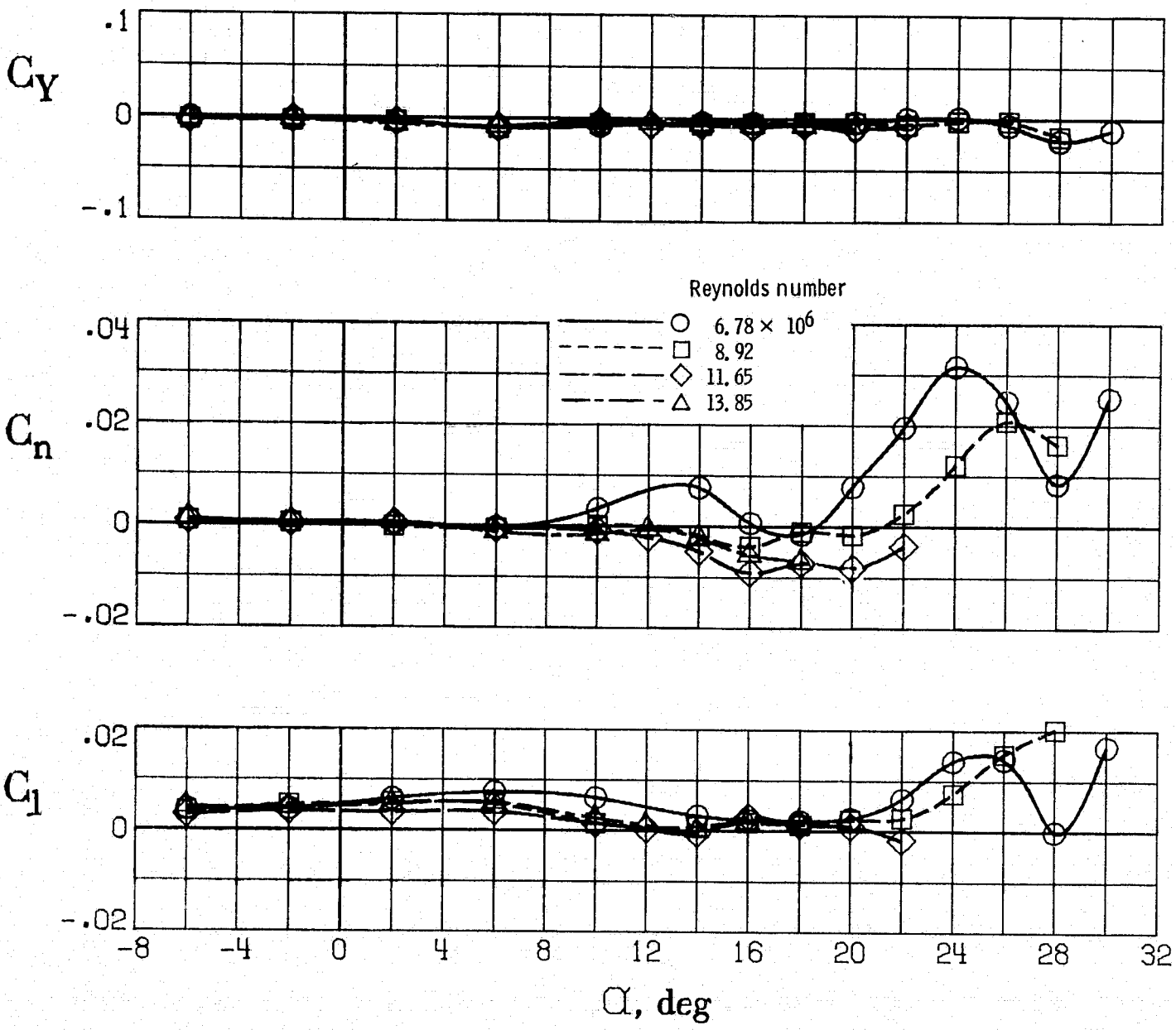

Figure 34. - Effect of Reynolds number on the lateral and directional characteristics of the clean wing with vertical tails. $\beta = 0°$, $T_c = 0$.

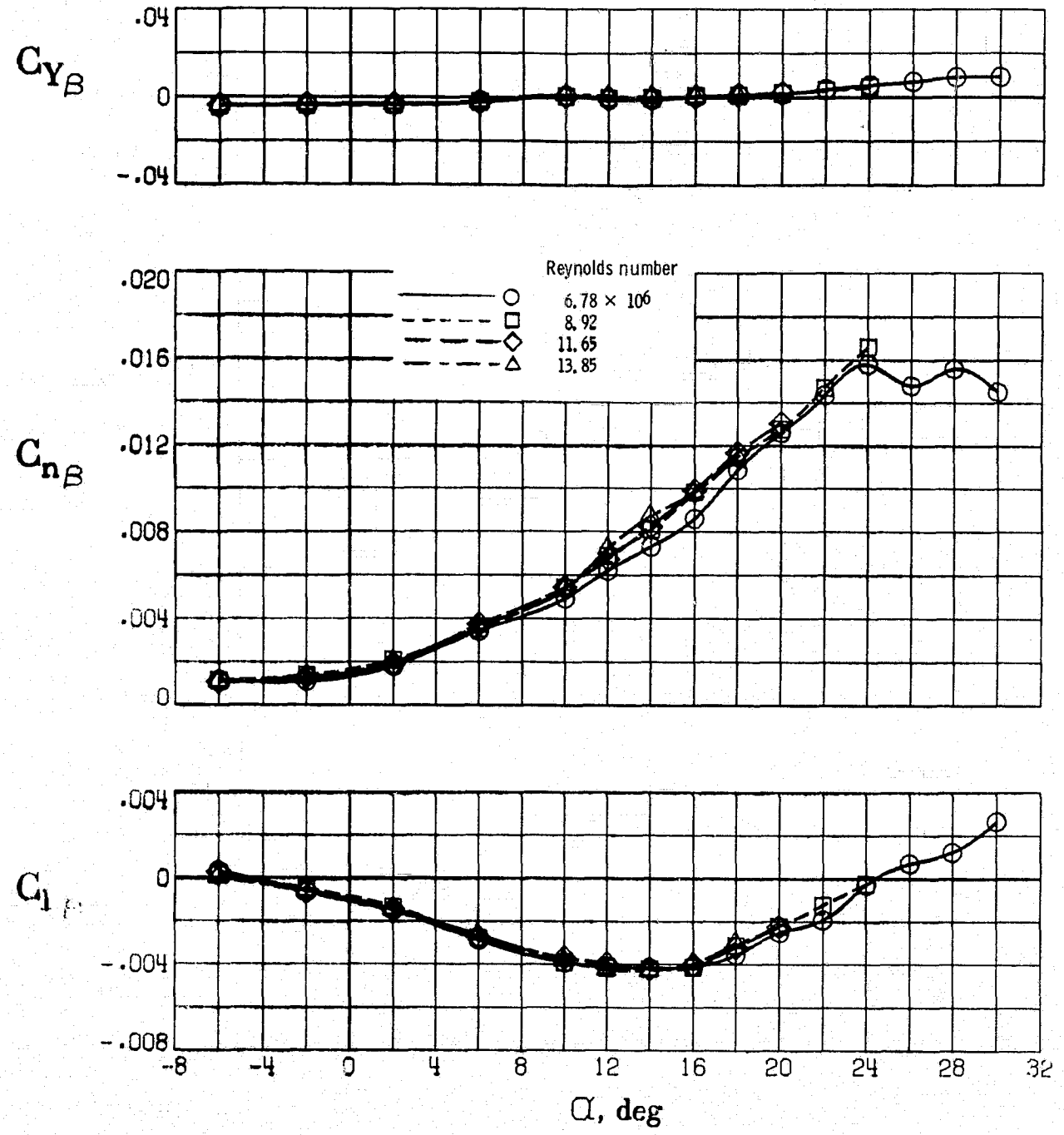

Figure 35. - Effect of Reynolds number on the static lateral - directional stability derivatives of the clean configuration. Vertical tails on. $T_C' = 0$.

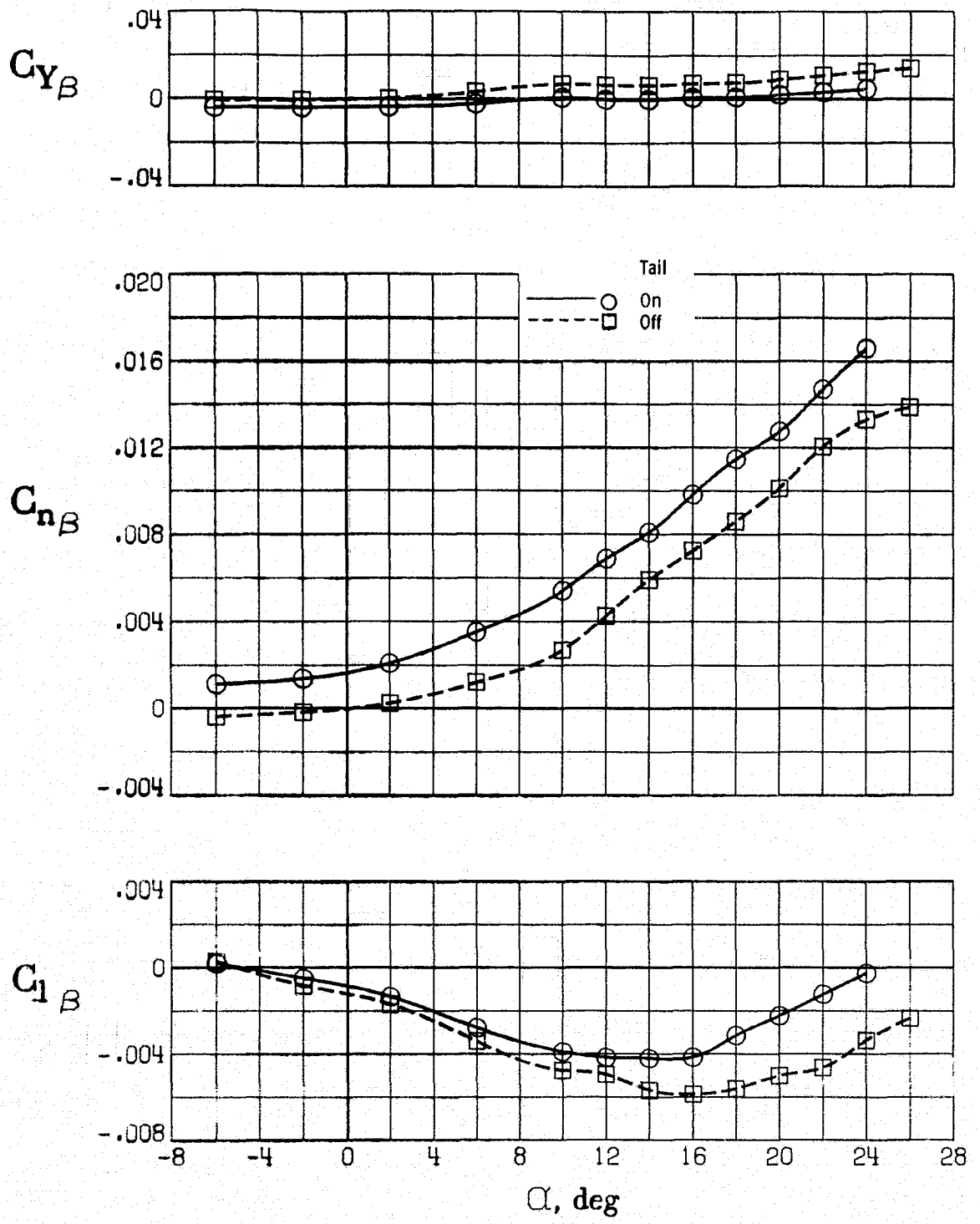

Figure 36. - Effect of vertical tails on the static lateral - directional stability derivatives of the clean configuration. $T_C' = 0$.

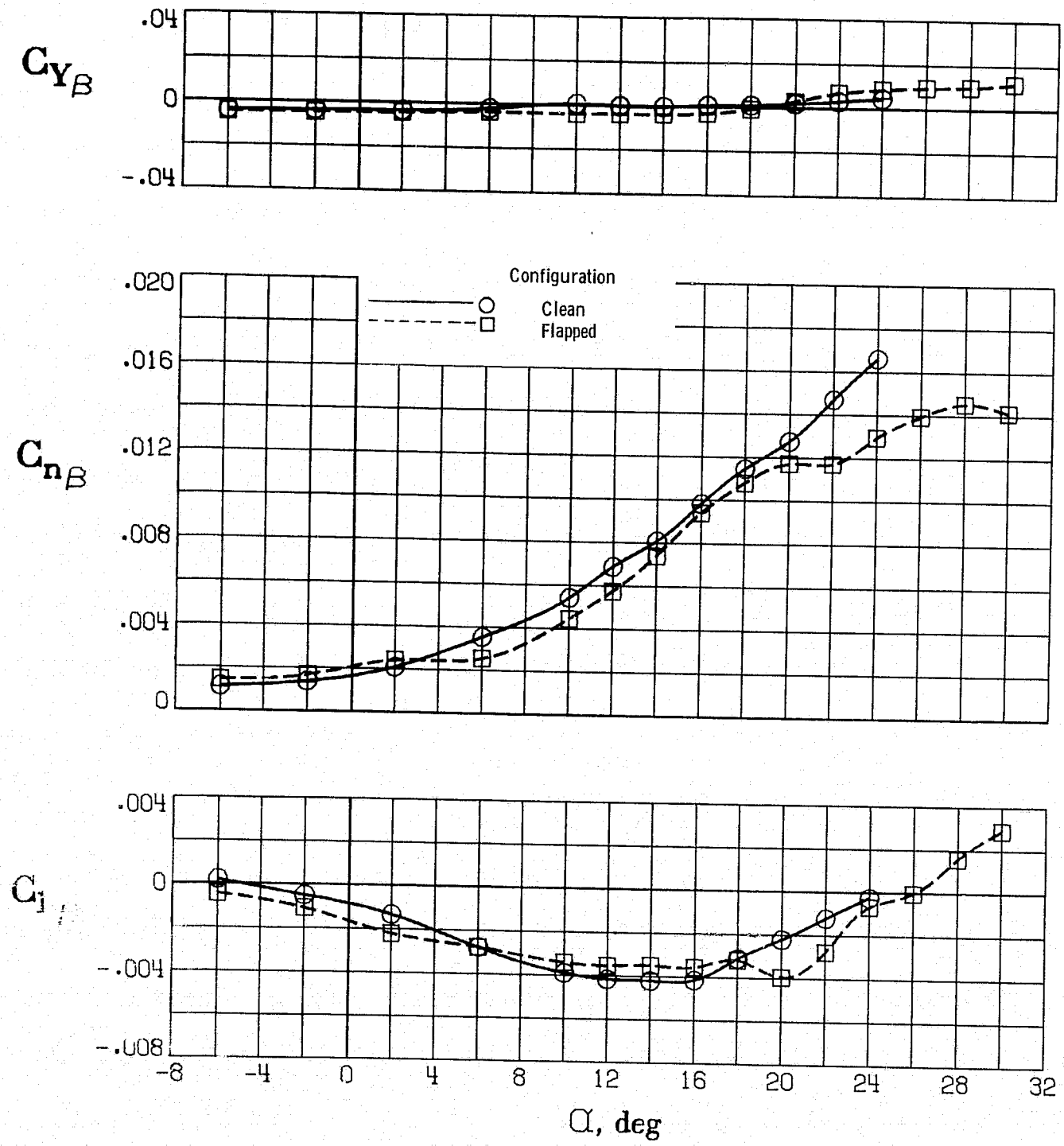

Figure 37. - Effect of L.E. and T.E. flaps on the static lateral - directional stability derivatives. $\delta_{f,1,2,3,}$ = 20°, 30°, 30°, $\delta_{n,1,2,3,4}$ = 45°, $\delta_{n,5,6,7}$ = 60°, T_c' = 0.

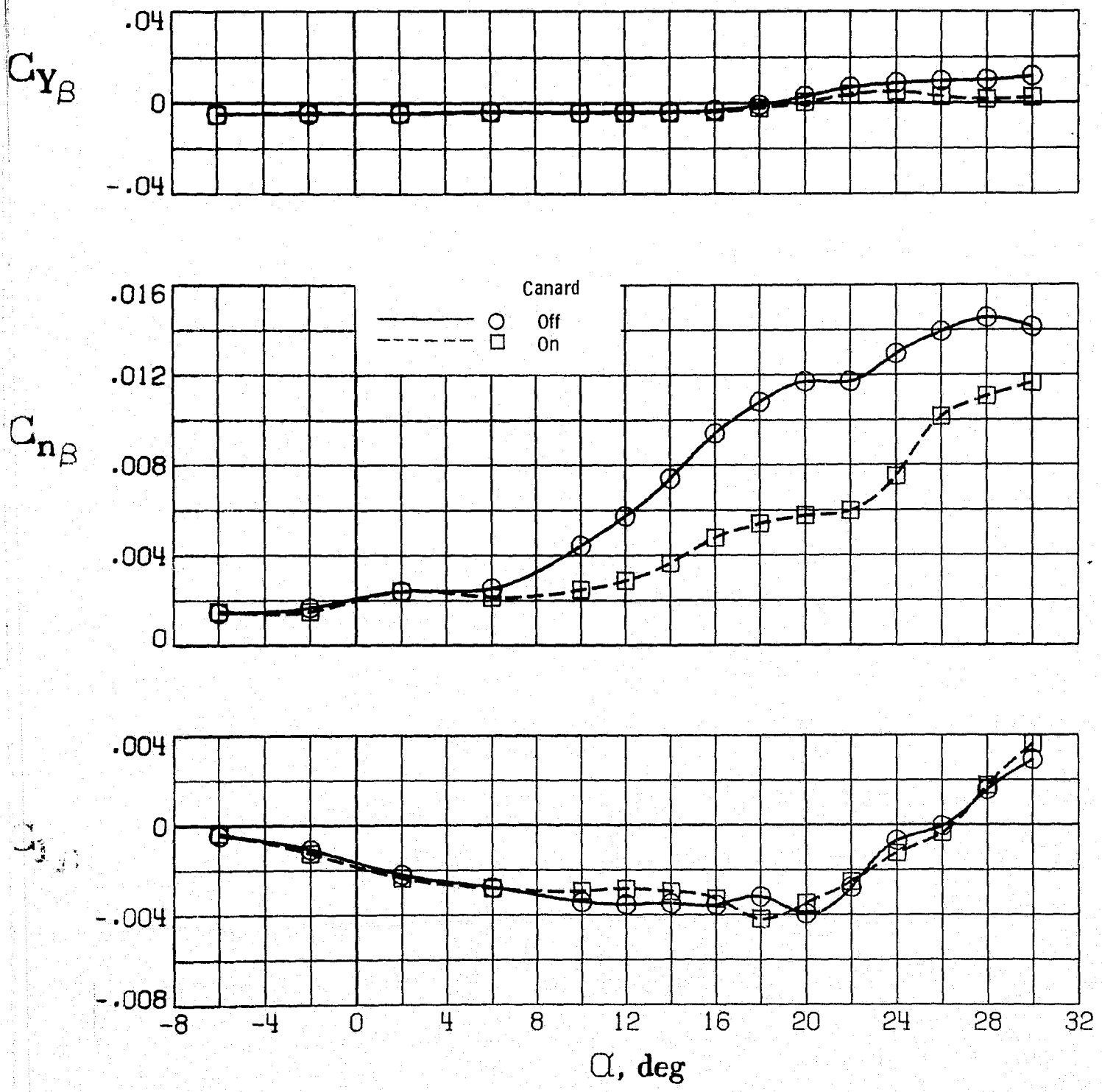

Figure 38. - Effect of 0.020 S canard on the static lateral - directional stability derivatives. $\delta_{n,1,2,3,4} = 45°$, $\delta_{n,5,6,7} = 60°$, $T_c' = 0$.

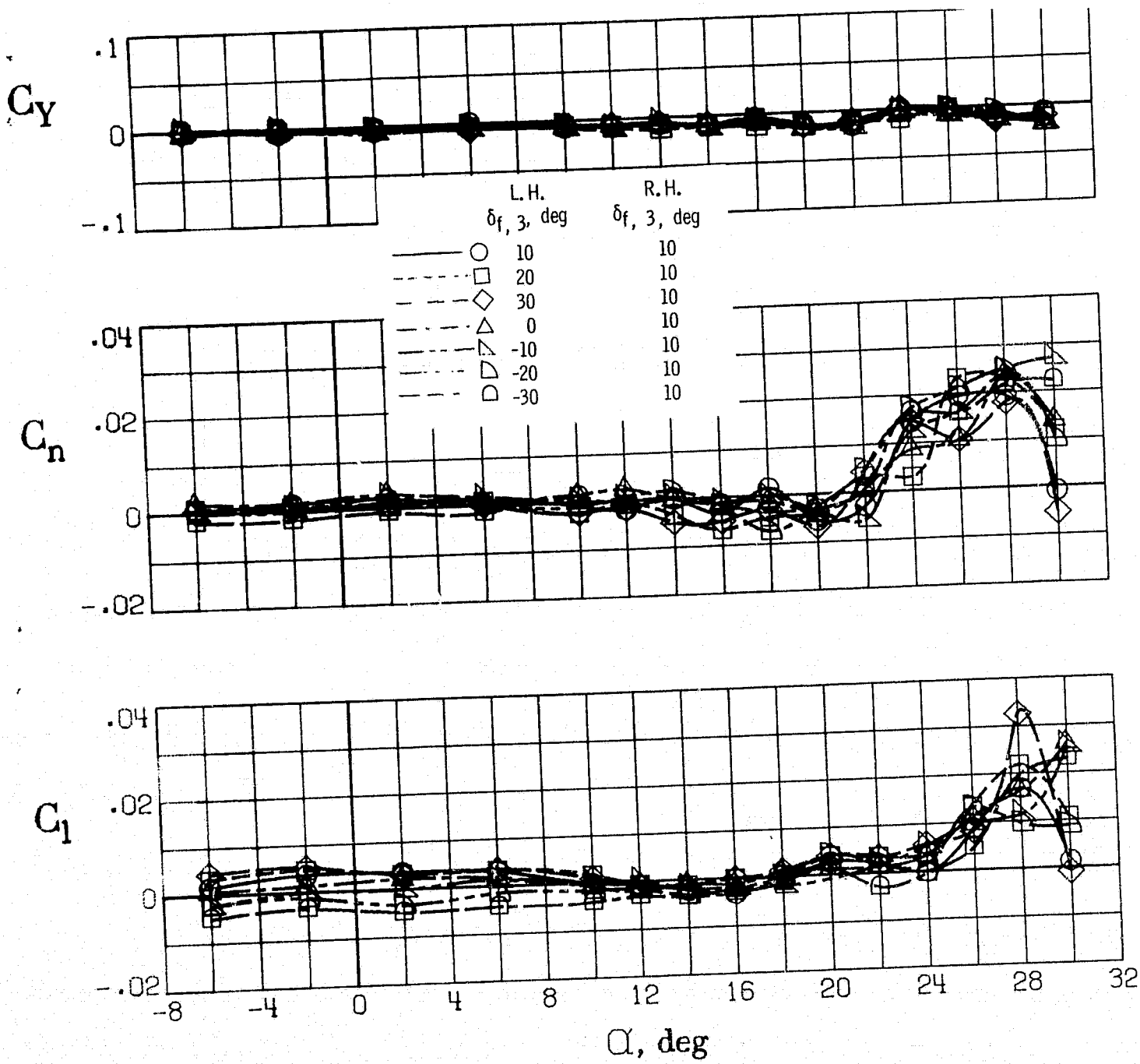

Figure 39. - Lateral control effectiveness of outboard T.E. flaps. $\delta_{f,1,2} = 30^\circ$, $\delta_{n,1,2,3,4} = 45^\circ$, $\delta_{n,5,6,7} = 60^\circ$, $\beta = 0^\circ$, $T_c' = 0$.

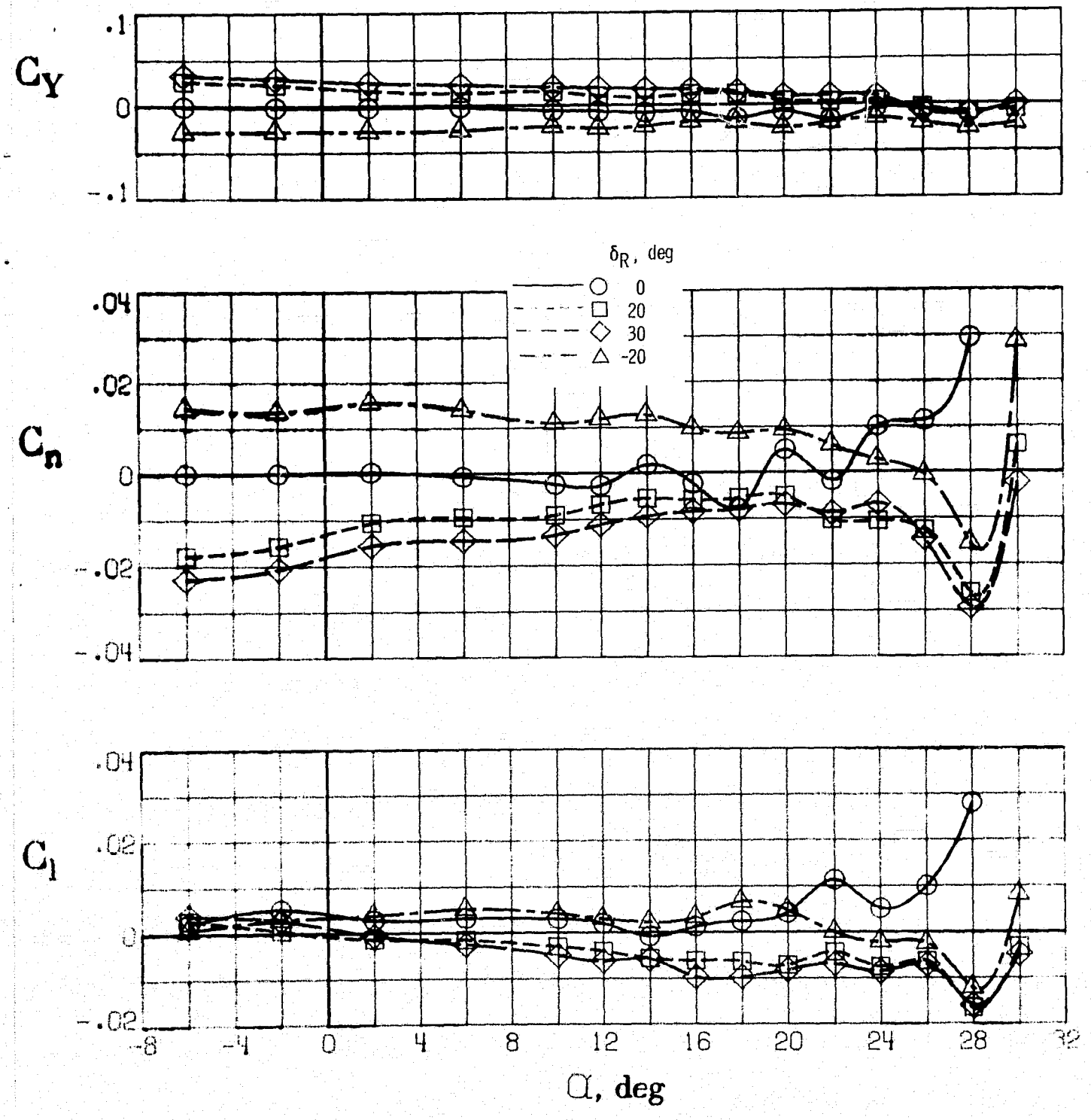

Figure 40. - Effect of rudder deflection on the lateral-directional characteristics. $\delta_{f,1,2,3} = 30°$, $\delta_{n,1,2,3,4} = 45°$, $\delta_{n,5,6,7} = 60°$, 0.025S canard, $T'_C = 0$.